Using the eddy covariance technique to measure gas exchanges in a beef cattle feedlot

by

Prajaya Prajapati

B.S., Institute of Forestry, 2010
M.S., Indiana University, 2013

AN ABSTRACT OF A DISSERTATION

submitted in partial fulfillment of the requirements for the degree

DOCTOR OF PHILOSOPHY

Department of Agronomy
College of Agriculture

KANSAS STATE UNIVERSITY
Manhattan, Kansas

2018

Abstract

Measurements of methane (CH_4) emissions from livestock production could provide invaluable data to reduce uncertainties in the global CH_4 budget and to evaluate mitigation strategies to lower greenhouse gas (GHG) emissions. The eddy covariance (EC) technique has recently been applied as an alternative to measure CH_4 emissions from livestock systems, but heterogeneities in the source area and fetch limitations impose challenges to EC measurements. The main objectives of this study were to: 1) assess the performance of a closed-path EC system for measuring CH_4, CO_2, and H_2O fluxes; 2) investigate the spatial variability of the EC fluxes in a cattle feedlot using flux footprint analysis; 3) estimate CH_4 emission rates per animal (F_{animal}) from a beef cattle feedlot using the EC technique combined with two footprint models: an analytical footprint model (KM01) and a parametrization of a Lagrangian dispersion model (FFP); and 4) compare CH_4 emissions obtained using the EC technique and a footprint analysis with CH_4 emission estimates provided by a well-stablished backward-Lagrangian stochastic (bLS) model. A closed-path EC system was used to measure CH_4, CO_2, and H_2O fluxes. To evaluate the performance of this closed-path system, a well-stablished open-path EC system was also deployed on the flux tower to measure CO_2 and H_2O exchange. Methane concentration measurements and wind data provided by that system were used to estimate CH_4 emissions using the bLS model. The performance assessment that included comparison of gas cospectra and measured fluxes from the two EC systems showed that the closed-path system was suitable for the EC measurements. Flux values were quite variable during the field experiment. A one-dimensional flux footprint model was useful to interpret some of the flux temporal and spatial dynamics. Then, a more comprehensive data analysis was carried out using two-dimensional footprint models (FFP and KM01) to interpret fluxes and scale fluxes measured at landscape to

animal level. The monthly average F_{animal}, calculated using the footprint weighed stocking density ranged from 83 to 125 g animal^{-1} d^{-1} (KM01) and 75–114 g animal^{-1} d^{-1} (FFP). These emission values are consistent with the results from previous studies in feedlots however our results also suggested that in some occasions the movement of animals on the pens could have affected CH_4 emission estimates. The results from the comparisons between EC and bLS CH_4 emission estimates show good agreement (0.84; concordance coefficient) between the two methods. In addition, the precision of the EC as compared to the bLS estimates was improved by using a more rigorous fetch screening criterion. Overall, these results indicate that the eddy covariance technique can be successfully used to accurately measure CH_4 emissions from feedlot cattle. However, further work is still needed to quantify the uncertainties in F_{animal} caused by errors in flux footprint model estimates and animal movement.

Using the eddy covariance technique to measure gas exchanges in a beef cattle feedlot

by

Prajaya Prajapati

B.S., Institute of Forestry, 2010
M.S., Indiana University, 2013

A DISSERTATION

submitted in partial fulfillment of the requirements for the degree

DOCTOR OF PHILOSOPHY

Department of Agronomy
College of Agriculture

KANSAS STATE UNIVERSITY
Manhattan, Kansas

2018

Approved by:

Major Professor
Eduardo Alvarez Santos

Copyright

Abstract

Measurements of methane (CH_4) emissions from livestock production could provide invaluable data to reduce uncertainties in the global CH_4 budget and to evaluate mitigation strategies to lower greenhouse gas (GHG) emissions. The eddy covariance (EC) technique has recently been applied as an alternative to measure CH_4 emissions from livestock systems, but heterogeneities in the source area and fetch limitations impose challenges to EC measurements at these systems. The main objectives of this study were to: 1) assess the performance of a closed-path EC system for measuring CH_4, CO_2, and H_2O fluxes; 2) investigate the spatial variability of the EC fluxes in a cattle feedlot using flux footprint analysis; 3) estimate CH_4 emission rates per animal (F_{animal}) from a beef cattle feedlot using the EC technique combined with two footprint models: an analytical footprint model (KM01) and a parametrization of a Lagrangian dispersion model (FFP); and 4) compare CH_4 emissions obtained using the EC technique and a footprint analysis with CH_4 emission estimates provided by a well-stablished backward-Lagrangian stochastic (bLS) model. A closed-path EC system was used to measure CH_4, CO_2, and H_2O fluxes. To evaluate the performance of this closed-path system, a well-stablished open-path EC system was also deployed on the flux tower to measure CO_2 and H_2O exchange. Methane concentration measurements and wind data provided by that system were used to estimate CH_4 emissions using the bLS model. The performance assessment that included comparison of gas cospectra and measured fluxes from the two EC systems showed that the closed-path system was suitable for the EC measurements. Flux values were quite variable during the field experiment. A one-dimensional flux footprint model was useful to interpret some of the flux temporal and spatial dynamics. Then, a more comprehensive data analysis was carried out using two-dimensional footprint models (FFP and KM01) to interpret fluxes and scale fluxes measured at

landscape to animal level. The monthly average F_{animal}, calculated using the footprint weighed stocking density ranged from 83 to 125 g animal^{-1} d^{-1} (KM01) and 75–114 g animal^{-1} d^{-1} (FFP). These emission values are consistent with the results from previous studies in feedlots; however, our results also suggested that in some occasions the movement of animals in the pens could have affected CH_4 emission estimates. The results from the comparisons between EC and bLS CH_4 emission estimates show good agreement (concordance coefficient = 0.84) between the two methods. In addition, the precision of the EC as compared to the bLS estimates was improved by using a more rigorous fetch screening criterion. Overall, these results indicate that the eddy covariance technique can be successfully used to measure CH_4 emissions from feedlot cattle. However, further work is still needed to quantify the uncertainties in F_{animal} caused by errors in flux footprint model estimates and animal movement.

Table of Contents

List of Figures

List of Tables

Nomenclature

$\overline{u}$	horizontal wind speed, m s^{-1}
u^*	friction velocity, m s^{-1}
w	vertical wind speed, m s^{-1}
z	measurement height, m
ϕ	footprint function, m^{-2}
τ_c	characteristic time constant of the EC system, s
ρ	molar density, mol m^{-3}
n_m	dimensionless frequency
α	stability dependent constant
θ	potential temperature, °K
χ_v	water vapor mixing ratio, μmol mol^{-1}
χ_c	carbon dioxide mixing ratio, μmol mol^{-1}
χ_m	methane mixing ratio, μmol mol^{-1}
ρ_c	molar density of carbon dioxide, mol m^{-3}
ρ_m	molar density of methane, mol m^{-3}
$fC_{w'x'}$	normalized cospectra
T_a	sonic anemometer temperature, °K
CP	closed path analyzer
OP	open-path analyzer
σ_F/F	fractional flux error
z_m	measurement height above the displacement height, m
L	Monin–Obukhov length, m
d	displacement height, m
z_0	aerodynamic roughness length, m
Ψ_m	integral profile similarity function for momentum
k	von Karman constant
y	crosswind distance from the sensor, m
x	along wind distance from the sensor, m

σ_y	standard deviation of the cross-wind distance, m
h	boundary layer height, m
Ω_p	isopleth describing source area level describing specific fraction of the measured flux (P)
C_f	normalized aggregated flux footprint
P_t	normalized footprint contribution
F_{pens}	methane flux from pens, μmol m^{-2} s^{-1}
F_{obs}	eddy covariance measured CH_4 flux, μmol m^{-2} s^{-1}
F_{animal}	methane flux per animal, g $animal^{-1}$ day^{-1}
sd_k	stocking density, m^2 $head^{-1}$
$\phi_{\Omega k}$	footprint weight allocated to a pen, m^{-2}
$x_{80\ or\ 90}$	downwind distance contributing 80 or 90% of the total flux, m
FFP	Kljun et al. (2015) model
KM01	Kormann and Meixner (2001) footprint model
bLS	Backward Lagrangian Stochastic technique
SF_6	Sulphur hexafluoride technique
SF	scaling factor

Acknowledgements

The work presented in this dissertation would not have been possible without the important contributions of several people.

First and foremost, I would like to express my deep appreciation and gratitude to my advisor, Dr. Eduardo Alvarez Santos, for his guidance and mentorship from the start to the completion of my PhD studies.

I would also like to thank my committee members: Dr. Gerard J. Kluitenberg, Dr. Ronaldo Maghirang and Dr. Xiaomao Lin for their guidance in my research and suggestion in improving my dissertation.

I would like to acknowledge the support by Kansas Agricultural Experiment Station at Kansas State University for funding this project. I am very much thankful to the collaborators in the feedlot industry for their assistance in this project. I am thankful to Kyle Stropes for his help in the field visits and instrumentation. I would like to acknowledge Fred Caldwell for his help with the field experiment.

Finally, I would like to thank my parents for their love and support throughout my study at K-State. I wish to thank my loving and supportive wife, Ramita and my wonderful son, Pramit, who have made me stronger, better and more fulfilled in my life.

Chapter 1 - General Introduction

The global demand for animal products has tripled over the last four decades and increased 20 percent in the last decade resulting in an expansion of livestock production (FAO, 2009; Vranken et al., 2014). The livestock sector accounts for the emission of 7.1 Gigatonnes of CO_2 equivalent per year, which corresponds to 14.5% of total anthropogenic greenhouse gas (GHG) emissions. It has been estimated that dairy and beef cattle contribute to 65 to 80%, while swine and poultry (non-ruminants) production contributes to 8 to 9% to the total livestock sector GHGs emissions (Gerber et al., 2013; Opio et al., 2013). It is noteworthy that the CO_2 emitted by animals is not included in the GHG emissions by ruminants since the CO_2 produced by livestock is originated from carbon assimilated by plants during photosynthesis. However, the conversion of natural ecosystem such as forest to pasture for feed production indirectly contribute to GHG emissions by releasing CO_2 from the decomposition of soil organic matter to the atmosphere (IPCC, 2006; Steinfeld et al., 2006). Nevertheless, the majority of GHG emissions by the livestock sector is originated from CH_4 and N_2O, which are powerful GHGs with global warming potential 25 and 298 times larger than CO_2, respectively over the period of 100 years (IPCC, 2014).

Confined animal feeding operations (CAFOs), such as beef cattle feedlots, contribute to more than 40% of the global meat demand and are the most rapidly expanding production system worldwide (Hudson, 2009). CAFOs are large-scale industrial livestock facilities that raise animals at high density using nutrient concentrated diets for the production of meat, eggs or milk. However, the growth of CAFOs has cause several environmental issues. The animal waste produced at CAFOs can affect ground and surface water quality (Burkholder et al., 2007). In addition, the decomposing manure produces air pollutants such as ammonia (NH_3), H_2S

(hydrogen sulphide), volatile organic compounds (VOCs), and particulate matter (PM) affecting the ambient air quality. CAFOs are also a source of greenhouse gases (GHGs) such as CH_4, CO_2 and NO_2 that contribute to global climate change (EPA, 2017).

Manure storage is an important source of CH_4 emission in livestock production systems. CH_4 emission from manure is mainly due to decomposition of organic material present in animal waste by anaerobic and facultative bacteria. The resulting products of this decomposition are CH_4, CO_2, and stabilized organic material. The amount of methane produced from manure depends on the composition of the manure, which, in turn, depends on the composition and digestibility of the animal diet. Additionally, the amount of CH_4 produced during manure decomposition is influenced by several factors such as temperature, moisture content and manure management practices (Chadwick et al., 2011). Manure management practices affect methane production by modifying oxygen (O_2) and moisture content; pH levels; and nutrient availability in the manure. Optimal conditions for CH_4 production include low O_2 levels, high water content, high level of nutrients needed for bacterial growth, a neutral pH (close to 7.0), and warm conditions (Buendia et al., 2006).

In ruminant production systems, the majority of the CH_4 emissions result from the microbial decomposition of plant carbohydrates inside the animal digestive system (O'Mara, 2011). Ruminant animals (e.g. cattle, buffalo, sheep, goats, and camels) have a large "fore-stomach" or rumen, within which microbial fermentation breaks down long-chain carbohydrates into soluble nutrients that can be assimilated by the animal (Gibbs and Leng, 1993). The digestion of feed components by the microbiota (bacteria, protozoa, fungi) results in the production of volatile fatty acids. These acids, mainly acetate, propionate, and butyrate are used by the animal as a source of energy. The metabolism of fatty acids results in the production of

gases, such as hydrogen (H_2), which are mainly eliminated through eructation. However, part of the H_2 is used by methanogenic bacteria to reduce CO_2 into CH_4 in a process called enteric fermentation. The enteric methane produced by ruminants also results in loss of feed energy, so the methane production by ruminants is also an indicator of the efficiency of feed utilization. It has been estimated that methane production by enteric fermentation represents a loss of 2% to 12% of the animal gross energy intake (Klevenhusen et al., 2011; Pinares-Patiño et al., 2007). Many factors affect CH_4 production in ruminants, including physical and chemical characteristics of the feed, animal feed intake, ration addictive, feeding schedule, and the overall health of the animal (Johnson and Johnson, 1995; Shibata and Terada, 2010). The feed characteristics and animal intake play a major role in methane production. The conversion of CH_4 production by ruminant animals depends upon amount of feed intake that is turned into CH_4 gas (EPA, 2016).

Different strategies have been evaluated to reduce enteric CH_4 production. Such CH_4 mitigation measures include: feed manipulation (Beauchemin et al., 2009; Knapp et al., 2011; Knapp et al., 2014), increasing animal productivity by improving animal health, nutrition and genetics (Havlík et al., 2014), and immunization with anti-methanogen vaccines (Subharat et al., 2015; Wright et al., 2004). Changing feed composition has shown potential for reducing CH_4 emission. The use of feed containing high level of dietary fat such as crushed oilseeds (sunflower seed, canola seed or flaxseed) or dried corn distillers grain reduced the energy lost as CH_4 by up to 40% (Sejian et al., 2012). Feeding cattle with whole cottonseed, plant oils, and some ethanol byproducts have also shown to lower methane production (Beauchemin et al., 2009). Adding more grain in ruminant's ration also reduces methane emissions, but this mitigation strategy is limited in scope as one of the main advantages of cattle production is the ability of these animals

to convert fibrous feeds, unsuitable for direct human consumption, to high-quality protein sources: milk and meat. Diets based on corn grain, compared with barley grain, reduce methane emissions, as does feeding high quality forages such as corn silage and alfalfa. Alternatively, the use of ionophores, antimicrobials that target the ruminal bacterial population and increase production efficiency, also reduce methane emissions at least for a short time (Eckard et al., 2010; Grainger and Beauchemin, 2011; Martin et al., 2010).

The evaluation of the CH_4 emission mitigation strategies requires reliable measurements of CH_4 emissions from livestock systems. In addition, CH_4 measurements are crucial to: (1) understand the environmental impacts of livestock sector at a regional and global scale, (2) to reduce uncertainty in greenhouse gas national inventories, (3) and to meet commitments of monitoring progress under the United Nations Framework Convention on Climate Change (UNFCCC) and subsequent agreements (Laubach and Kelliher, 2005).

Methane emissions from individual animals are measured using face masks (Place et al., 2011), head-hood chambers (Hill et al., 2016), whole-animal respiration chambers (Pinares-Patiño et al., 2011), tunnels (Lockyer and Jarvis, 1995) and tracer methods (Grainger et al., 2007; Johnson et al., 1994). The respiration chamber is considered the standard technique for measuring livestock GHG emissions. Results from chamber studies have been used to develop predictive models and equations for national greenhouse gas inventories (Danielsson et al., 2017; Ramin and Huhtanen, 2013). However, this method can create measurement artifacts by affecting animal behavior and is not suitable for measuring CH_4 emissions from large number of animals (McGinn et al., 2004; Storm et al., 2012).

The tracer method is based on the assumption that the controlled released of a tracer gas, usually within the animal rumen, is correlated to the animal CH_4 production and, therefore, can

be used to predict enteric methane production. Some of the commonly used tracer gases are carbon monoxide (CO), CO_2, various radioactive gases, and sulfur hexafluoride (SF_6) (McGinn et al., 2006). The SF_6 is commonly used as a tracer because it is nontoxic, nonflammable, and can be easily detected even at low concentration. The SF_6 tracer method has been used for studying effect of feeding and nutrition such as level of feeding, effect of feedstuff, effect of chemical and physical composition of feed on CH_4 emissions (Johnson et al., 1994; Lassey et al., 2011; Pinares-Patiño et al., 2011). However, the SF6 method is labor intensive and unsuitable for farm scale studies (Storm et al., 2012). In addition, SF_6 is a strong greenhouse gas and its use has been banned in several European countries. The CH_4:CO_2 tracer method is based on the assumption that CH_4 and CO_2 emissions from ruminants are correlated since the CO_2 production by animals is closely related to biochemical reactions in the animal rumen (Madsen et al., 2010). The accuracy of the CH_4 estimates using the CH_4:CO_2 ratio method depends on various factors that include the source of gases in the air sampled and diel variation in the ratio of CH_4: CO_2 concentration due to differences in animal activity and feeding frequency (Hammond et al., 2016).

Micrometeorological techniques have been applied for measuring ammonia (NH_3), CO_2, N_2O and CH_4 emissions from livestock systems (Baldocchi, 2003; McGinn and Flesch, 2018; Phillips et al., 2007; Sun et al., 2015). The benefits of these techniques are that they are non-intrusive, can integrate fluxes from large herds of cattle reducing measurement uncertainties due to animal to animal variability, and provide high temporal resolution (< 1h) flux measurements (McGinn, 2013). However, uncertainties associated with heterogeneities in the source area and fetch limitations in livestock systems impose challenges to the implementation of micrometeorological approaches (Baum et al., 2008; Coates et al., 2017). The

micrometeorological methods can be grouped in different methods based on: spatial gradients of concentration in the direction of scalar diffusion, inverse Lagrangian models and concentration fluctuation-based methods (Raupach, 2001).

The integrated horizontal flux technique (IHF) is based on mass balance principles and uses the difference between the upwind and downwind horizontal scalar concentration from the source area of interest to estimate the vertical flux (McGinn, 2006). Previous studies have used the IHF method for quantifying total CH_4 emission from livestock (Griffith et al., 2008; Harper et al., 1999; Laubach and Kelliher, 2004). The benefit of using IHF is its simple theoretical basis, simple instrumentation requirements and its suitability in heterogonous source areas. However, this technique is only suitable for small and well-defined source areas (Denmead, 2008).

The flux-gradient technique (FG) also applies gradients of concentration to estimate fluxes. This technique has been applied to measure CH_4 emission from grazing sheep (Judd et al., 1999) and grazing cattle (Laubach et al., 2008). The FG approach is based on the assumption that the vertical flux of scalars can be related to vertical gradients of concentration measured above a homogeneous surface using an eddy diffusivity coefficient. Like other micrometeorological methods, the FG technique requires the measurements to be taken within a fully adjusted internal boundary layer, so that the flux measurements represent the underlying surface over which flux measurements are made (Vesala et al., 2008).

The backward Lagrangian stochastic technique (bLS) is a well-stablished inverse dispersion model used to determine scalar exchange from well-defined source areas. The bLS technique is particularly useful to quantify gas emissions from livestock systems within well-defined boundaries, such as manure storage lagoons (Ro et al., 2013) , CAFOs (Flesch et al., 2007; Loh et al., 2008; Todd et al., 2011; Todd et al., 2008), barns (Gao et al., 2010; Harper et

al., 2009), and land application of livestock waste (Sanz et al., 2010). The bLS approach uses the rise of concentration downwind from the source and wind statistics to determine the source emission rate. One of the advantages of the technique is its simplicity, i.e. wind and concentration measurements are straightforward, and it can be used to measure emissions from point sources and source areas of variable sizes. Numerous validation studies have been conducted under field conditions by releasing a tracer gas at known flow rate and estimating the recovery rate with the bLS technique (Flesch et al., 2005a; Flesch et al., 2004; Gao et al., 2010; Gao et al., 2009; Loh et al., 2009; McBain and Desjardins, 2005). These studies have reported an emission rate accuracy of ±10%. The limitation of bLS technique is that it requires the source area of emission to be well defined or that location of point sources to be known. Another limitation is the bLS technique does not provide accurate emission measurements under very convective or stable atmospheric (Flesch et al., 2009).

The EC technique measures the exchange of energy and mass between land surface and the atmosphere by monitoring instantaneous fluctuations of concentration (c') and vertical wind velocity (w'). The eddy flux (F) is given by:

$$F = \overline{\rho_a}\overline{w'c'} \tag{1.1}$$

where: ρ_a is air density, the overbars represent time averages and primes represent instantaneous fluctuations from the mean. The measured EC flux represents the averaged gas exchange from an area located upwind of the sensors. The extent of this source area (i.e., area of influence) can be estimated using a flux footprint model and is dependent on wind direction, atmospheric stability and surface characteristics (Fig 1.1a and b) (Schmid and Lloyd, 1997). The flux footprint ϕ is given by:

$$F(0,0,z_m) = \int_{\Omega} Q_c(x,y,0)\,\phi\,(x,y,z_m)dxdy \tag{1.2}$$

where: F (x = 0, y = 0, z_m) is the turbulent EC flux measured at measurement height (z_m) in the center of the Cartesian plane, Q_c (x, y, 0) is the spatial distribution of source strength, and Ω is the source area. Flux footprint models can be categorized into: analytical models, Lagrangian-stochastic particle dispersion models, large-eddy simulations, and ensemble-averaged closure models (Schmid, 2002). The Lagrangian-stochastic particle dispersion models, large-eddy simulations, and ensemble-averaged closure models are relatively accurate; however, these models are also complex and computing-intensive. The analytical models are easy and simple to use; however their validity is constrained to a narrow range of sensor heights and atmospheric boundary layer conditions (Kljun et al., 2015; Vesala et al., 2008). Alternatively, a parameterized version of Lagrangian stochastic models retain most of the complex model predicting skills while reducing computation demands compared to the full models (Kljun et al., 2015; Schmid, 2002) .

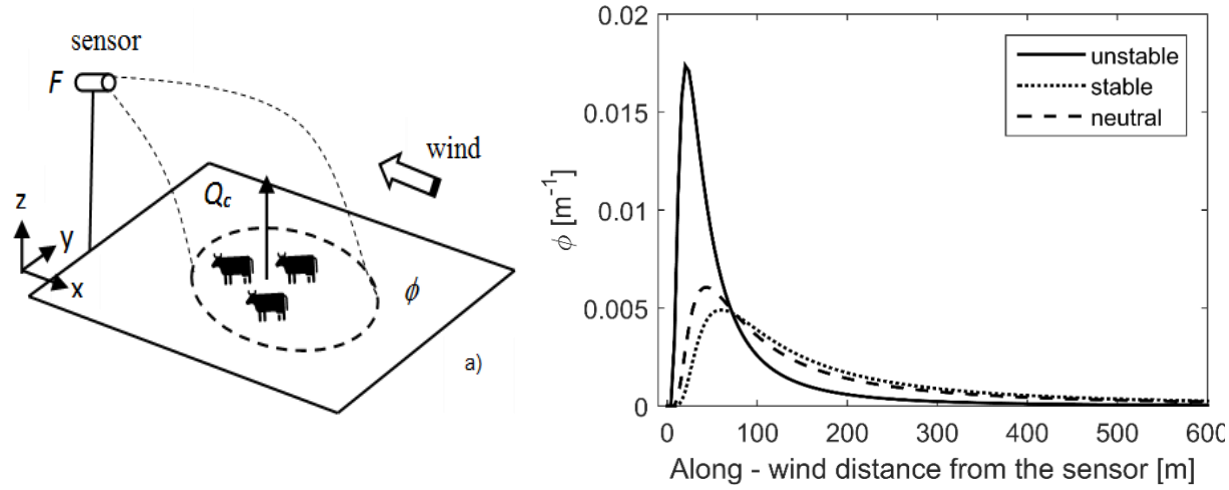

Figure 1.1 a) The scalar flux (F) measured at the sensor height depends on flux footprint (ϕ) and scalar source strength (Q_c). b) Relationship between cross-wind integrated flux footprint with the atmospheric stability conditions (unstable: - 100 < L < 0, stable: 0 < L < 100 and neutral: |L| > 100).

The EC approach implementation in livestock systems faces two major challenges: heterogeneities of the source area and fetch limitations. In feedlots for example, the presence of non-emitting surfaces such as roads, transfer alleys and the movement of animals can increase uncertainty in flux measurements and scaling from landscape to animal scale from livestock production system like a cattle feedlot (Baum et al., 2008; Sun et al., 2015). In principle, information about the number of animals, their spatial position relative to the sensor location and flux footprint models can be used to screen EC fluxes for fetch limitations (Dengel et al., 2011; Sun et al., 2015; Taylor et al., 2017) and to scale measured fluxes from feedlot to animal scale (Baum et al., 2008; Felber et al., 2015). Only a few studies have evaluated the use of EC technique and the scaling approach using a flux footprint model in estimating CH_4 emissions from the livestock systems (Baum et al., 2008; Felber et al., 2015).

1.1. Outline and Objectives

This dissertation is divided into 5 chapters, chapters 2 to 4 have been published in Agricultural and Forest Meteorology (Prajapati and Santos, 2017; Prajapati and Santos, 2018a; Prajapati and Santos, 2018b). The overall objective of this dissertation was to investigate the performance of the EC technique to measure gas emissions from a commercial beef cattle feedlot in Kansas.

In chapter 2, a closed-path EC system was used to measure CH_4 emissions from an open-air beef cattle feedlot. The objectives of this specific study were 1) to assess the performance of a closed-path EC system for measuring CH_4, CO_2, and water vapor (H_2O) fluxes in a beef cattle feedlot against a well-stablished EC open-path system, and 2) to investigate the spatial variability of EC fluxes measured above the surface of a beef cattle feedlot using an analytical flux footprint analysis.

Chapter 3 describes the use of a flux footprint scaling approach to scale CH_4 EC fluxes from feedlot to animal scale. The specific objectives of this chapter were to: 1) investigate the effect of fetch limitations and feedlot surface heterogeneities on EC CH_4 flux measurements and 2) estimate and compare the CH_4 emission rate per pen area and per animal from the feedlot using an analytical flux footprint model and the parameterized version of a Lagrangian stochastic particle dispersion model.

The chapter 4 main objective was to compare CH_4 emissions obtained using the EC technique, combined with a footprint analysis (EC_{FFP}), with CH_4 emission estimates provided by the bLS model. The influence of the flux footprint extent and fetch limitations on the EC and the bLS CH_4 estimates were also investigated in this chapter.

Chapter 5 provide an overall summary of the results and conclusions of the studies in chapters 2, 3 and 4, along with the possible directions for future research.

Chapter 2 - Measurements of Methane Emissions from a Beef Cattle Feedlot using the Eddy Covariance Technique

2.1. Abstract

The eddy covariance (EC) technique has been extensively used in several sites around the world to measure energy fluxes and CO_2 exchange at the ecosystem scale. Recent advances in optical sensors have allowed the use of the EC approach to measure other trace gases (e.g. CH_4, NH_3 and N_2O), which has expanded the use of eddy covariance for other applications, including measuring gas emissions from livestock production systems. The main objectives of this study were to assess the performance of a closed-path EC system for measuring CH_4, CO_2, and H_2O fluxes in a beef cattle feedlot and to investigate the spatial variability of eddy covariance fluxes measured above the surface of a feedlot using an analytical flux footprint analysis. A closed-path EC system was used to measure CH_4, CO_2, and H_2O fluxes. To evaluate the performance of this closed-path system, an open-path EC system was also deployed on the flux tower to measure CO_2 and H_2O exchanges. The performance assessment of the closed-path EC system showed that this system was suitable for EC measurements. The frequency attenuations, observed for the closed-path system CO_2 and CH_4 cospectra in this study, are in agreement with results from previous instrument comparison studies. For the water vapor closed-path cospectra, larger attenuations were likely caused by water vapor molecule interaction with the sampling tube walls. Values of R^2 for the relationship between H_2O and CO_2 fluxes, measured by open-path and closed-path systems, were 0.94 to 0.98, respectively. The closed-path EC system overestimated the CO_2 by approximately 5% and underestimated the latent heat fluxes by about 10% when compared with the open-path system measurements. Measured CH_4 and CO_2 fluxes

during the study period from the feedlot averaged 2.63 μmol m^{-2} s^{-1} and 103.8 μmol m^{-2} s^{-1}, respectively. Flux values were quite variable during the field experiment and the footprint analysis was useful to interpret flux temporal and spatial variation. This study shows indication that consideration of atmospheric stability condition, wind direction and animal movement are important to improve estimates of CH_4 emissions per pen surface or per head of cattle.

2.2. Introduction

Methane is an important GHG with a global warming potential 28 times greater than CO_2 over a 100-year period. Methane, originating from microbial fermentation in the digestive system of ruminants (enteric fermentation) and manure management, accounts for approximately 30% of the total anthropogenic CH_4 emissions in the United States (USEPA, 2015). Accurate measurements of CH_4 from animal production systems are crucial for reducing uncertainties in national GHG inventories and evaluating mitigation strategies to reduce GHG emissions from agriculture.

Chamber and tracer techniques are often used to measure emissions from livestock. These techniques are useful in comparison studies aiming to evaluate the effect of different diets and mitigation strategies to minimize GHG emissions (Makkar and Vercoe, 2007). However, chambers and tracer techniques are intrusive. They can alter typical animal behavior, management conditions, and gas emission rates. In addition, their application is constrained to a limited number of animals increasing measurement uncertainties (Harper et al., 2011).

Micrometeorological approaches have also been used to estimate GHG emissions from livestock production systems and offer some advantages compared to chamber and tracer techniques (Bai et al., 2015; Baum et al., 2008; Flesch et al., 2007; Laubach, 2010; Laubach et al., 2013). For instance, micrometeorological methods are non-intrusive and integrate flux

measurements from larger areas and from a larger number of animals in their natural environment, reducing uncertainties in the fluxes caused by small sample sizes and changes in animal behavior (Harper et al., 2011; McGinn, 2013).

The eddy covariance technique is considered the most direct micrometeorological method to measure gas exchanges between the land and the atmosphere (Baldocchi, 2003; Dabberdt et al., 1993). The EC approach requires fast response sensors (typically 10-20 Hz sampling rate) to capture fluxes measured by small turbulent eddies. Recent advances in optical sensors have allowed the development of fast response sensors capable of measuring other trace gases, such as CH_4, nitrous oxide (N_2O), and ammonia (NH_3), at a rate suitable for EC measurements (Detto et al., 2011; McDermitt et al., 2011; Peltola et al., 2013; Sun et al., 2015). The EC approach has been used to measure gas exchange from different surfaces, including: agricultural sites (Abraha et al., 2015; Baker and Griffis, 2005), urban plots (Feigenwinter et al., 2012; Velasco et al., 2005), landfills (McDermitt et al., 2013), and bodies of water (Nordbo et al., 2011; Norris et al., 2012). Recent studies have also applied the EC technique to estimate CH_4 emissions from grazing animals (Dengel et al., 2011; Felber et al., 2015).

Previous studies have also applied the EC technique to measure gas exchange from beef cattle feedlots and the atmosphere (Baum et al., 2008; Sun et al., 2015). These whole farm emission measurements can be useful to improve current GHG modeling approach uncertainties (Crosson et al., 2011). One of the basic assumptions of the EC technique is that measurements are taken above an extensive and homogeneous source area. In feedlots, fluxes measured using the EC approach integrate contributions from different surfaces, such as: pens, roads and alleys, which will influence the flux magnitudes (Baum et al., 2008). Flux footprint analyzes have been used to interpret flux variation in animal production systems and to investigate how changes in

the underlying source surface affect flux measurements (Baum et al., 2008; Dengel et al., 2011; Sun et al., 2015). Baum et al. (2008) applied the eddy covariance technique to measure carbon dioxide (CO_2) and water vapor fluxes from a commercial beef cattle feedlot in Kansas. They utilized an analytical footprint model to determine the contributions of non-pen surfaces to the EC flux. They found alleys and roads contribute to 2 and 10% of the total flux, respectively. They also reported that the effect of these surfaces on the fluxes varied depending on the wind direction. More recently, Sun et al. (2015) used the EC approach to measure NH_3 fluxes in a beef cattle feedlot in Colorado. They were able to identify in their two-week measurement that the diel variation in the NH_3 flux was also influenced by the flux footprint.

Most of the CH_4 emission measurements from ruminants using micrometeorological techniques are restricted to short field campaigns ranging from a few days to weeks. Long-term studies are necessary to investigate how changes in environmental conditions affect GHG fluxes from livestock production systems and to reduce the uncertainties of current GHG inventories and emission factors. In addition, long-term studies could bring new insights into the factors affecting the performance of micrometeorological techniques. In this study, we evaluate the performance of a closed-path EC system to measure CH_4 and CO_2 emissions from a commercial beef cattle feedlot during an 8-month period. Few studies have applied the EC technique to quantify gas emissions from a beef cattle feedlot (Baum et al., 2008; Sun et al., 2015) and to our knowledge, this is the first study to utilize the EC technique to estimate long-term CH_4 emissions from a confined animal feeding operation. The main objectives of this study were (i) to assess the performance of a closed-path EC system for measuring CH_4, CO_2, and water vapor (H_2O) fluxes in a beef cattle feedlot against a well-established open-path gas analyzer, and (ii) to

investigate the spatial variability of EC fluxes measured above the surface of a beef cattle feedlot using an analytical flux footprint analysis.

2.3. Material and Methods

2.3.1. Site description

The field experiment was carried out in a commercial beef cattle feedlot in western Kansas from August 2013 to May 2014. This feedlot has a near rectangular shape with a total pen surface of approximately 59 ha surrounded by agricultural fields. The feedlot has the capacity to hold 30,000 head of cattle and was near full capacity (~30,000) during the experiment. The experimental site is on a near flat terrain (slope < 5%) and located in one of the windiest regions of the United States (National Climatic Data Center, 2017), making this site ideal to evaluate micrometeorological methods.

2.3.2. Flux measurements

Fluxes of CH_4, CO_2, latent heat, and sensible heat were measured using the EC technique. Wind velocity, three orthogonal components, and temperature were measured using a sonic anemometer (CSAT3, Campbell Sci., Logan, UT). A wavelength-scanned cavity ring-down spectroscopy closed-path gas analyzer (G2311-f, Picarro Inc., Santa Clara, CA) was used to measure CH_4, CO_2 and H_2O concentrations. To evaluate the performance of the closed-path EC system, a well-established open-path gas analyzer (LI-7500, LI-COR, Lincoln, NE) was also deployed on the flux tower to measure CO_2 and H_2O concentrations.

The closed-path analyzer air intake consisted of a rain diverter connected to an inline filter (Polypropylene/polyethylene 10 μm membrane, Pall Corporation, AnnArbor, MI) and was positioned at 8 cm from the sonic anemometer. The air was drawn from the intake through a 7-m long high-density polyethylene tube with an inner diameter of 5.3 mm and then to a second filter

(Acrodisc Gelman 1μm, PTFE membrane, Pall corporation), which was connected to the closed-path analyzer inlet. The feedlot is a very dusty environment, so the use of two filters in series was necessary to prevent clogging of the analyzer's internal filter by particulate material. A vacuum pump (MD 4 NT, Vacuubrand GmbH, Wertheim, Germany) and the analyzer internal mass flow controller kept the flow rate in the sampling line at 5 L min^{-1}. The sampling line was heated using a pipe heating cable and covered with pipe insulation material to lower the relative humidity within the sampling tube and minimize the adsorption of water by the tube walls. Field calibrations were performed in two-week intervals using certified calibration tanks (Tank 1: CH_4 = 1.9 ppm and CO_2 = 350.1 ppm, and Tank 2: CH_4 = 4 ppm and CO_2 = 450.3 ppm, ±1% accuracy, Matheson, Joliet, IL).

The sonic anemometer, closed-path analyzer air inlet, and open-path analyzer were setup on a tower at approximately 5 m above the ground. The tower was mounted on the top of a flatbed trailer at the northern edge of the feedlot. The instrumentation setup location was chosen to maximize air flow over the source area within the feedlot and to maximize the distance between the tower and buildings at the south side of the feedlot that could disturb the air flow. The open-path analyzer was set up with a slight angle from the vertical (~15^o) to minimize the accumulation of rain droplets on the analyzer windows after rain events. To minimize synchronization errors among the instruments, the signals of the sonic anemometer, open-path and closed-path gas analyzers were recorded at 10 Hz by a single datalogger (CR1000, Campbell Sci.). The sensors and the datalogger were connected using synchronous devices for measurement (SDM, Campbell Sci) cables for sonic anemometer and open-path analyzer and a serial (RS232) cable for the closed-path analyzer.

2.3.3. Flux calculations

The high-frequency raw data files were converted into half-hour files using Matlab (version 8.3.0.532, The Mathworks Inc., Natick, MA) functions. These functions were also used to check the consistency of time stamps and to apply the calibration corrections, obtained during field calibrations, to the closed-path analyzer raw signals.

The half-hour high frequency data were then analyzed using the EC package software EddyPro (v. 6.0, Licor). Spikes in the data time series were eliminated following the methodology proposed by Vickers and Mahrt (1997). Averages, covariances, and other statistics were then calculated for 30-min intervals. The block average method was used for calculating turbulent fluctuations and the double rotation method was used to nullify the average cross-stream and components of the wind velocity (Wilczak et al., 2001).

2.3.3.1. Time lag compensation

Time lags among sonic anemometer and gas analyzer signals arise due to several reasons, such as spatial separation between wind and gas analyzers, as well as differences in computation and digitalization of electronic signals (Aubinet et al., 2012). In addition, in closed-path systems the travelling time of air parcels through the sampling tube and the interaction between gases and tube walls cause gas concentrations to always be measured with a certain delay with respect to the wind velocity measurements. Determining the time lags correctly is an important step of flux calculations as it prevents flux underestimation (Moravek et al., 2013). In our study, compensations for time lags were performed using the covariance maximization method (Fan et al., 1990). For the closed-path EC system, these time lags were determined within a plausible search window. The determination of the plausibility of the time lags is particularly important for low flux conditions when the measured signals contain a large amount of noise leading in some cases to physically unrealistic values of time lag (Detto et al., 2011). The plausibility window was determined by the Eddy Pro software in a preprocessing step that statistically determined the

time lags for the closed-path system and their range of variation. Considering the dependence between the water vapor time lags and the relative humidity, the nominal time lags and plausibility windows are determined for different relative humidity classes.

2.3.3.2. Air density corrections

Fluctuations in temperature and water vapor in the air lead to fluctuations in trace gas concentrations that are not associated with the turbulent transport of the trace gas of interest. Thus, the use of appropriate density corrections is necessary for correct flux computations. For the open-path analyzer, fluxes of CO_2 ($\overline{F_c}$) and H_2O ($\overline{F_v}$) were corrected using the method proposed by Webb et al. (1980), given by:

$$\overline{F_c} = \overline{w'\rho_c{}'} + \mu_m(\overline{\rho_c}/\overline{\rho_d})\overline{w'\rho_v'} + (1 + \mu_m\sigma)(\overline{\rho_c}/\bar{\theta})\overline{w'\theta'} \quad (2.1)$$

$$F_v = (1 + \mu_m\sigma)\left[\overline{w'\rho_v'} + (\overline{\rho_v}/\bar{\theta})\overline{w'\theta'}\right] \quad (2.2)$$

where w is the vertical wind velocity, ρ is the molar density, the subscripts c, d and v denote: CO_2, dry air and water vapor, respectively; $\mu_m = m_d/m_v$ is the ratio of molar masses of dry air and water vapor; and $\sigma = \overline{\rho_v}/\overline{\rho_d}$ and θ is the potential temperature. Overbars represent the mean and the prime symbols are the departure from the mean.

The closed-path analyzer converts CO_2 and CH_4 mole fractions to mixing ratios, using high frequency measurements of H_2O mixing ratio in the air and an internal algorithm (Chen et al., 2010), which eliminates the need for density corrections. This approach was evaluated as described in section 2.3.3.2.

2.3.3.3. Spectral corrections

Frequency losses in EC systems are caused by different factors including: inadequate sampling frequency by sensors, sensor separation, and finite sampling duration. In closed-path

systems, the existence of sampling tubes and filters, and the residence time in the sampling cell are major causes of spectral attenuation and flux underestimation (Aubinet et al., 2012). Low frequency losses were corrected following the method proposed by Moncrieff et al. (2004) to compensate frequency loss due to finite averaging length and detrending. The analytical method proposed by Moncrieff et al. (1997) was used to correct high-frequency losses by the open-path analyzer. For the closed-path system, we applied the spectral correction procedure proposed by Horst (1997), given by:

$$(\overline{w's'})_m/(\overline{w's'})_t = \frac{1}{1+(2\pi n_m \tau_c \overline{u}/z)^{\alpha}} \quad (2.3)$$

where $(\overline{w's'})_m$ is measured scalar flux or the covariance between *w* and the scalar concentration *s*, $(\overline{w's'})_t$ is the un-attenuated scalar flux or expected covariance between *w* and *s*, $\overline{u}$ is the average horizontal wind speed at the measurement height *z*, τ_c is the characteristic time constant of the EC system, α is a stability dependent constant (α = 7/8 for neutral and unstable stratification, $z/L \leq 0$, and α = 1 for stable stratification, $z/L > 0$), *L* is the Obukhov length, and n_m is the dimensionless frequency at which the logarithmic cospectrum attains its maximum value. Values of n_m for different conditions of atmospheric stability were estimated using the parameterization proposed by Horst (1997). The time constant τ_c is a function of the transfer function cut-off frequency, which was determined following Ibrom et al. (2007).

2.3.4. Flux Footprint calculation

The upwind distance from the flux tower for a given fraction of the source area contributing to the total flux was estimated using the analytical footprint model proposed by Kormann and Meixner (2001). This model is based on the solution of the two-dimensional advection and power law profiles of mean horizontal wind velocity and eddy diffusivity. This

simple analytical model is numerically robust and has a reasonable computational time when applied to long-term datasets, as in our study. In addition, the Kormann and Meixner (2001) footprint model has shown good agreement with estimates provided by Lagrangian Stochastic models (Kljun et al., 2003). Following Kormann and Meixner (2001), the cross-wind integrated flux (F_x) at the downwind distance ($x > 0$) from the flux tower is given by:

$$F_x = \frac{1}{\Gamma(\mu)} \frac{\xi^{\mu}}{x^{1+\mu}} e^{-\xi/x} \tag{2.4}$$

where ξ is a flux length scale, μ is a dimensionless model constant and $\Gamma(\mu)$ is the gamma function. In this study, Eq. 2.4 was used to estimate x for which the cumulative F_x equals the fraction of the flux contribution of interest (e.g. 70%). The upwind distance, x was calculated for each half hour and combined with wind direction values to assist with the interpretation of the temporal and spatial variabilities of fluxes at the feedlot.

The flux length scale ξ is given by:

$$\xi = \frac{Uz^r}{r^2 \kappa} \tag{2.5}$$

where U and κ are proportionality constants in the power-law profile of the wind velocity and r is the so-called shape factor. The calculation of ξ was performed following the procedure described by Kormann and Meixner (2001) that requires the use of wind velocity, the Obukhov length and the displacement height. The displacement height was determined to be 0.65 m and was calculated using the formulation for sparse plant canopies applied by Baum et al. (2008) for the same feedlot of this study.

2.4. Results and Discussion

2.4.1. Flux data quality control and atmospheric conditions

During the experimental period, power outages and instrument malfunction resulted in the loss of 5% of the 30-min data. In addition, approximately 4% of open-path system data were excluded due to the accumulation of dust particles and water on the open-path analyzer windows. Regular cleaning of the open-path system window may have limited the data gap.

The remaining half-hourly flux data were screened using the quality control protocol developed by Foken et al. (2004) to test for the development of turbulence and steady state conditions suitable for flux measurements. Using this system, each half-hour period was assigned a quality grade ranging from 1 (best) to 9 (poorest). Foken et al. (2004) recommended the use of flag values smaller than 7 for continuously running EC systems. In our study, we used a slightly stricter criterion excluding flux values associated with quality flags greater than 5 as well as when more than 10% of data points were missing for a given 30-min interval. By using this criterion, 12, 22, and 19% of half-hourly fluxes of CO_2, CH_4, and H_2O, respectively, for the closed-path EC system were excluded from our analysis. The same criterion removed approximately 13% of CO_2 and H_2O half hourly flux data measured by the open-path EC system.

The time lag values for CO_2 and CH_4 were very similar and ranged from 4.5 s to 4.7 s. The small variation in time lag values shows that the flow rate in the closed-path system sampling line was quite constant. For the water vapor, the average time lag was 5.3 s. The greater lag time for H_2O of 5.3 s implies interaction of H_2O with the sampling tube walls. The average horizontal wind velocity during the experimental period was 4.9 m/s, with prevailing southerly winds greater than 5 m/s being observed in 40% of the time intervals (Fig. 2.1). The atmospheric stability conditions at the feedlot during the study period were near neutral ($|L| > 100$), unstable ($-100 < L < 0$), and stable ($0 < L < 100$) for 54, 26, and 19% of the time periods,

respectively. These prevailing near-neutral conditions at the experimental site are due to the high horizontal wind speeds, low surface heating during the winter months, and the presence of urine and fecal matter on the pen surface, keeping the pen surfaces wet, even during dry and hot days (Baum et al., 2008).

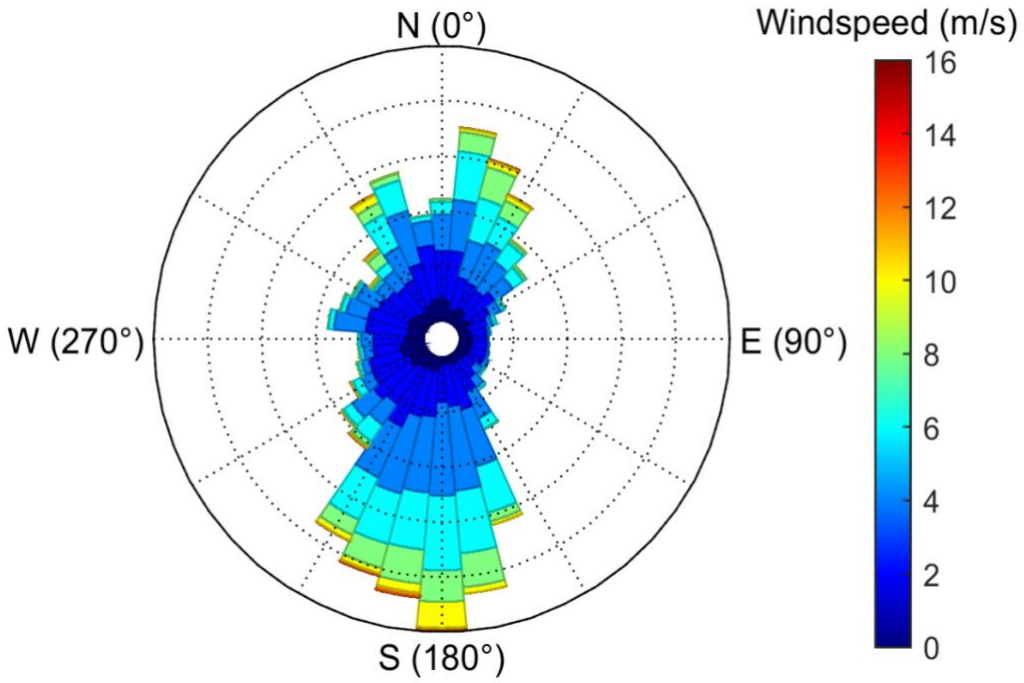

Figure 2.1. Frequency distribution of wind direction (North = 0º, East =90º) and average wind speed during the experimental period**.**

2.4.2. Density corrections

The closed-path analyzer outputs the gas concentrations for CO_2 and CH_4 in molar density and mixing ratios (χ, number of moles gas per mole dry air). Molar density values of CO_2 (ρ_c) and CH_4 (ρ_m) are converted into mixing ratios of CO_2 (χ_c) and CH_4 (χ_m) using high frequency measurements of water vapor mixing ratio and the following quadratic polynomial functions (Chen et al., 2010):

$$\frac{\rho_c}{\chi_c} = 1 + a\chi_v + b\chi_v^2 \quad (2.6)$$

$$\frac{\rho_m}{\chi_m} = 1 + c\chi_v + d\chi_v^2 \quad (2.7)$$

where χ_v is the water vapor mixing ratio reported by the closed-path analyzer at 10 Hz, a = -0.012, b = -2.674 x 10^{-4}, c = -0.00982, and d = -2.393 x 10^{-4} are adjusted coefficients for Eq. 2.6 and 2.7, derived from laboratory experiments.

The use of mixing ratios, obtained from Eq. 2.6 and 2.7, for flux calculations theoretically eliminates the need for density corrections for the closed-path analyzer flux calculations. To evaluate the performance of this approach, we applied the procedure proposed by Burba et al. (2012) to correct fluxes calculated using molar densities given by the closed-path analyzer. The effects of water vapor and temperature fluctuations on trace gas fluxes are expected to be proportionally higher when the magnitude of the trace gas flux of interest is low and when the latent heat flux is high (Eq. 2.1). For our closed-path system, with a relatively long sampling tube and a temperature-controlled sampling cell, the effect of temperature fluctuations on flux measurements is expected to be negligible. For this analysis, we selected periods in which the area sampled by the flux tower was located outside the feedlot, so that density corrections are expected be large with respect to the CH_4 fluxes.

The relationships between the latent heat flux and CH_4 fluxes, corrected and uncorrected for density effects, are shown in Fig. 2.2. The non-density corrected CH_4 fluxes became more negative as the magnitude of latent heat flux increased. This apparent CH_4 uptake by the surface is a result of fluctuations in CH_4 concentration caused by fluctuations in air humidity that are not associated with the turbulent transport. Thus, density corrections were applied to the CH_4 fluxes. The average CH_4 fluxes were -0.0055 µmol m^{-2} s^{-1} for non-density corrected fluxes, and equal to -0.0028 µmol m^{-2} s^{-1} and -0.0023 µmol m^{-2} s^{-1} for corrected fluxes following Burba et al. (2012) and the analyzer reported mixing ratio (Chen et al., 2010), respectively. A t-test showed that the

slopes for the relationships between latent heat and CH_4 fluxes (Fig. 2.2), corrected using the two density correction methods were not significant at a 5% probability level. This indicates that the use of the analyzer reported mixing ratios eliminates the need of density corrections.

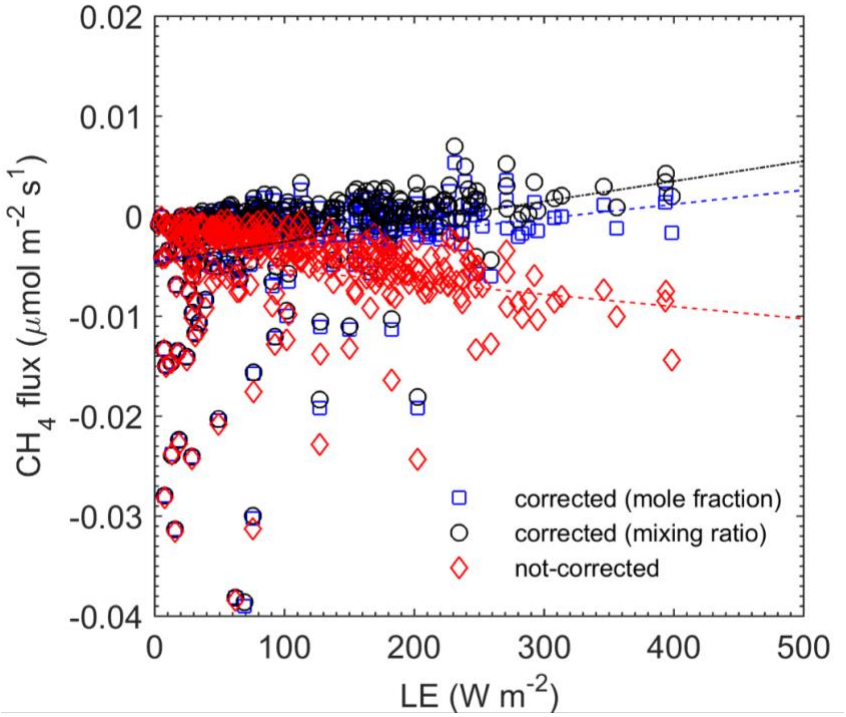

Figure 2.2. Relationship between the latent heat flux (LE) and corrected and uncorrected CH_4 fluxes for air density effects. The air density effects were corrected using the close-path analyzer internal algorithm to estimate the CH_4 mixing ratio (circles) and the method proposed by Burba et al. (2012) to correct fluxes calculated using the mole fraction (squares). The non-corrected values are represented by the diamond symbol. Dashed lines represent regression lines for uncorrected fluxes (red line), corrected using the closed-path internal algorithm (black line) and calculated using the mole fraction (blue line). For these analyzes, only small CH_4 fluxes associated with northerly wind directions were selected.

2.4.3. Spectral corrections

The ensemble-averaged cospectra, computed for midday (12:00 – 15:00 h) over the entire study period, were used to investigate closed-path and open-path analyzers' frequency responses (Fig. 2.3). The sensible heat cospectrum was used as a reference since it is expected to closely follow the cospectrum theoretical predictions when measured at a suitable height under well-

developed turbulence conditions (Kaimal et al., 1972). Comparisons with the sensible heat, obtained from the sonic anemometer, and CO_2 and H_2O, measured using a well-established open-path analyzer (LI-7500), were used to evaluate the ability of the closed-path system to measure signals at different frequencies responsible for scalar turbulent transport.

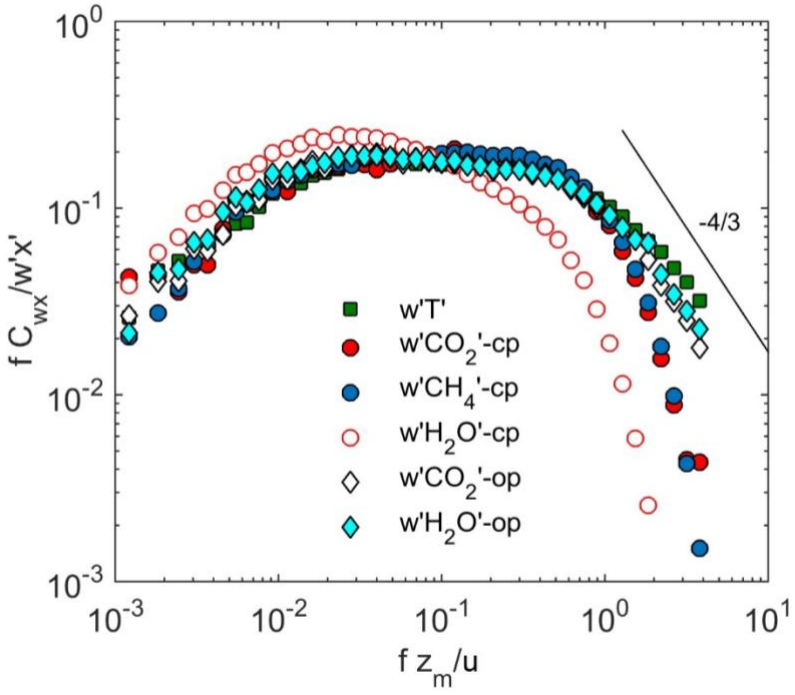

Figure 2.3. Normalized cospectra of vertical wind velocity (w) with sonic anemometer temperature (T_a), CO_2, CH_4 and H_2O calculated using half hourly periods from 12-15 h during the experimental period. The symbols op and cp denote open-path and closed-path EC systems, respectively, and f is the frequency, z_m is the measurement height and u is the horizontal wind speed.

The sensible heat flux cospectrum was slightly less negative than the theoretical slope (-4/3) for the inertial subrange (Kaimal et al., 1972), which has also been previously observed (Baum et al.; 2008) and confirms that the sensible heat flux cospectrum is a suitable reference to evaluate the flux losses for other gases (Fig. 2.3). The ensemble-averaged cospectra for all gas species showed different degrees of frequency attenuation at the inertial sub-range. For the closed-path system, the CH_4, CO_2, and H_2O cospectra showed steeper slopes at the higher

frequency band (normalized frequency > 1) when compared to CO_2 and H_2O cospectra, measured using the open-path EC system. The ensemble-averaged CH_4 cospectrum was noisier than the other gas curves at the higher frequency end. With the exception of the water vapor closed-path system cospectra, the extent of attenuation was minimal at low frequencies, given the good agreement between the curves at the low frequency band.

The frequency attenuations for the close-path system in this study are in agreement with results from previous comparison studies of CH_4 analyzers (Detto et al., 2011; Peltola et al., 2013). High frequency losses are inherent to closed-path systems and caused by the presence of the sampling line and air filters. For the water vapor, more severe attenuations are mostly likely a result of water vapor molecule interaction with the tubing walls. The EC fluxes were corrected for spectral losses following Horst (1997). The averaged spectral correction factors were: 1.17 for the OP analyzer (CO_2 and H_2O), and 1.22 for CH_4, 1.23 for CO_2 from closed-path system, which are close to the range reported in previous studies by Detto et al. (2011), Haslwanter et al. (2009). However, a much higher spectral correction factor (2.06) was found for the H_2O flux measured using the closed-path system. Our cospectral analysis suggests that the closed-path system was capable of reasonably measuring CO_2 and CH_4 concentrations for the entire spectrum of frequencies.

2.4.4. Random error uncertainties

Trace gas flux measurements using the EC technique are prone to random uncertainty errors resulting from instrument errors, changes in flux footprint and the stochastic nature of the turbulence (Finkelstein and Sims, 2001). The random uncertainty error was calculated following the approach by Finkelstein and Sims (2001), which estimates variance of the calculated covariance.

The results of this analysis were expressed in terms of distribution of the normalized absolute value of flux error following Peltola et al. (2013) for both the open-path and closed-path EC systems (Fig. 2.4). All distribution curves were skewed to the left and peaked at low values (0.02-0.03) of fractional flux error. Both closed-path and open-path EC systems showed similar random error uncertainty distribution. The cumulative frequency of occurrence is shown on the right panel of Fig. 2.4. Approximately 85% of the half-hourly flux values had a random error smaller than 7%. These observations further suggest that the closed-path EC system performed well at the feedlot.

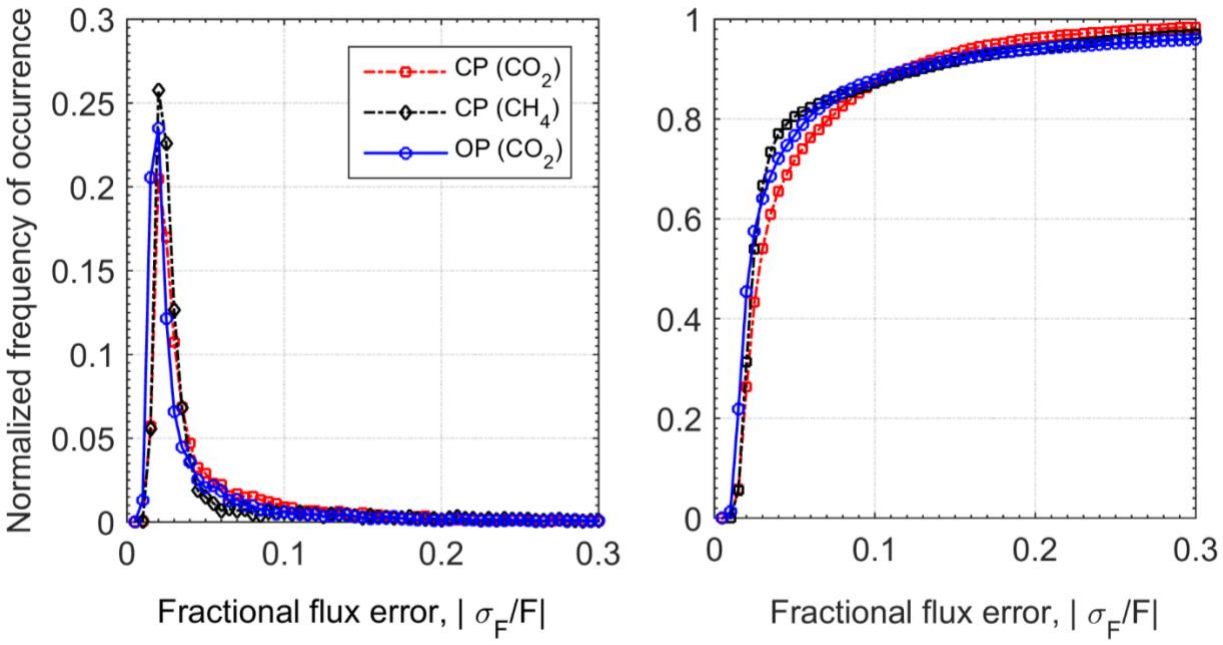

Figure 2.4. Distribution curves of absolute value of fractional flux error ($|\sigma_F / F|$) (left plot), and cumulative sums of relative frequency of occurrence of respective flux (right plot). CP denotes close-path eddy covariance system and OP denotes open-path eddy covariance system.

2.4.5. Open-path and closed-path flux comparisons

Fig 2.5 shows the comparisons between CO_2 and H_2O fluxes estimated using the closed-path and open-path EC systems. The regression of CO_2 against H_2O (Fig. 2.5) for closed-path

and open-path EC systems gave R^2 values of 0.94 and 0.98, respectively. The closed-path EC system overestimated CO_2 flux by 5% and underestimated latent heat fluxes by 10% when compared with the open-path system measurements (Fig. 2-5).

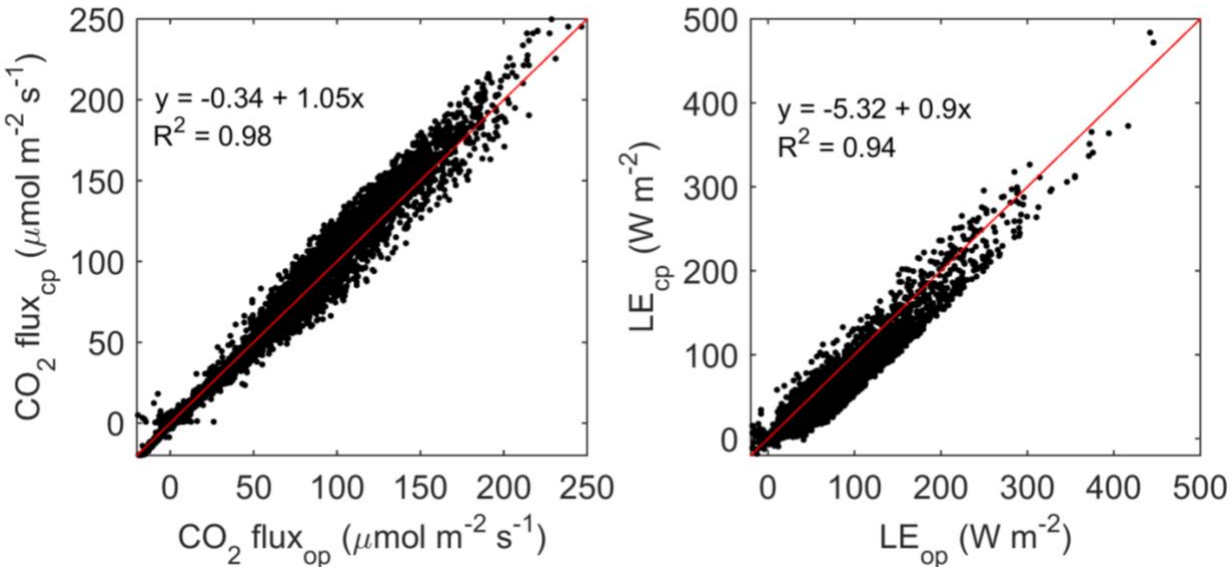

Figure. 2.5. Comparisons between a) CO_2 (left) and b) latent heat fluxes (LE, right), obtained using two different EC systems: closed-path (cp) and open-path (op) systems. Data on the graphs are half-hourly fluxes from August 2013 – May 2014, which were screened using the method proposed by Foken et al. (2004).

A paired t-test showed that closed-path and open-path CO_2 fluxes differences were not significant at a 5% probability level, but the same test indicated that the latent heat fluxes measured by open-path and closed-path EC system were statistically different.

The good agreement between the measurements of open-path and closed-path EC systems indicates that the closed-path EC system is suitable to measure fluxes of passive gases, such as CO_2 and CH_4. However, measurements of water vapor fluxes using closed-path EC systems are more challenging. In the present study, we observed strong dampening of the water vapor signal in the closed-path system (Fig. 2.3). That signal attenuation by the sampling line is likely to be the main reason for flux underestimations. Physical adsorption and desorption of water vapor by

dust particles in the short (~50 cm) stainless tubing located upstream of the air filter, as well as within the walls of the sampling tube, and filters were likely to attenuate the high frequency concentration fluctuations. In future studies, the length of the air intake tubing (between rain diverter and air filter) should be shortened to minimize the accumulation of dust and water vapor adsorption in this section of the sampling line. Furthermore, other hydrophobic tubing materials, such as Teflon and Synflex tubing, and other types of air filters (e.g. Vortex air cleaner, Campbell Sci.) could be an option to improve frequency responses for active gases such as NH_3 and H_2O measured by closed-path EC systems.

Considering the underestimation of the latent heat flux by the closed-path EC system, we hereafter used the latent heat flux provided by the open-path EC system to evaluate the temporal and spatial variability of fluxes at the feedlot. Despite these issues with the water vapor flux measurements, our spectral analysis and instrument comparisons indicate that the closed-path EC system is appropriate for measuring CO_2 and CH_4 fluxes in long-term studies.

2.4.6. Flux temporal and spatial variability

Half-hourly EC measurements of CH_4, CO_2, latent heat and sensible heat fluxes for the entire experimental period are shown in Fig. 2.6. The large data gaps in Fig. 2.6 were the result of equipment malfunctions and power outages. The latent and heat fluxes showed a clear diel and seasonal variation that was related to changes in the availability of solar radiation at the experimental site (Fig. 2.6 top panels). On the other hand, the fluxes of CH_4 and CO_2 showed large temporal variability (Fig. 6 bottom panels). Higher values of CH_4 and CO_2 fluxes were observed for the months of September and October. The average CH_4 and CO_2 fluxes were equal to 2.63 μmol m^{-2} s^{-1} and 103.8 μmol m^{-2} s^{-1}, respectively, for wind directions ranging from 120º to 240º, assumed to characterize fluxes originated from the feedlot. The magnitude of these

fluxes are in agreement with the range of values (1.5 - 4.6 μmol m^{-2} s^{-1}) reported for CH_4 fluxes by Sun et al. (2015) and for CO_2 fluxes (124.6 – 374.1 μmol m^{-2} s^{-1}) by Baum et al. (2008) in their respective feedlot studies. In contrast, the average CH_4 and CO_2 fluxes were: 0.032 μmol m^{-2} s^{-1} and 0.63 μmol m^{-2} s^{-1}, respectively, for wind directions ranging from 300° to 60°, which are expected to characterize fluxes originating from the agricultural fields at the north edge of the feedlot. These results show that the feedlot and surrounding fields have very distinct CH_4 and CO_2 source strengths.

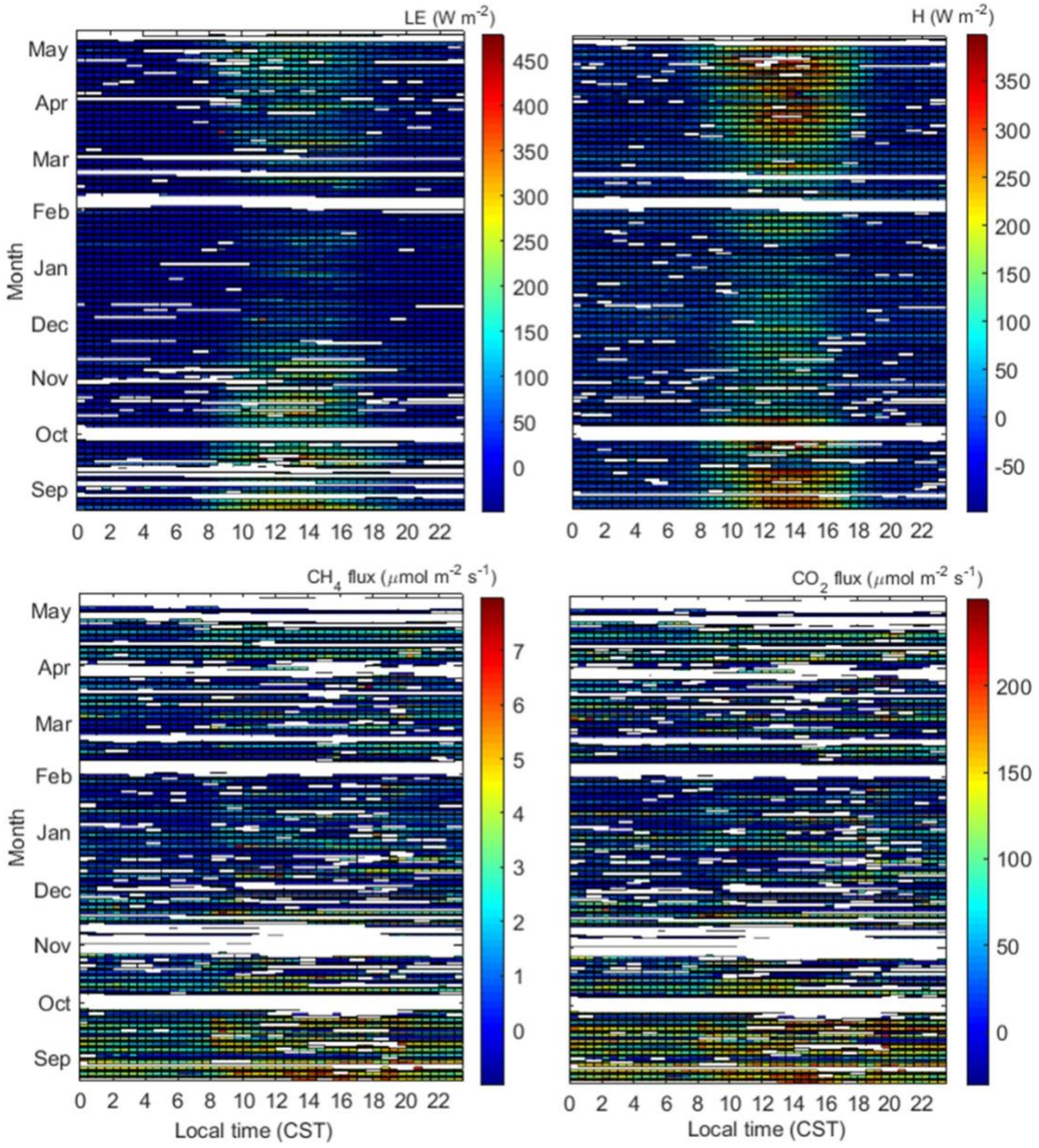

Figure 2.6. Diurnal and seasonal variation of CH_4 flux (top left), CO_2 (top right), latent heat (LE) (bottom left), and sensible heat (bottom right) fluxes during the experimental period.

The ensemble average half-hourly CO_2 and CH_4 fluxes for wind directions ranging from 120º to 240º, assumed to characterize feedlot fluxes, are shown in Fig. 2.7. Lower values for CH_4 and CO_2 fluxes were observed at night and in the morning while the higher values were observed during the daytime. Sun et al. (2015) used the EC technique to measure gas emissions from a beef cattle feedlot in Colorado. Their ensemble diel CO_2 and CH_4 fluxes showed smaller

variation throughout the day when compared to their composite diel sensible and latent heat fluxes. They reported maximum CH_4 fluxes in the late afternoon and evening.

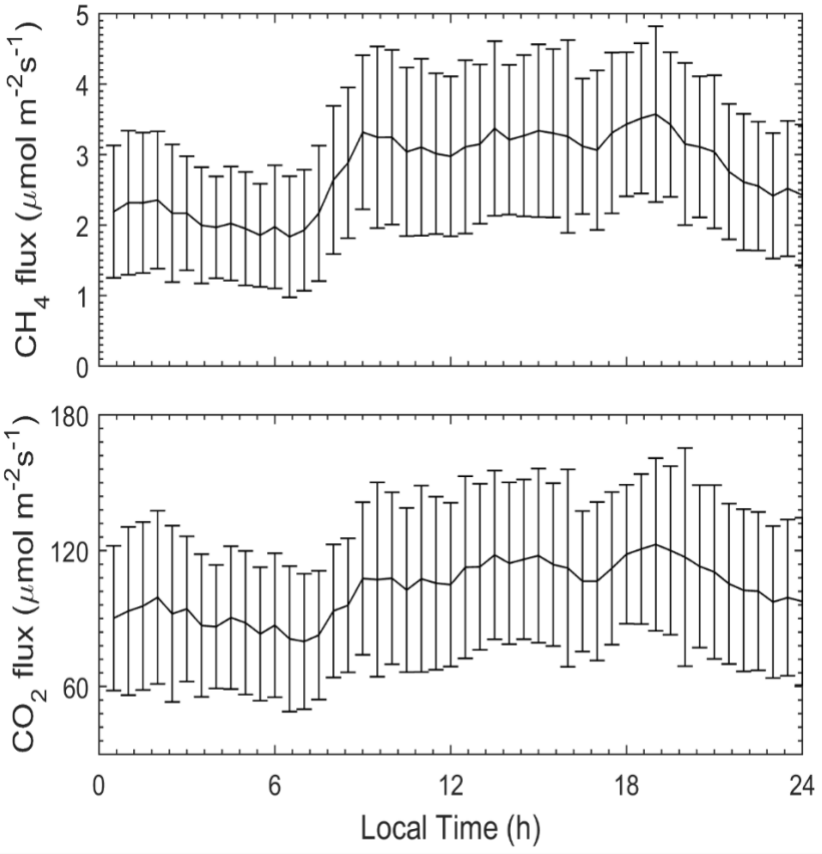

Figure 2.7. Daily ensemble average CO_2 and CH_4 fluxes at the study site. Half-hourly fluxes were averaged from August 2013 – May 2014 and screening the data for wind directions ranging from 120º to 240º to include gas emissions originating mostly from the feedlot surface.

A similar daily pattern for CO_2 fluxes was observed by Baum et al. (2008) for a beef cattle feedlot in Kansas. Our daily ensemble average CO_2 and CH_4 fluxes did not show a distinct peak in the later afternoon and evening as reported in those previous studies. The discrepancies between our results and the ones from previous studies could be related to two factors: 1) differences in management practices among the feedlots, which may affect animal behavior and the temporal dynamics of CO_2 and CH_4 emitted by the cattle; and 2) changes in the source area sampled by the flux tower caused by environmental conditions at the site. To investigate the

latter hypothesis, we utilized an analytical footprint model (Kormann and Meixner, 2001), described in section 3.3.3.1, to estimate the upwind distance from the sonic anemometer contributing to 70% of the total fluxes (x_{70}), following previous feedlot studies (Baum et al., 2008; Sun et al., 2015).

The estimated values for x_{70} for day and night periods are shown in Fig. 2.8. This average distance was 199 m and 352 m for the day and nighttime, respectively. These differences in x_{70} between day and night can be explained by the conditions of atmospheric stability. Under stable atmospheric conditions, often common during the nighttime, the flux footprint stretches over a large distance.

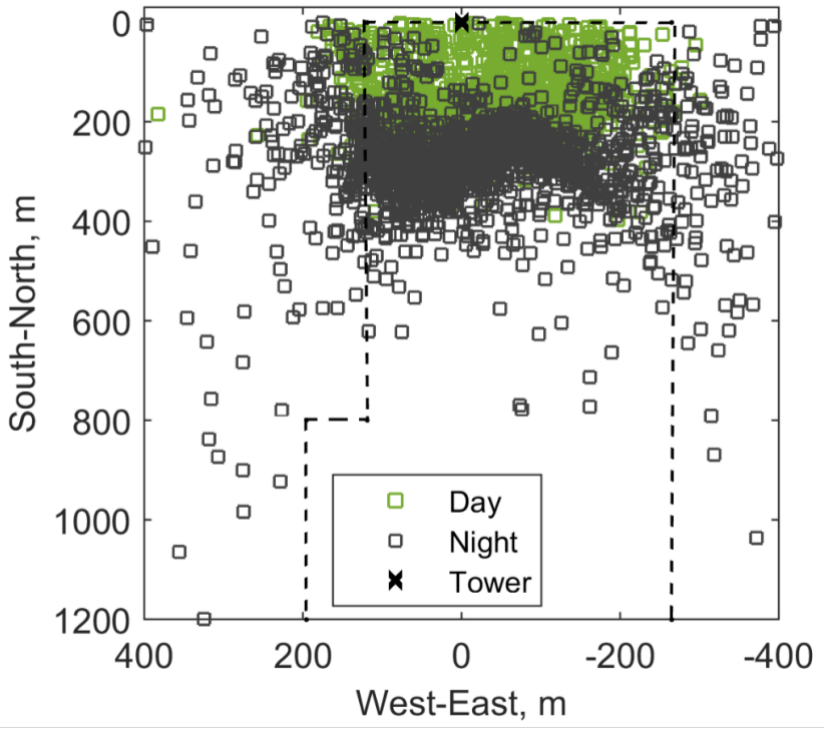

Figure 2.8. Upwind distance from the flux tower contributing to 70% of total flux, estimated using an analytical footprint analysis (Kormann and Meixner, 2001) during day time and night time. Only half hourly periods with wind directions ranging from 90° to 270° were included in this analysis. The dotted line indicates the boundary of the feedlot.

In contrast, during daytime, solar radiation warms the surface of the feedlot making the

atmosphere unstable and convective, resulting in upward motion of scalars that also travel over a short distance (Eugster and Merbold, 2015).

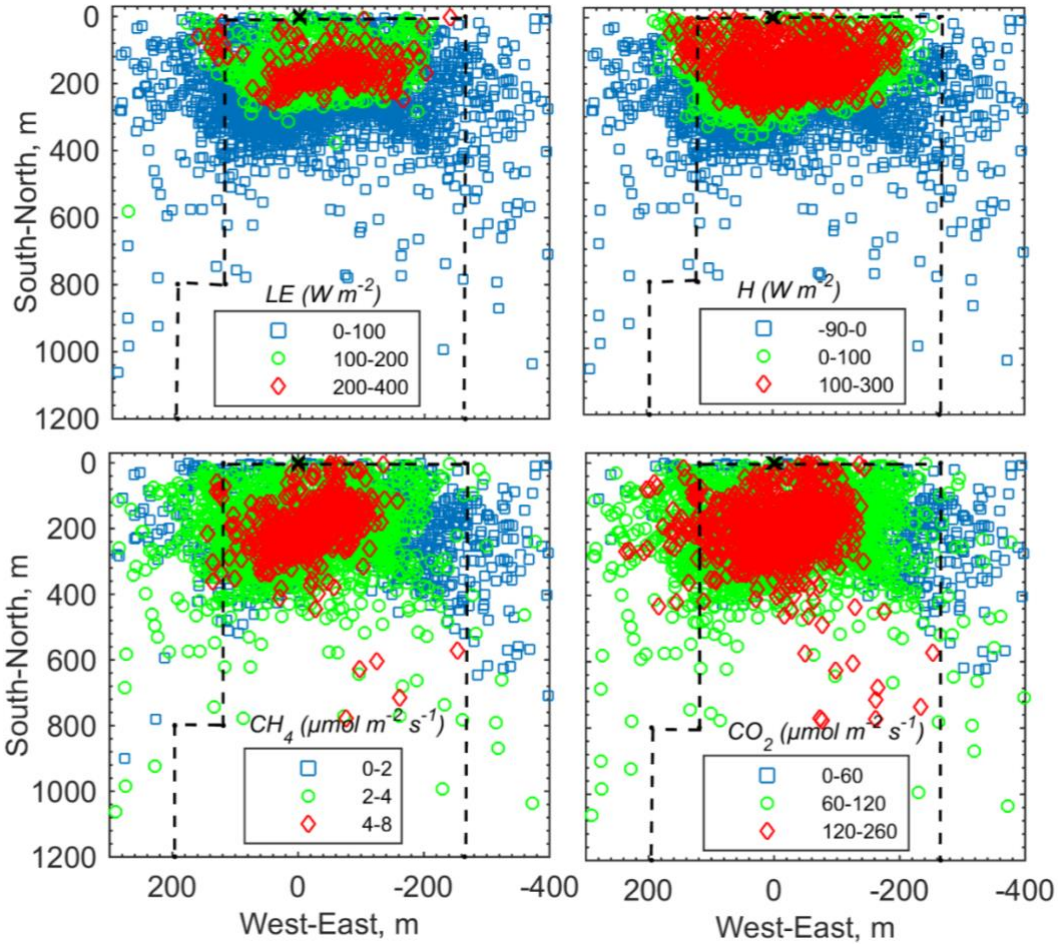

Figure 2.9. Spatial distribution of 30 min latent heat (LE), sensible heat (H), CH_4 and CO_2 fluxes in the feedlot during the experimental period. The flux data associated with the footprint distance contributing to 70% of the total flux (Kormann and Meixner, 2001) and wind direction values were grouped in different classes of flux values to investigate the spatial variability of fluxes.

The spatial variation of scalar fluxes was investigated using polar plots of wind direction and footprint distance, expressed by x_{70}, and by grouping scalar fluxes into classes with different magnitudes. All scalar fluxes showed a similar spatial pattern (Fig. 2.9). In general, higher latent and sensible heat fluxes were associated with x_{70} smaller than 300 m. These higher fluxes were

observed during the daytime under convective conditions. Methane and CO_2 fluxes showed a similar spatial variability, with maximum values of fluxes observed for $x_{70} \approx 200$ m and southerly winds. As the wind shifted to eastern and western sectors, flux magnitude tended to decrease, which is explained by the increase of contributions from areas outside the feedlot to eddy fluxes. Higher CO_2 and CH_4 fluxes on the southwest side were likely due to emissions from a manure storage lagoon located at the west side of the feedlot.

Furthermore, as x_{70} increases CO_2 and CH_4 fluxes are more likely to be diluted by non-emitting surfaces within the feedlot. Approximately 28% of the feedlot area is composed of alleys and roads that are used for cattle movement and feed delivery. These sections of the feedlot are expected to have negligible CO_2 and CH_4 emissions, given that animal metabolic processes were the main source of CO_2 and CH_4 at the feedlot. Fluxes that originated from areas further from the tower were likely to be diluted by those surfaces. Baum et al. (2008) combined estimates given by a one-dimensional analytical footprint model and the map with pens and non-pen surfaces, to investigate the impact of changes in the flux tower footprint on their CO_2 flux EC measurements. They found similar effects of non-pen surfaces on the flux calculation. Their raw CO_2 fluxes typically increased by 11% when the bias caused by non-emitting surfaces (roads and alleys) was removed from their raw flux measurements. However, under easterly wind conditions, their correction factor was as much as 31% of the raw fluxes due to a larger proportion of roads and alleys in the flux footprint.

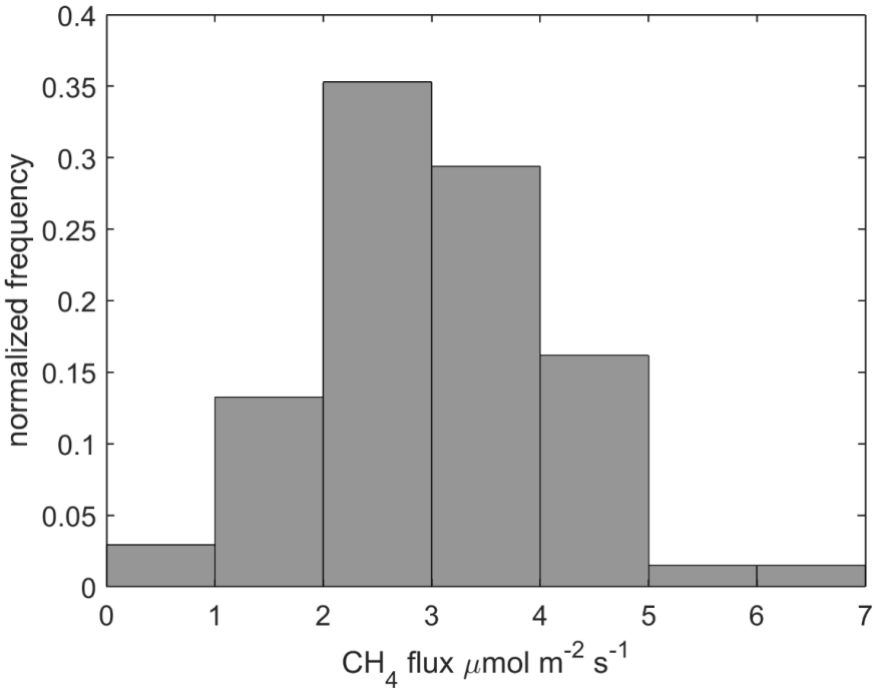

Figure 2.10. Frequency distribution of the CH_4 fluxes obtained from pens closer to the flux tower. CH_4 fluxes displayed in this graph were associated with the footprint distance contributing to 70% of the total flux (Kormann and Meixner, 2001) and wind direction values raging from 165° to 205° to minimize the effect road, alleys and other non-emitting surfaces on CH_4 fluxes.

To investigate the variability of the CH_4 fluxes within the pens, we screened the CH_4 flux data based on x_{70} (< 150m) and wind direction (175° < wind dir. > 195°). By using this screening criterion, we ensured that most of the contributions to the total CH_4 flux originated from the two pens closest to the flux tower, minimizing the dilution effects from non-emitting surfaces on the CH_4 fluxes. However, results from this analysis still show large variation in fluxes values, with CH_4 flux values ranging from 0.82 to 6.2 μmol m^{-2} s^{-1} (Fig. 2.10). Several factors could have affected the variability of CH_4 fluxes within the pens, such as: 1) changes in stocking rate in the pens, 2) variations in animal diet, 3) increase in CH_4 production in the pen surface by soil microbes during wet periods and 4) changes in animal position. In this feedlot there was a small reduction in the stocking rate (10-15%) during the winter months (*feedlot manager, personal*

communication) and animals from some pens were also replaced, which could account for some long-term flux variability. However, there were no major changes in nutrient content of the diet (data not shown). During the dry cold season, the CH_4 emissions from pen surfaces are expected to be small in comparison with animal emissions. Changes in animal position seems to be the major reason for the short-term CH_4 flux variability in this study.

Animal movement imposes additional challenges to EC measurements of CH_4 emissions from ruminants by creating heterogeneities in the source surface and uncertainties in flux measurements. The effect of animal movement in free grazing systems on CH_4 flux measurements has been investigated in recent studies (Baldocchi et al., 2012; Dengel et al., 2011; Felber et al., 2015; Laubach et al., 2013; McGinn et al., 2011). Laubach et al. (2013) measured CH_4 emissions from a herd of cattle using the external tracer technique and two micrometeorological approaches: an inverse dispersion model and a mass balance technique. Their results show that the discrepancies between the mass balance approach and the tracer technique could be explained by uneven animal distribution in the pasture. Felber et al. (2015) used the EC technique combined with a footprint analysis and individual animal position, recorded by GPS units, to estimate CH_4 emissions from dairy cows grazing in paddocks. Their results show that for their grazing system, the inclusion of the position of each animal did not lead to substantial differences in flux estimates per head when compared to similar estimates obtained using only the paddock occupational time. Feedlots have a higher stocking rate than grazing systems which could contribute to a more even flux source area. However, during this experiment, we observed that the cattle in the feedlot gathered near the feed bunks during feeding times leaving the center of the pen nearly empty. In addition, under cold conditions, animals tended to gather in one of the pen corners to minimize heat exchange with the

environment. Hence, consideration of animal movement could be important in a confined animal system like a feedlot. In depth investigation of the influence animal positions have on EC measurements is out of the scope of this study but will be addressed in next chapter.

2.5. Conclusions

The performance assessment of the closed-path EC system showed that this system was suitable for EC measurements. The frequency attenuations, observed for the close-path system CO_2 and CH_4 cospectra in this study, are in agreement with results from previous studies. For the water vapor closed-path cospectra, larger attenuations were most likely caused by water vapor molecule interaction with the tubing walls. Values of R^2 for the relationship between H_2O and CO_2 fluxes, measured by open-path and closed-path systems, were 0.94 to 0.98, respectively. The closed-path EC system overestimated the CO_2 by approximately 5% and underestimated the latent heat fluxes by about 10% when compared with the open-path system measurements. In a dusty environment, such as the feedlot in our study, closed-path EC gas analyzers are likely to result in better data retention compared to narrow-band open-path EC analyzers, which are sensitive to the deposition of particulate matter on the sensor window.

Average fluxes of CH_4 and CO_2 from the feedlot were 2.63 μmol m^{-2} s^{-1} and 103.8 μmol m^{-2} s^{-1}, respectively, during the study period. These emission rates were in agreement with other reported studies using micrometeorological methods in feedlots. In general, the flux densities were higher in the pens near the tower under stable conditions, but were lower as the source distance increased under stable conditions, probably due to the dilution effect from road and alleys. However, highly variable flux densities were observed near the tower, which could be related to changes in source strength and homogeneity, caused by for example, animal

movement.

This study shows further indication that consideration of atmospheric stability condition, wind direction and animal movement are important to improve the measurement of animal emissions in a feedlot using the EC technique. Additional work is necessary to investigate how heterogeneities in the source area and animal movement affect the flux measurements at the feedlot.

Chapter 3 - Estimating methane emissions from beef cattle in a feedlot using the eddy covariance technique and footprint analysis

3.1. Abstract

Measurements of CH_4 emissions from cattle could provide invaluable data to reduce uncertainties in the global CH_4 budget and to evaluate mitigation strategies to lower greenhouse gas emissions. The EC technique has recently been applied as an alternative to measure CH_4 emissions from livestock systems, but heterogeneities in the source area and fetch limitations impose challenges to EC measurements. The main objective of this study was to estimate CH_4 emissions rates per pen surface (F_{pens}) and per animal (F_{animal}) from a beef cattle feedlot using the EC technique combined with two footprint models: an analytical footprint model (KM01) and a parametrization of a Lagrangian dispersion model (FFP). Fluxes of CH_4 were measured using a closed-path EC system in a commercial feedlot. The footprint models were used to investigate fetch requirements and to estimate F_{pens} and F_{animal}. The aggregated footprint area predicted by KM01 was 5 to 6 times larger than FFP estimates. On average, F_{pens} was 8 (FFP) to 14% (KM01) higher than the raw EC flux, but differences between F_{pens} and EC flux varied substantially depending on the location and size of the flux footprint. The monthly average F_{animal}, calculated using F_{pens} and the footprint weighed stocking density, ranged from 83 to 125 g animal^{-1} d^{-1} (KM01) and 75 to 114 g animal^{-1} d^{-1} (FFP). The emission values are consistent with the results from previous studies in feedlots. These results suggest that the EC technique can be combined with footprint analysis to estimate gas emissions from livestock systems.

3.2. Introduction

Enteric fermentation and manure management are major agricultural sources of CH_4 and account for about one third of the total CH_4 emissions from anthropogenic activities in the United States (EPA, 2017). Beef and dairy cattle production systems are estimated to account for about 71% and 25%, of enteric CH_4 emissions in the US, respectively (EPA, 2017). Accurate measurements of CH_4 emissions from livestock are necessary to reduce uncertainties in the CH_4 global budget and to identify appropriate mitigation strategies to reduce greenhouse gas (GHG) emissions from agriculture.

Micrometeorological techniques have been used to measure GHG from livestock production systems (Bai et al., 2015; Flesch et al., 2007; Laubach et al., 2013; McGinn, 2013). These techniques are non-intrusive and integrate fluxes over large areas, which minimizes flux uncertainties due to source heterogeneities commonly observed in livestock systems (Harper et al., 2011). In addition, micrometeorological approaches provide flux measurements at a high temporal resolution (< 1 hour) over extended periods of time (months to years) which is required to improve the understanding of the mechanisms controlling GHG emissions from livestock and to improve whole-farm GHG models.

The eddy covariance (EC) technique has been the standard micrometeorological method to measure fluxes of CO_2 and energy in ecosystems around the world (Baldocchi, 2008). Recently, with the development of new optical sensors, the EC method has been also used to measure the fluxes of other trace gases such as CH_4, ammonia (NH_3) and nitrous oxide (N_2O) (Baldocchi et al., 2012; Famulari et al., 2010; Peltola et al., 2013; Sun et al., 2015) . The major challenges for applying the EC technique to measure GHG emissions from livestock systems are: 1) fetch limitations and 2) heterogeneity of the underlying source area (Baum et al., 2008; Felber

et al., 2015; Prajapati and Santos, 2018b; Sun et al., 2015). Baum et al. (2008) used the EC technique to measure CO_2 and energy fluxes from a beef cattle feedlot in Kansas. They showed systematic errors were introduced in their CO_2 flux measurements by fetch limitations as well as by the presence of weak CO_2 source areas (roads and alleys) within the feedlot. These challenges need to be addressed to improve the accuracy of GHG emission measurements from livestock systems using the EC technique. Furthermore, EC measurements of GHG emissions from livestock systems usually integrate contributions from different source areas, e.g. in a feedlot, fluxes can be a result of contributions from different surfaces: pens, lagoons, alleys and roads. Integrated flux measurements from different GHG sources at the farm level can provide useful datasets to validate whole-farm GHG models (Crosson et al., 2011; Taylor et al., 2017) but for other applications, such as dietary studies, GHG inventories and regulatory purposes, GHG emissions are usually expressed as fluxes per source unit, e.g.: CH_4 emissions per head of cattle and N_2O fluxes per paddock surface.

Footprint models have been used for about three decades to investigate the effect of the underlying surface on point flux measurements (Gash, 1986; Leclerc and Thurtell, 1990; Schmid and Oke, 1990; Schuepp et al., 1990). In livestock systems, footprint models have been applied to study the effect of source area heterogeneities on EC flux measurements and to scale EC measurements per unit of source area (Baum et al., 2008; Dengel et al., 2011; Felber et al., 2015). Baum et al. (2008) aggregated the results from a one-dimensional footprint model to determine the contributions from pen, road, and alley surface areas to EC flux measurements in a beef cattle feedlot. Felber et al. (2015) combined EC flux measurements, obtained from paddocks grazed by dairy cows, with an analytical footprint model and the location of the dairy cows to estimate the CH_4 emission rate per animal (F_{animal}). The analytical footprint models used

in those studies are attractive for their simplicity and computation speed which makes them suitable to estimate the flux footprint for long-term datasets (Leclerc and Foken, 2014). However, analytical footprint models are often limited to homogeneous surface layer similarity conditions and to some specific atmospheric stability conditions (Schmid, 2002). More complex models, such as backward Lagrangian models, can overcome some of those problems but are usually computationally expensive. Parameterized versions of complex models could retain some of the skills of the complex models while requiring less computer resources and time for simulations (Hsieh et al., 2000; Kljun et al., 2015; Schmid, 2002).

Currently, only a few studies in livestock systems have applied the EC technique with footprint models to estimate CH_4 emissions per animal (Dengel et al., 2011; Felber et al., 2015). Additional studies are necessary to investigate the performance of footprint models and the EC technique to estimate GHG emissions from different livestock production systems under a wide variety of atmospheric conditions. To our knowledge, this is the first study to apply this new methodology to estimate F_{animal} in an outdoor feedlot. Cattle feedlots are an important component of the beef cattle industry in North America. A total of 20.4 million heads of cattle were placed in feedlots for the slaughter market in 2015 (USDA, 2016).

The main objective of this study was to estimate CH_4 emissions from cattle in a feedlot using the EC technique combined with existing footprint models. The specific objectives of this study were to: 1) investigate the effect of fetch limitations and feedlot surface heterogeneities on EC CH_4 flux measurements and 2) estimate and compare the CH_4 emission rate per pen area and per animal from the feedlot using an analytical footprint model and the parameterized version of a Lagrangian stochastic particle dispersion model.

3.3. Material and Methods

3.3.1. Site description

Field measurements were carried out at a commercial beef cattle feedlot in Kansas from August 2013 to May 2014. The total monthly precipitation ranged from 7 to 83 mm and average monthly air temperature ranged from 2 to 26 ^{o}C (Fig. 3.1) in the nearby weather station located 6 km west from the site (National Climatic Data Center, 2017). The site is located at an elevation of 622 m above the sea level over a near flat terrain (slope < 5%). The feedlot has near rectangular shaped pens with a total surface area of approximately 59 ha surrounded by agricultural fields and a holding capacity of 30,000 head of cattle. Roads and alleys accounted for approximately 21% of the total feedlot surface area.

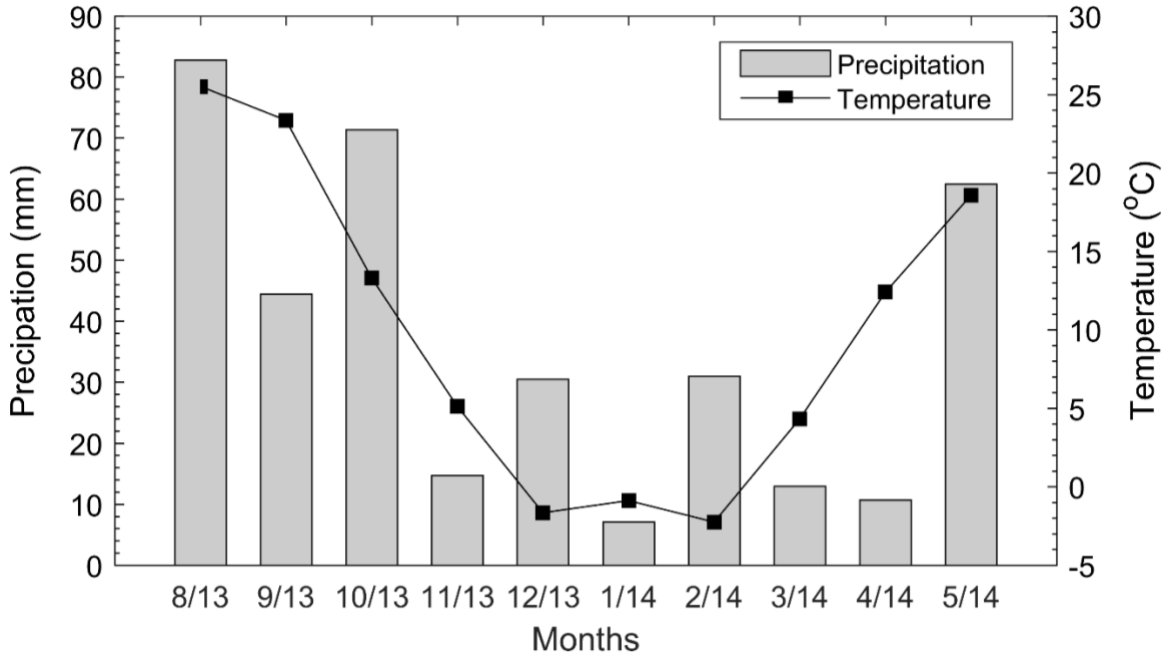

Figure 3.1. Monthly mean temperature and monthly total precipitation measured at a weather station near the feedlot from August 2013–May 2014.

The pens near the north edge of the feedlot were occupied by steers and heifers weighing 300-350 kg at the beginning of the experiment. In this feedlot, the cattle spent about three to six months, gaining 250-300 kg in weight. The average stocking density in the pens was 19 m^2

animal^{-1} (~526 animals ha^{-1}), with a total of 24,116 head of cattle during the summer and early fall months (August 2013 to November 2013). In the late fall and spring months (December to April), the number of animals was reduced by about 15% resulting in an average stocking density in the pens of 22 m^2 animal^{-1} (~455 animals ha^{-1}).

Ration samples from three pens immediately south of the flux tower were collected during the experiment on two different dates. The reason for the selection of those pens was that they were expected to contribute to the majority of the measured flux (section 3.4.2). The composition of the cattle ration is shown in Table 3.1. During the experiment, there were no substantial changes in the cattle ration (*feedlot manager personal communication*).

Table 3.1. Average composition ration on dry matter basis (DM) collected at the feed bunks of three pens immediately south from the flux tower in two dates (December 12, 2013 and January 14, 2014) during the experiment. Std denotes the mean standard deviation.

Parameters	(Mean ± 1 std)
	(% DM)
Crude Protein	15.9 ± 0.3
Acid detergent Fiber	9.2 ± 1.0
Crude Fiber	5.9 ± 0.6
Crude Fat	7.0 ± 0.1
Total Digestible Nutrients	90.5 ± 1.2
	(MJ/kg)
Net Energy, Maintenance	9.2 ± 0.09
Net Energy, Gain	6.4 ±0.09
Net Energy, Lactation	8.3 ±0.09
Digestible Energy	16.5 ±0.18
Metabolic. Energy, Beef	13.8 ±0.18

3.3.2. Flux measurements

A detailed description of the fluxes measurements is provided in chapter 2 (section 2.3.2), a summary of flux measurement and calculations are provided in this study for completeness. Fluxes of CH_4 were measured using the eddy covariance method. The wind velocity orthogonal

components were measured using a sonic anemometer (CSAT3, Campbell Sci., Logan, UT). A wavelength-scanned cavity ring-down spectroscopy closed-path gas analyzer (G2311-f, Picarro Inc., Santa Clara, CA) was used to measure CH_4, CO_2 and H_2O mixing ratios, but only CH_4 mixing ratio data were used for flux calculations in this study. The closed-path analyzer air intake consisted of a rain diverter connected to an inline filter (Polypropylene/polyethylene 10 µm membrane, Pall Corporation, AnnArbor, MI). The air was drawn from the intake through a 7-m long high-density polyethylene tube with an inner diameter of 5.3 mm to a second filter (Acrodisc Gelman 1µm, PTFE membrane, Pall corporation), which was connected to the closed-path analyzer inlet. A vacuum pump (MD 4 NT, Vacuubrand GmbH, Wertheim, Germany) drew air through the sampling tube. The flow rate was kept at 5 L min^{-1} by the closed-path analyzer's internal mass flow controller. The sampling line was heated using a heating cable to minimize the adsorption of water by the tube walls. Field calibrations were performed at least every two weeks using certified calibration tanks (Tank 1: CH_4 = 1.9 ppm and Tank 2: CH_4 = 4 ppm, ±1% accuracy, Matheson, Joliet, IL).

The sonic anemometer and closed-path analyzer air intake were set up on a tower at approximately 5 m above the ground. The closed-path analyzer air intake was positioned with a vertical separation of 8 cm, a northward separation of 18 cm and an eastward separation of 31 cm from the sonic anemometer. The flux tower was set up at the north edge of the feedlot with the sonic anemometer and the gas analyzer air intake oriented towards the south to maximize air flow over the source area within the feedlot and avoid potential air flow disturbances caused by buildings at the south edge of the feedlot. The signals of the sonic anemometer and closed-path gas analyzer were recorded at 10 Hz using a datalogger (CR1000, Campbell Sci.).

Prior to flux calculations, calibration corrections were applied to the raw concentration data and the consistency of time stamps was verified using a Matlab (version 8.3.0.532, The Mathworks Inc., Natick, MA) function. The half-hour high frequency files, generated by the same Matlab function, were analyzed following the procedures described by Aubinet et al. (2012) using the software package EddyPro (v. 6.0, Licor). The flux calculations included the following procedures: spike removal, double coordinate rotation, time lag compensation (Fan et al., 1990), and spectral corrections (Horst, 1997). Half-hourly fluxes were screened to ensure adequate turbulence development and steady state conditions suitable for flux measurements using the quality control flag system proposed by (Foken et al., 2004).

3.3.3. Flux footprint analysis

In this study, an analytical footprint model and a parameterized footprint model were used to investigate the effect of fetch limitations and the source area heterogeneities on CH_4 flux measurements. In addition, the footprint model weight functions were combined with EC flux measurements to estimate the CH_4 fluxes per unit of F_{pens} and $F_{animals}$ (sections 3.3.5 and 3.3.6).

3.3.3.1. Kormann and Meixner (2001) model

The footprint model proposed by Kormann and Meixner (2001), hereafter denoted as KM01, is based on the solution of the advection diffusion equation and power law profiles of mean horizontal wind velocity and diffusivity. The two-dimensional footprint function (ϕ_{KM}) for a fixed measurement height is given by:

$$\phi_{KM} = \left[\frac{1}{\sqrt{2\pi}Dx^{E}}\exp\left(\frac{-y^{2}}{2(Dx^{E})^{2}}\right)\right]Cx^{-A}\exp\left(\frac{-E}{x}\right) \quad (3.1)$$

where the terms *A*, *B*, *C*, *D* and *E* are functions of the following input parameters: measurement height above the displacement height (z_m), friction velocity (u_*), Monin–Obukhov length (L),

standard deviation of the cross-wind component, wind direction, and mean horizontal wind speed (u). The (x, y) values indicate upwind location of the unit point source that contribute to the measured flux. These input parameters were measured or derived from the sonic anemometer measurements. The term in Eq. 3.1 within the square brackets describes the Gaussian crosswind distribution while the remaining terms describe the crosswind-integrated longitudinal distribution. The displacement height (d) of 0.65 m was calculated following Baum et al. (2008), who applied the formulation proposed by Raupach (1994) for sparse canopies to estimate the displacement height for a feedlot. This formulation assumption is that the cattle behave like buff-rough elements on the feedlot surface. The aerodynamic roughness length (z_0) was calculated for 30-min intervals following Businger et al. (1971) and Dyer (1974) by rearranging the wind profile equation:

$$z_0 = \frac{z - d}{\exp[k\,u(z)/u_* + \Psi_m(z/L)]} \tag{3.2}$$

where Ψ_m is the integral profile similarity function for momentum, k is the von Karman constant (0.4) and z is the measurement height.

3.3.3.2. Kljun et al. (2015) model

Kljun et al. (2015) proposed a two-dimensional flux footprint parameterization (FFP, hereafter) based on the Lagrangian stochastic particle dispersion model LPDM-B (Kljun et al., 2002). This parameterization provides a source weigh footprint function (ϕ_K) for a broad range of boundary layer conditions and measurement heights:

$$\phi_K = \overline{f^y}(x)\frac{1}{\sigma_y\sqrt{2\pi}}exp\left(\frac{-y^2}{2\sigma_y^2}\right) \quad (3.3)$$

where $\overline{f^y}$ is the crosswind-integrated footprint, y is the crosswind distance from the x axis of the footprint and σ_y is the standard deviation of the cross-wind distance. The expression on the right side of the term $\overline{f^y}(x)$ is the crosswind dispersion function.

The crosswind-integrated footprint is given by:

$$\overline{f^y} = F^{y*}(X*)\left(1-\frac{z_m}{h}\right)\frac{u^*}{\bar{u}(z_m)kz_m} \quad (3.4)$$

where F^{y*} is the non-dimensional scaled crosswind-integrated footprint, X^* is the scaled non-dimensional upwind distance, z_m is the measurement height above displacement height (i.e. z-d), u^* is the friction velocity (m/s), $\bar{u}(z_m)$ is the average horizontal wind velocity (m/s) at z_m, k is the von Karman constant (0.4), and h is the boundary layer height (m). The dimensionless parameters F^{y*} and X^* were obtained by Kljun et al. (2015) using Buckingham Π dimensional analysis (Stull, 1988) and 200 simulations run using a Lagrangian stochastic particle dispersion model (Kljun et al., 2002) for measurement heights ranging from 1 to 1000 m and boundary layer conditions extending from strongly convective (Obukhov length (L) = -200 m) to strongly stable (L = 200 m).

In this study, the boundary layer height was calculated as suggested by Kljun et al. (2015), following Batchvarova and Gryning (1991). In addition, the roughness length (Eq. 3.2), used in F^{y*} and X^* estimations (Kljun et al., 2015), was calculated by rearranging the wind profile equation following Businger et al. (1971) and Dyer (1974):

3.3.4. Footprint climatology calculation

To investigate long-term contributions from different surfaces in the feedlot to the measured flux, a normalized aggregated flux footprint (C_f), i.e. the footprint climatology, was calculated for the study period (Amiro, 1998). To do that, the estimated half-hourly footprint functions (ϕ) for both models (Eqs. 3.1 and 3.3) were rotated along the wind direction and accumulated for the experimental period to yield C_f values for KM01 and FFP following Kljun et al. (2015):

$$C_f(x, y, z_m) = \frac{\iint_{\Omega_p} \sum_{n=1}^{N} \phi(x, y, z_m) dx dy}{N} \tag{3.5}$$

where n is the half-hour time step, N is the total number of half-hour periods used to estimate C_f and Ω_p is the isopleth that describes the source area contributing to a specific fraction (P) of the measured flux. A P value of 0.1 to 0.9 at a step of 0.1 is used to determine the respective contour line representing 10 to 90% of the aggregate source areas.

3.3.5. Estimation of CH_4 flux per pen surface

The CH_4 flux per pen surface was estimated by scaling EC flux measurements using the relative contributions of pens and non-emitting surfaces (roads and alleys) in the feedlot to the measured fluxes based on the methodology proposed by Baum et al. (2008) and Neftel et al. (2008). For the time intervals in which the large majority of contributions to the measured flux are from areas within the feedlot, the measured EC CH_4 flux (F_{obs}) can be assumed to be the result of contributions from pens and non-pen surfaces in the feedlot:

$$F_{obs} = P_t . F_{pens} + (1 - P_t) F_{other} \tag{3.6}$$

where P_t is the normalized footprint contribution from pens ranging from 0 to 1 calculated using Eq. 3.8; F_{pens} is the CH_4 flux from the pens and F_{other} is the CH_4 flux from non-pen surfaces. By assuming F_{other} to be negligible, Eq. 6 can be rearranged to estimate F_{pens}, as follows:

$$F_{pens} = \frac{F_{obs}}{P_t} \tag{3.7}$$

Eq. 3.7 was used to scale F_{obs} at feedlot level (landscape scale) to F_{pens} (source area scale). To do that, half-hourly values of P_t were estimated by superimposing arrays of ϕ_{KM} and ϕ_K on a digital map of the feedlot with polygons representing different feedlot surfaces. For illustration, the feedlot map and source weight function calculated for a selected half-hour period are shown in Fig. 3.2.

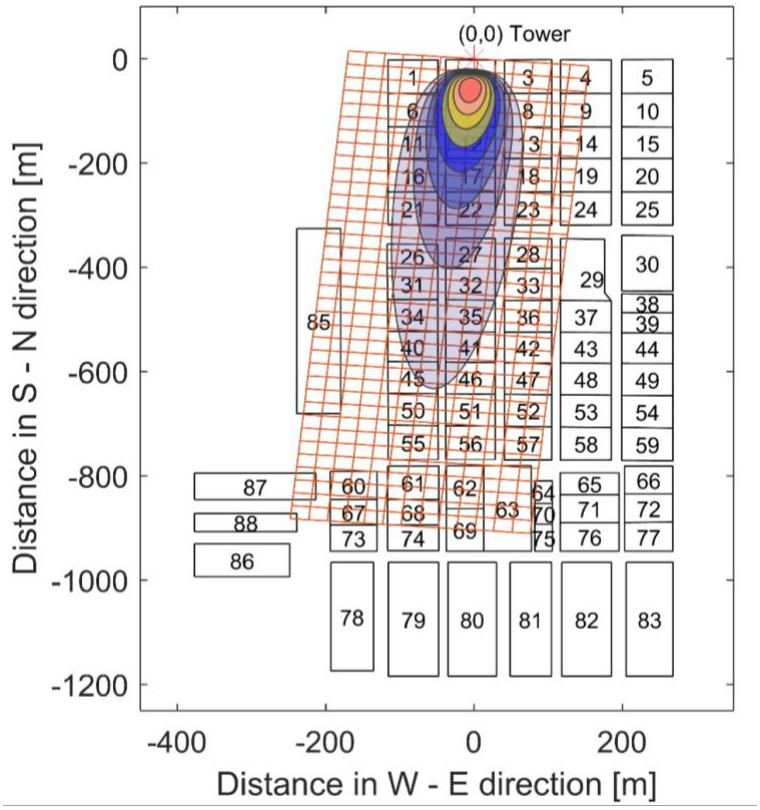

Figure 3.2. Schematic diagram showing the grid cell overlaid on the feedlot map. The footprint weight, $\phi(x, y)$ was calculated for each grid cell for 30 min periods. The cumulative distribution of $\phi(x, y)$ is shown by the contour lines ranging from 10 to 80% of the source area. The outer limit of the contour line represents the footprint fetch or source area (Ω_P, P = 0.8 or 80%). The $\phi(x, y)$ values for each polygon within the footprint was added to estimate contributions from different feedlot surfaces (e.g. pens, roads and alleys.).

The digital map of the feedlot was generated using a high resolution satellite image of the feedlot (Google Earth, resolution: 15 x 15 cm, accuracy < 1 m) that was georeferenced using a GIS software (ArcGIS 10.0, ESRI, Redlands, CA) and GPS coordinates of control points collected in the feedlot using a survey grade GPS (AgGPS 214, Trimble Navigation Limited, Sunnyvale, CA). The Cartesian coordinates of the vertices of the polygons representing different feedlot surfaces were extracted from the georeferenced map of the feedlot.

Arrays of ϕ_{KM} and ϕ_K were calculated using Eqs. 3.1 and 3.3, respectively, for a grid cell in the *x*-*y* plane. The *x* and *y* coordinates of the grid cells and feedlot digital map were specified so that the flux tower was located at the origin ($x = 0$, $y = 0$). Half-hourly values of ϕ_{KM} and contributions of different feedlot surfaces to the measured flux were calculated using an R (ver. 3.3.2, R Core Team) routine provided by Felber et al. (2015) that was developed based on the original footprint tool developed by Neftel et al. (2008). Similarly, ϕ_K was used to estimate the contributions from feedlot surfaces using Matlab functions. For ϕ_{KM} calculations, the grid size was fixed to 1.5 x 1.5 km, with each cell measuring 4 x 4 m. The Matlab function utilized to compute ϕ_K used a variable grid size, ranging in this study from 100 × 100 m^2 to 2.5 × 2.5 km^2, with cell dimensions varying from 0.2 × 0.2 m^2 to 4 × 4 m^2, depending on the atmospheric conditions. A sensitivity analysis was performed by reducing the cell dimensions used in both model calculations by half. This reduction had negligible (< 2%) influence on flux contribution estimates from pens and non-emitting surfaces (data not shown); however, it considerably increased the computing time. Thus, the original cell dimensions were considered adequate for this study.

Values of ϕ_{KM} and ϕ_K for all grid cells inside each polygon (*i*) were added to calculate the integral footprint contribution (P_t) from a given feedlot surface, as follows:

P_t is the relative contribution of all pens to the measured flux, given by

$$P_t = \sum_{i=1}^{M} P_i \tag{3.8}$$

where *M* is the number of pens in the source area and (P_i) is the relative contribution of different surfaces in the feedlot (P_i) to the total 30-min average flux given by:

$$P_{\mathrm{i}} = \frac{\iint_{A_i} f(x, y, z_{\mathrm{m}})\, dx\, dy}{\iint_{\Omega} f(x, y, z_m)\, dx\, dy} \tag{3.9}$$

where A_{i} is the area of a specific pen represented by polygons on the feedlot vector map and Ω is the flux footprint function integration domain determined by a fraction of the total flux footprint.

3.3.6. Estimation of CH_4 emission rate per animal

The average CH_4 emissions rate per animal were estimated using F_{pens} and the footprint weighted stocking density assuming homogeneous distribution of the cattle inside the pens, as follows:

$$F_{\mathrm{animal}} = SF_{\mathrm{pens}} \tag{3.10}$$

where S is the footprint averaged stocking density, given by:

$$S = \frac{\sum_{\mathrm{i}=1}^{M} S_{\mathrm{i}} P_{\mathrm{i}}}{\sum_{\mathrm{i}=1}^{M} P_{\mathrm{i}}} \tag{3.11}$$

where S_{i} is the stocking density for each pen.

3.4. Results and Discussion

3.4.1. Flux footprint model comparisons

The aggregated flux footprint or footprint climatology (section 3.3.4) was estimated using FFP and KM01 for half-hourly time steps for the entire experimental period. The aggregated footprints obtained for each model were then overlaid on the feedlot map (Fig. 3.3).

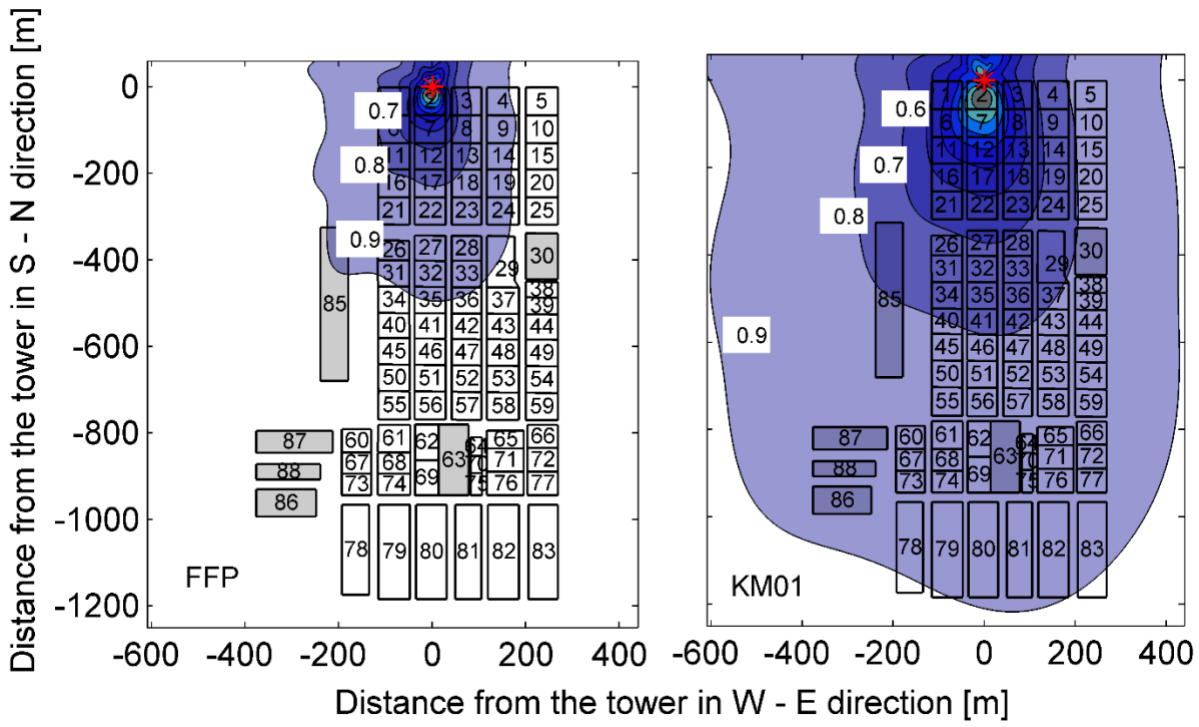

Figure 3.3. Footprint climatology estimated using the models proposed by Kljun et al., 2015 (FFP) and Kormann and Meixner, 2001 (KM01). The footprint contour lines are shown in 10% increments ranging from 10 to 90%. The background map shows the location of the flux tower (red asterisk) with respect to different feedlot surfaces. Pens are represented by unfilled polygons. Polygons: 63, 85, 86 and 87 represent run-off storage lagoons and polygon 30 represents a barn. Roads and transfer alleys are in between the pens and around the edges of the feedlot. (For interpretation of the references to color in this figure legend, the reader is referred to the web version of this article).

Southerly winds prevailed at the experimental site during the experimental period (Prajapati and Santos, 2017) which explains the elongated shape along the north-south axis of the aggregated footprints. Despite the similar shape, the KM01 aggregated footprint was much greater than the footprint climatology estimated using FFP. The average source areas contributing to 10% to 90% of the measured flux estimated by the KM01 model were 5 to 6 times greater than the ones for FFP (Table 3.2).

Table 3.2. Average source weight per area (Wp) for different level of isopleths relative to the source weight per area for the isopleth level 0.1 ($W_{0.1}$). Wp and Wp/W0.1 values are for areas between isopleths P and $(P - 0.1)$.

P	Area (m^2)		Source weight/m^2 (W_p)		$W_p/W_{0.1}$	
	FFP	**KM01**	**FFP**	**KM01**	**FFP**	**KM01**
0.1	223	1185	4.5×10^{-4}	8.4×10^{-5}	1	1
0.2	576	3149	2.8×10^{-4}	5.0×10^{-5}	0.63	0.60
0.3	1121	6455	1.8×10^{-4}	3.0×10^{-5}	0.40	0.35
0.4	1997	12,012	1.1×10^{-4}	1.8×10^{-5}	0.25	0.21
0.5	3580	21,449	6.3×10^{-5}	1.1×10^{-5}	0.14	0.12
0.6	6513	40,044	3.4×10^{-5}	5.4×10^{-6}	0.07	0.063
0.7	13,269	82,255	1.5×10^{-5}	2.4×10^{-6}	0.032	0.028
0.8	33,595	208,510	4.9×10^{-6}	7.9×10^{-7}	0.010	0.009
0.9	155,360	922,803	8.2×10^{-7}	1.4×10^{-7}	0.0018	0.0016

The differences between the KM01 and FFP estimates varied depending on the atmospheric stability conditions. The downwind distance contributing 80% of the total flux (x_{80}) was estimated using KM01 and FFP for different atmospheric stability conditions. Half-hourly values of x_{80} for both models were calculated by finding the maximum distance between the flux tower and the farthest point on the ellipse representing the source area (Fig 3.2). The average value of x_{80} under unstable conditions (-100 m < L < 0 m) was 1.5 times greater for KM01 than for FFP while the differences between the x_{80} values estimated by KM01 and FFP models widened for neutral and stable conditions. The value of x_{80} estimated using the KM01 model was 2.3 to 3 times larger on average, for neutral (|L| > 100 m) and stable conditions (0 m < L < 100 m), when compared to FFP x_{80} values. In addition, the average crosswind-width of the source area (Ω_{80}) by KM01 was 2 times larger than the one estimated by FFP.

Kljun et al. (2003) compared estimates provided by the backward Lagrangian particle dispersion model LPDM-B (Kljun et al., 2002), which was used to test and parameterize FFP, with KM01 estimates for different atmospheric stability regimes for the surface layer and a range of measurement heights. Their results showed discrepancies between the two models especially under neutral and stable conditions. During the experimental period, most of the 30 min periods were under neutral atmospheric conditions (54%, $|L| > 100$) while about 19% of the half-hour periods were under stable ($0 < L < 100$) atmospheric conditions (Prajapati and Santos, 2017). The predominance of neutral and stable atmospheric stability conditions explain part of the large differences between the FFP and KM01 footprints (Fig. 3.3).

Kljun et al. (2003) attributed these differences primarily to along wind velocity fluctuations which are not incorporated into KM01 calculations. The differences between KM01 and FFP estimates in this study were also in agreement with the results of KM01 and FFP comparisons reported by Kljun et al. (2015). Kljun et al. (2015) also observed the larger footprint extents predicted by KM01 when compared to FFP estimates for most atmospheric conditions, except for their free convection and mixed layer scenarios when the FFP footprint extended further than the one predicted by KM01. They also reported that for most of the scenarios, the footprint, estimated by KM01, was wider downwind of the footprint peak.

Wilson (2015) compared footprints computed using eddy diffusion models, including KM01, with first-order Lagrangian stochastic models or Langevin models (LSM). He also found similar discrepancies between KM01 and LSM footprints as the ones observed for KM01 and FFP in this study. However, Wilson (2015) found that the agreement between KM01 and LSM improved by tuning the effective Schmidt number (S_c) in KM01. The parameter S_c represents the ratio of eddy viscosity to the tracer eddy diffusivity and was assumed to be unity for KM01 by

Kormann and Meixner (2001). Wilson (2015) showed that KM01 and LSM agreement was better for $S_c = 0.64$ in comparison to KM01 original model simulations ($S_c = 1$). Part of the differences between KM01 and FFP simulations in this study could also be explained by discrepancies in *Sc* values for these two models, since the LPDM-B model by Kljun et al. (2002), used to parametrize FFP, has an implicit *Sc* value of 0.61. Despite the better agreement between KM01 and LSM simulations after S_c tuning, Wilson (2015) concludes that his results suggest that the eddy diffusion solutions, such as KM01, misrepresent the flux footprint in comparison to LSM simulations. This assertion is also supported by other studies (Kljun et al., 2015; Sawford, 2001; Wilson and Yee, 2007). Considering the results from these previous studies, one could speculate that the FFP simulations are probably more accurate than KM01 estimates. Yet, field studies are still needed to investigate the accuracy of those footprint models under different atmospheric conditions. The validation of footprint models is beyond the scope of this study. Instead, we will investigate how the differences between FFP and KM01 footprints influence fetch requirements for EC measurements and CH_4 emission estimates in the feedlot in the following sections.

3.4.2. Fetch requirements

The rectangular shape of the feedlot resulted in a variable distance between the flux tower location and the feedlot boundaries. The downwind distance between the flux tower and the feedlot boundary ranged from 1200 m under southerly winds, to less than 270 m for east and west wind directions (Fig. 3.3). The effect of fetch limitations on CH_4 flux measurements is evident in Fig. 3.4. The average CH_4 fluxes originating from the SE (90 ° to 180 °), SW (180 ° to 270 °), NW (180 ° to 270 °), and NE (0 ° to 90 °) sectors were 2.7, 2.5, 0.08 and 0.02 µmol m^{-2} s^{-1}, respectively.

Fig 3.4 illustrates that as wind directions departed from the south, there was a progressive reduction in CH_4 flux magnitudes. This flux reduction is related to an increase in contribution of surrounding agricultural fields to the measured fluxes. The FFP and KM01 footprint functions were used to evaluate the fetch requirements for flux measurements at the feedlot. The fetch is the area bounded by a footprint function isopleth, also referred to as the source area (Ω_P). Values of *P* ranging from 0.6 to 0.9, which defines the outer limit of Ω_P (section 3.3.4), were used to exclude time intervals in which Ω_p extended beyond the feedlot boundary. As the value of *P* increased, less data points were retained (Fig. 3.4). For the same *P* value, there was a large data retention for FFP relative to KM01 because KM01 tended to overestimate Ω_p in comparison to FFP (section 3.4.1). The selection of the *P* value to screen flux data should maximize the data retention while minimizing the influence of areas outside the feedlot to the measured CH_4 fluxes. In theory, the scaling approach described in section 3.3.4 could also be used to minimize the effect of surfaces outside the feedlot on the measured fluxes by assuming that CH_4 fluxes from those surfaces are negligible. Nevertheless, the reduction in contributions from the area of interest (pens) to the measured CH_4 fluxes would also reduce the representativeness of EC measurements and introduced uncertainties in the scaled fluxes.

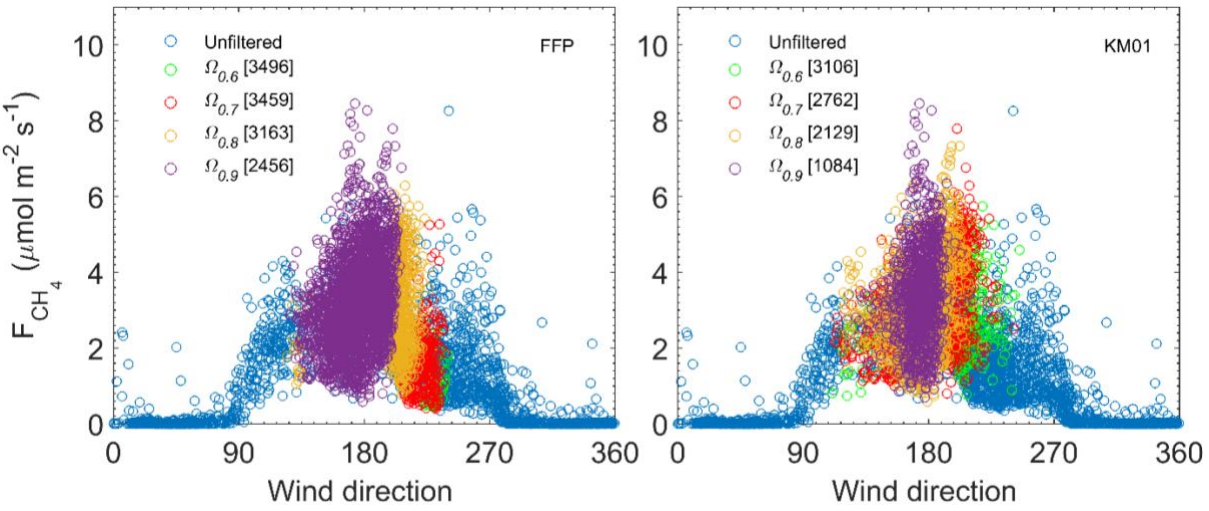

Figure 3.4. Relationship between CH_4 fluxes (F_{CH_4}) and wind direction. The flux data were screened using different fractions of the source weight area (Ω_P), estimated using FFP and KM01 models. For example, when $\Omega_{0.7}$ was used the flux data were screened to ensure that more than 70% of source weight area contributing to the flux was inside of the feedlot.

Schmid (1994) proposed the use of the source weight distribution to evaluate the extent to which flux measurements describe the area of interest. Using this approach, the outer limit for Ω_P can be determined for a *P* value above which the contributions to measured fluxes are negligible. We estimated the averaged maximum source weight values (ϕ_{max}) for KM01 [Eq 22 in Kormann and Meixner (2001)] and FFP [Eqs. 14 and 22 in Kljun et al. (2015)], which were used as a reference to estimate the outer limit source weight corresponding to 1% of ϕ_{max}. The average values for the outer limit source weight were equal to 4×10^{-6} m^{-2} for FFP and 7.7×10^{-7} m^{-2} for KM01. These values are in close agreement with the source weight per area (W_p) values for areas between isopleths 0.7 and 0.8 for both models shown in Table 3.2. The $W_p/W_{0.1}$ values, which provide relative importance of disturbance at the area between the isopleths compared to similar disturbance at $\Omega_{0.1.}$, also showed limited contributions to the measured flux from source areas beyond $\Omega_{0.8}$. This suggests $\Omega_{0.8}$ would be adequate to screen time intervals in which

contributions to the measured flux from areas outside the feedlot are relatively high. We adopted a value of $\Omega_{0.8}$ for FFP, but assuming that KM01 overestimates the footprint extent (section 3.4.1) and to maximize data retention (Fig. 3.4), we decided to use $\Omega_{0.7}$ for KM01. The use of $\Omega_{0.8}$ (FFP) and $\Omega_{0.7}$ (KM01) allowed for the retention of 3163 and 2762 data points respectively, which corresponded to 72% and 63% of total flux data points (4377).

3.4.3. Contributions of different feedlot surfaces to the measured fluxes

The contributions from the different feedlot surfaces were calculated using $\Omega_{0.8}$ in FFP and $\Omega_{0.7}$ for KM01. As we were also interested in investigating the contribution of run-off storage lagoons located outside the feedlot to the measured flux, we did not exclude intervals in which the footprint extended beyond the feedlot boundaries. Instead, only data points associated with wind directions ranging from 90 to 270 $^{\circ}$ were included in this calculation. The results showed that the measured flux was dominated by contributions from pens within a distance of approximately 320 m from the flux tower. The total contributions from these pens (1-25 in the feedlot map) were 87% and 81% for FFP and KM01, respectively (Table 3.3).

Although the two pens immediately south from the flux tower represented less than 2% of the feedlot surface, they were responsible for 71% (FFP) and 48% (KM01) of the contributions to the measured fluxes (Table 3.3). The differences in contributions predicted by the models for the two pens can be attributed to the differences in the FFP and KM01 footprint extent (section 3.4.1). The analyses also showed that the average contribution of run-off storage lagoons to the measured flux was negligible (< 0.1%). The average contributions from roads and alleys ranged from 9 to 12%, although those surfaces account for 21% of the feedlot area.

Table 3.3. Relative contribution to eddy flux measurements from different surfaces within and outside the feedlot estimated using FFP and KM01 models.

Surface	Polygon i.d.	Area (%)	Contribution to the measured flux (%)[a]	
			FFP	KM01
Pens	2	0.8	59.5	30.6
	7	0.8	11.1	17.3
	1–25 (excluding 2 & 7)	19	16.6	33.3
	26–83 (excluding 63)	51	0.01	<0.1
Lagoons	85–88 & 63	7.4	<0.01	<0.1
Roads and alleys	–	21	8.5	12
Areas outside the feedlot boundary	–	–	4.29	6.7
Total	–	100	100	100

[a]Calculations were based on the source areas contributing to: 80% of the flux for FFP and 70% for KM01.

3.4.4. Effect of non-pen surfaces on measured CH_4 fluxes

Although the flux data can be screened to minimize the influence of areas outside the feedlot on the flux measurements (section 3.4.2), non-pen surfaces within the feedlot, such as: roads and transfer alleys, can still influence the magnitude of measured fluxes (Baum et al., 2008). These non-emitting surfaces are expected to affect the measured fluxes from the feedlot. Hence, the observed flux values should be scaled to minimize the influence of non-pen surfaces on the measured fluxes.

To assess the effect of non-pen surfaces within the feedlot on the observed CH_4 fluxes under different environmental conditions, F_{pens} and F_{obs} were used to estimate the magnitude of the scaling factor (SF) for each half-hour interval, which is given by:

$$SF = (F_{pens} - F_{obs}) / F_{obs} \quad (3.12)$$

where F_{pens} was estimated using KM01 and FFP footprints using the approach described in section 3.4.5.

Fig. 3.5 shows the relationship between wind direction and the magnitude of the *SF*. The *SF* values were small for periods with southerly winds because the influence of roads in the flux footprint is small for these periods. Values of *SF* increased for southeasterly and westerly winds due to the increase in area of roads and alleys in the footprint. In addition, *SF* was larger for KM01 then FFP. This difference was likely the result of the larger proportion of non-pen surfaces in the source area estimated using KM01.

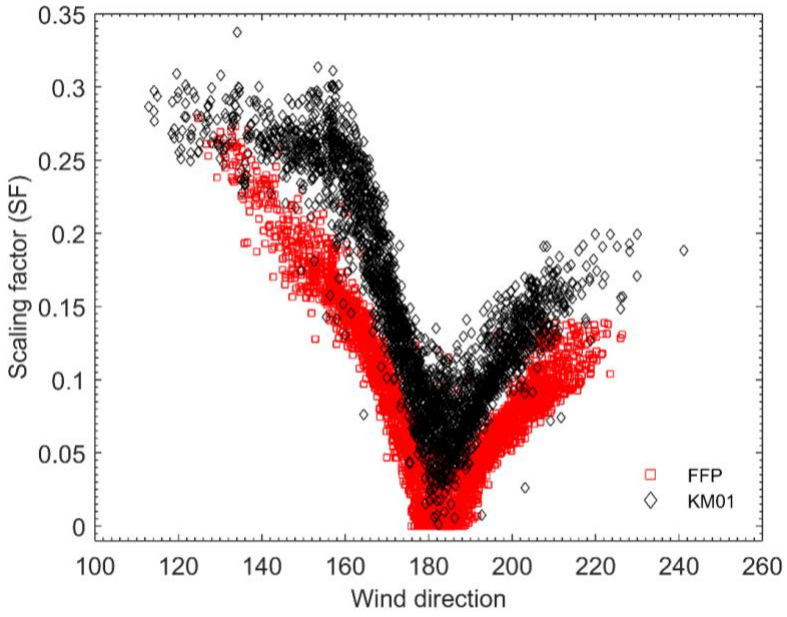

Figure 3.5. Relationship between wind direction and the flux scaling factor (*SF*, Eq. (11)) estimated using FFP and KM01.

To evaluate the ability of this footprint correction approach to minimize the effect of non-pen surfaces on the flux measurements, we divided half hour periods into two categories: 1) high-pen contribution periods with more than 90% of the flux contributions within the footprint originating from pen surfaces, and 2) lower-pen contribution periods with more than 10% of contributions within the source area originating from roads and alleys. Out of the retained data

points after fetch requirement screening (Fig. 3.4 section 3.4.2), 2269 (FFP, $\Omega_{0.8}$) and 1118 (KM01, $\Omega_{0.7}$) half-hour periods were in the high-pen contribution category while 894 (FFP) and 1164 (KM01) periods were in low pen contribution category. The high-pen contribution periods were typically associated with the southerly winds with directions ranging from 170 to 220°, while lower-pen contribution periods were associated with southeast and southwest wind directions.

Fig. 3.6 shows the ensemble averaged diel CH_4 fluxes for: high-pen contribution periods, lower-pen contribution periods and F_{pens}, which was calculated using data for both high pen and lower-pen contribution periods following the procedure described in section 3.3.5. Diel ensemble flux averages showed much higher CH_4 flux values for high-pen contribution periods in comparison to lower pen contribution periods. The reduction in average CH_4 fluxes in low-pen contribution periods were ~22 % (FFP) and ~19 % (KM01) compared to high-pen contribution periods. The average difference in CH_4 fluxes for the two categories were significant at a 5% significance level when tested with a two-sample t-test. These results clearly show that pens and alleys in the feedlot introduced biases in the measured fluxes.

We evaluated the ability of the procedure described in section 3.3.5 to correct biases in F_{obs} caused by the presence of non-pen surfaces in the feedlot by comparing F_{pens} with the ensemble averaged diel CH_4 fluxes for high-pen contribution periods. The corrected fluxes (F_{pens}) were in agreement with the averaged diel CH_4 fluxes for high-pen contribution periods with RMSE ranging from 0.01 μmol m^{-2} s^{-1} (FFP) to 0.03 μmol m^{-2} s^{-1} (KM01). The good agreement between F_{pens} with the ensemble averaged diel CH_4 fluxes for high-pen contribution periods suggests that both models were capable of correcting biases found in F_{obs} by non-pen surfaces. The larger extent of the KM01 footprint and inclusion of more non-pen surfaces in the

source area can explain the larger F_{pens} values derived from the model when compared to FFP (section 3.4.3).

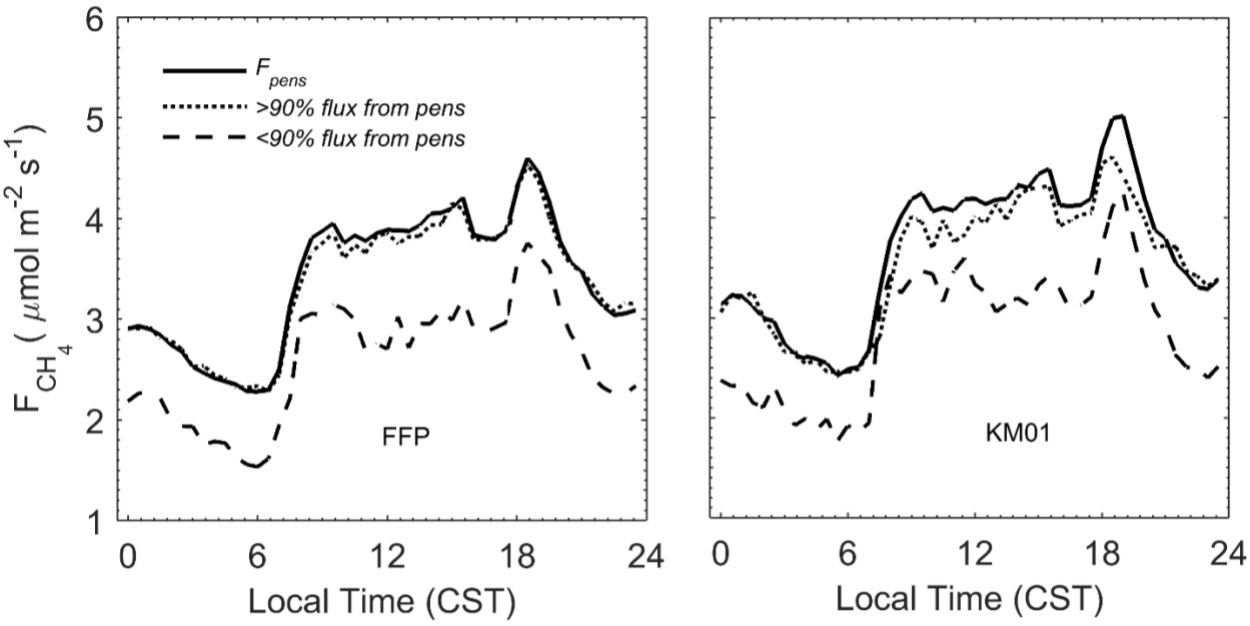

Figure 3.6. Ensemble average CH_4 flux for periods with different pen contributions: (i) periods that have majority (> 90%) of the flux contribution from the pens (dotted lines), (ii) periods with less than 90% of the contributions from pens (dashed lines) and (iii) CH_4 emissions from pens (F_{pens}), estimated taking into consideration the dilution effect caused by the presence non-pen surfaces in the flux footprint using FFP and KM01.

3.4.5. Methane fluxes per pen surface

The diel ensemble average F_{pens} showed high values during the day and low values at night (Fig. 3.6). Average ensemble values of F_{pens} started to increase after sunrise with a slight increase during the day and a peak in the early evening before decreasing during the nighttime. These larger F_{pens} values are related to feeding and ruminating during the daytime, which also has been reported in previous CH_4 emission studies with ruminants (Dengel et al., 2011; Felber et al., 2015; Laubach et al., 2013).

Fig. 3.7 shows the average monthly F_{pens} from August 2013 to April 2014. The flux data for the month of May 2014 were excluded due to the limited number of valid data points available. The average F_{pens}, estimated using FFP and KM01, were 3.4 and 3.7 µmol m^2 s^{-1}, respectively. Averaged monthly F_{pens} values were slightly higher for the fall months (August to November) in comparison to winter/spring months (December to March). The reduction in stocking density (~ 15%) in the winter months explains part of this variation, which will be further discussed in the next sections. Values of F_{pens} were on average 8% (FFP) to 14% (KM01) greater than F_{obs}.

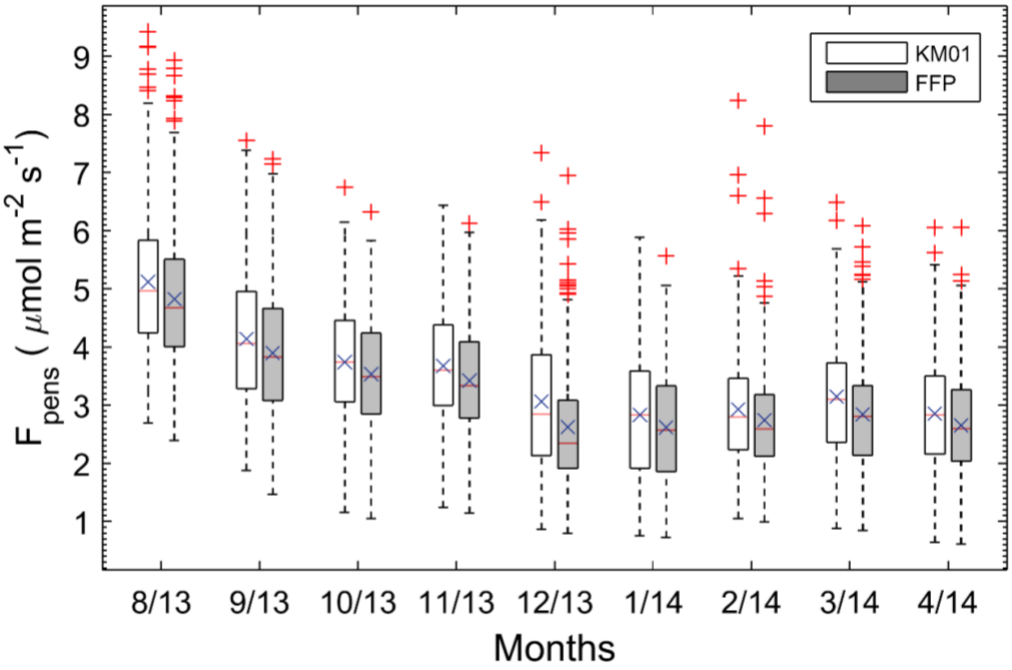

Figure 3.7. Monthly average of CH_4 flux per pen surface (F_{pens}) in a beef cattle feedlot. The central red line in each box indicates the median, central mark '×' indicates the mean, and the bottom and top edges of the box indicate the 25th and 75th percentiles, respectively. The whiskers are extended to the most extreme data point that is no more than 1.5 times the interquartile range (IQR) from the edge of the box. The '+' sign represents outliers that lie beyond the whiskers.

3.4.6. Estimation of CH_4 fluxes per animal

Half-hourly values of F_{animal} were estimated using F_{pens} and the footprint weighted average stocking density (Eq. 3.10). Average monthly CH_4 emissions, estimated based on KM01 model, ranged from 83 to 125 g animal^{-1} d^{-1} while F_{animal}, estimates using FFP ranged from 75 to 114 g animal^{-1} d^{-1} (Fig 3.8). Overall, the average emissions estimation based on FFP (95 g animal^{-1} d^{-1}) were about ~7% lower than KM01 values (102 g animal^{-1} d^{-1}). The highest monthly average F_{animal} was observed for the month of August (117.2 g animal^{-1} d^{-1}, FFP) and the lowest one (74.6 g animal^{-1} d^{-1}, FFP) for January. The average F_{pens} for the fall months (August to November) was 29% larger than the one for the winter months (December to April), and a reduction of 16% was observed for $F_{animals}$ from the fall to winter months. These results show that the reduction in stocking density (~15%) from the fall to winter months only explains part of the seasonal variability in CH_4 emissions from the feedlot. There may be other variables contributing for this flux reduction. A possible hypothesis is that the increase in CH_4 ground emissions, assumed to be negligible for $F_{animals}$ estimation (section 3.3.6), could explain some of the differences of $F_{animals}$ between the fall and winter months. During the late summer and early fall the higher precipitation and elevated ambient temperature (Fig. 3.1) could have led to CH_4 production by anaerobic decomposition of manure accumulated in the pen surfaces. This hypothesis as well as other sources of uncertainties in CH_4 scaled flux estimates will be discussed in section 3.4.7.

For comparison purposes, the CH_4 emissions per head of cattle was estimated following the Intergovernmental Panel on Climate Change (IPCC). The Tier 1 F_{animal} values reported for North American 'other cattle' category comprised of steers/heifers that are fed grain and finished in feedlots is 145 g animal^{-1} d^{-1} (FAO, 2009). The IPCC Tier 2 methodology is more

sophisticated and suggests using a fraction of the gross energy intake lost as CH_4 (Y_m) of 3.0% ± 1.0%. Todd et al. (2014) found averaged Y_m values ranging from 2.8% in the winter and 3.2% in the summer for a feedlot on the southern High Plains in Texas, so the recommended Y_m value by IPCC should be adequate for the feedlots in the region. The average F_{animal} was 167.8 ± 56 g animal^{-1} d^{-1} estimated using the methodology proposed by the IPCC Tier 2 methodology. The emission values in our study are closer to the lower end of the Tier 2 emission values.

Table 3.4 shows CH_4 emissions reported in selected studies with animal characteristics similar to the cattle in this study (Table 3.4). The CH_4 emissions ranged from 60 to 279 g animal^{-1} d^{-1} in these selected studies. Among those studies, Todd et al. (2014) used an inverse Lagrangian dispersion model to estimate CH_4 emission rates from cattle in a feedlot in the Southern high plains in Texas. They obtained CH_4 emissions per capita ranging from 71 to 118 g animal^{-1} d^{-1} in the winter to 70 to 130 g animal^{-1} d^{-1} in the summer. Our estimates of F_{animal} are in agreement with the CH_4 emissions reported in their study. However, the average Y_m derived from our scaled fluxes was about 2% which is lower than the values reported by Todd et al. (2014) and in the majority of studies shown in Table 3.4. Although comparisons between average F_{animal} estimates with CH_4 emission values found in the literature or estimated using existing models can provide some useful information on the performance of the EC technique, we acknowledge that this approach has limitations, including differences in measurement techniques, animal characteristics, feed type and management conditions among studies that are likely to affect CH_4 emission measurements. A thorough evaluation of the EC approach to estimate F_{animal} under different time scales and environmental conditions could be accomplished by a technique comparison study like the one carried out by Laubach et al. (2013). The results of such an evaluation study will be presented in chapter 4 of this thesis.

Table 3.4. Average CH_4 emissions from beef cattle reported in previous studies.

Reference	Animal (feed type)	CH_4 emission (g animal day^{-1})	Animal weight[a] (kg)	Y_m (%)	Measurement technique
Beauchemin and McGinn (2005)	Heifers (corn or Barley grains)	62–171	328	2.8–4	Chamber
Beauchemin and McGinn (2006)	Heifers (barley silage and grain, and additives)	114–151	328	6	Chamber
Harper et al. (1999)	Heifers (oats and lucerne)	60–70	436	1.9–2.2	Mass difference technique
McGinn et al. (2004)	Steers (barley silage with additives)	129–181	312	5–6.4	Chamber
McGinn et al. (2008)	Beef cattle – mixed animals (barley and corn silage and supplements)	166–214	442	4.5–5.1	bLS[c]
McGinn et al. (2009)	Steers (barley grain, corn grain and silage)	161–279 130–215	381	–	bLS[c] SF_6
Stackhouse et al. (2011)	Steers (mixed ration with corn, alfalfa, cottonseed, fat and limestone)	75–100	442	2.7–3.9	Chamber
Todd et al. (2014)	Beef cattle – mixed animals (SFC[b] and corn co-products)	70–130	301	2.7–3.1	bLS[c]

[a]Initial average weight of cattle in the beginning of study, [b]Steam-flaked corn, [c]Backward Lagrangian stochastic model.

3.4.7. Sources of uncertainties in CH_4 emission measurements

The scaling approach used to estimate F_{pens} and F_{animal} (sections 3.3.5 and 3.3.6) relies on the accuracy of footprint estimates. The footprint models used in this study were derived for smooth surface conditions, which are usually quantified by the roughness length. The average roughness length (z_0) was 3 cm for southerly winds and 4 cm for southeast and southwest wind directions with 87% of z_0 values data typically ranging from 1 cm to 10 cm. The presence of feed bunks probably led to slightly higher z_0 values for southeast and southwesterly wind directions.

These values are consistent with the z_0 values reported in previous feedlot studies (Baum et al., 2008; Flesch et al., 2007). Baum et al. (2008) attributed the smooth surface in feedlots to the predominance of a bare soil surface interspersed by cattle and feed bunks. They observed that the roughness length observed in their feedlot is in agreement with z_0 reported for sparse vegetation, such as vineyards and shrublands. Considering the typical z_0 values found for the feedlot, surface roughness characteristics are not expected to affect the footprint model performances in this study. However, we observed very large differences between KM01 and FFP footprint extents and in the estimated flux contributions from different feedlot surfaces (Table 3.3).

Surprisingly, F_{pens} and F_{animal} values derived from FFP and KM01 were in relative agreement (Figs. 3.7 and 3.8) considering the differences between the footprint models. A possible explanation for the agreement between KM01 and FFP F_{pens} estimates is that the tower was located near a contiguous block of pens which reduced the influence of non-pen surfaces to the measured fluxes, especially for the predominant wind direction (south) at the site (sections 3.4.4 and 3.4.5). In addition, the relative homogeneity in stocking density among the pens near the tower resulted in similar footprint weighing stocking densities (Eq. 3.10, data not shown) for the two models. Similar footprint weighed stocking densities and F_{pens} led to good agreement between KM01 and FFP F_{animal} estimates.

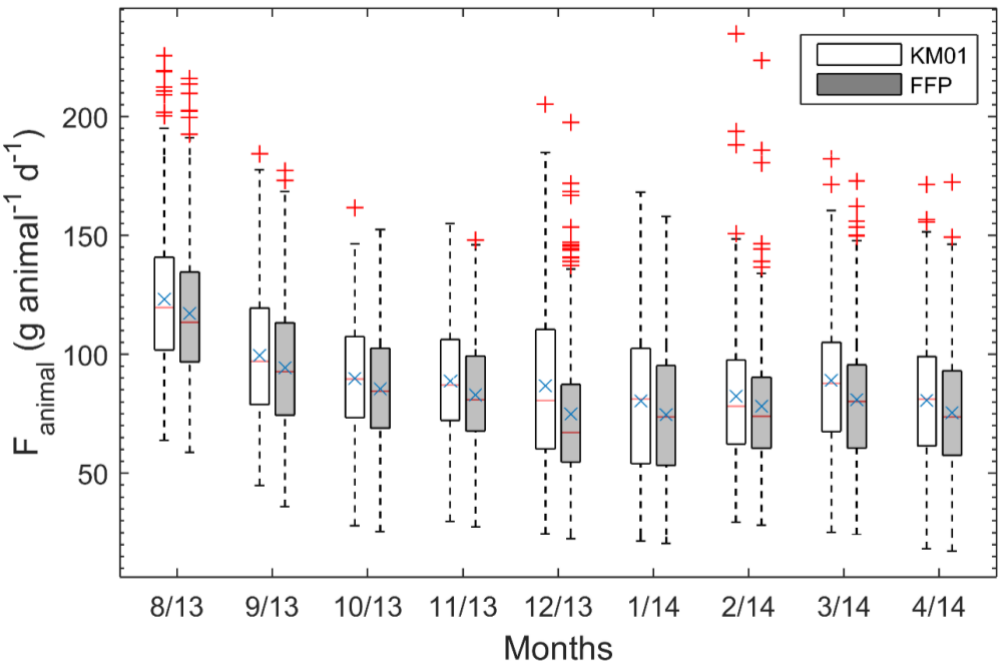

Figure 3.8. Monthly average CH_4 flux per animal (F_{animal}) in a beef cattle feedlot. The central red line in each box indicates the median, the central mark '×' indicates the mean and the bottom and top edges of the box indicate the 25th and 75th percentiles, respectively. The whiskers are extended to the most extreme data point that is no more than 1.5 times the IQR from the edge of the box. The '+' sign represents outliers that lie beyond the whiskers.

Nevertheless, larger differences between KM01 and FFP scaled fluxes would be expected for source areas with higher spatial heterogeneity than the feedlot of this study. Our results suggest that both models were able to correct the biases introduced in the flux data by the presence of non-pen surfaces in the source area (Fig. 3.6). However, KM01 overestimated the contribution of non-pen surfaces leading to an overestimation of F_{pens} when compared to FFP. Additional tracer release studies, as the one recently carried out by Coates et al. (2017), are necessary to improve the confidence of EC measurements from livestock systems and to validate footprint model estimates.

Heterogeneities in animal distribution are likely to be another source of uncertainties in CH_4 emission estimates in this study. Although the cattle were assumed to be evenly distributed

in the pens (section 3.4.4), the aggregation of animals near the feed bunks during feeding times likely violated this assumption. We hypothesize that fluxes measured under atmospheric conditions that lead to smaller footprints would be more sensitive to changes in stocking density within the source area. To test this hypothesis, F_{animal} was plotted against $\Omega_{0.8}$ (Fig 3.9). The F_{animal} values (> 180 g animal^{-1} d^{-1}) were associated with smaller footprints ($\Omega_{0.8}$ ~ 0.01 km^2), which occurred during the afternoon and evening feeding times when animals gathered near the feed bunks located in the east and/or west sides of the pens. In addition, the standard deviation of F_{animal} was slightly higher for smaller footprints (30 g animal^{-1} day^{-1} for $\Omega_{0.8}$ < 0.015 km^2) than for larger footprints (27 g animal^{-1} day^{-1} for $\Omega_{0.8}$ > 0.015 km^2). Similar results were observed for the relationship between F_{animal} and KM01 $\Omega_{0.7}$ (data not shown). Laubach et al. (2013) conducted an inter-comparison study with different methodologies to measure herd size CH_4 emissions. They performed a sensitivity test that indicated that animal movement affected CH_4 emission measurements for most microgeological methods. However, gradient profile techniques were more sensitive to the effect of animal movement in the source area. (Coates et al., 2017) conducted a controlled CH_4 release study to evaluate the capability of a Lagrangian stochastic dispersion model to interpret EC measurements from few individual artificial point sources. They observed that emission estimates with the EC sensors placed further away from the source area were slightly more accurate than the sensor near the source area. They suggested to increase the horizontal distance between the EC tower and the source area to improve the accuracy of the flux measurements. In this study, the relationship between F_{animal} and source area indicates that increasing the size of the area sampled by the tower could improve the EC CH_4 emission measurements. This could be accomplished by increasing the height of the EC sensors. The shortcoming of higher sensor heights would be the reduction of the data retention due to fetch

limitations. In this feedlot, for example, the tower could be placed closer to the center of the feedlot to increase data retention and the instrumentation could be set up at a higher height to minimize animal movement effects on the flux measurements.

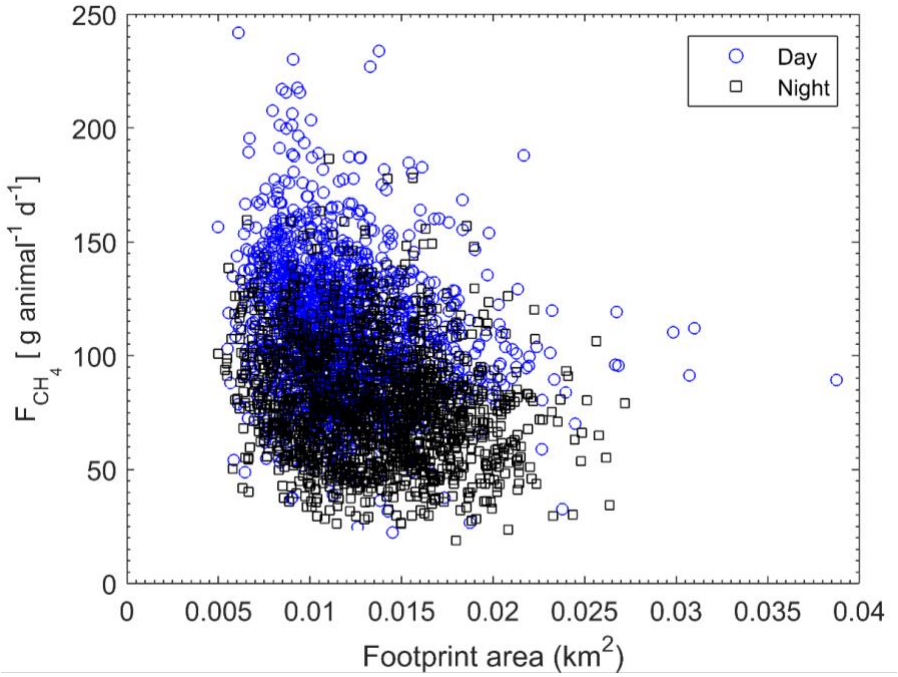

Figure 3.9. Relationship between daytime (8:00–20:00 CST) and nighttime (20:30–7:30 CST) CH_4 emissions per animal (F_{animal}) and the size of source area ($\Omega_{0.8}$) sampled by the flux tower. The size of the source area was calculated based on the FFP model. The daytime period was defined to represent the time with larger animal activity in the feedlot.

Alternatively, the animal position could be monitored to calculate the true stocking density in the tower footprint. Felber et al. (2015) used GPS units to monitor the position of dairy cows with respect to the footprint. The use of GPS units to monitor cattle movement in feedlots is not practical because of the large stocking density. In addition, unlike dairy systems, feedlot cattle are not handled on a daily basis imposing practical challenges for retrieving the data from the GPS units. An alternative would be the use of digital photograph and computer algorithms (Benvenutti et al., 2015) to determine the cattle position as suggested by Taylor et al. (2017). A

comprehensive analysis of the effect of animal movement on EC measurements is out of the scope of this study, but will be addressed in the future.

Furthermore, changes in CH_4 emissions from ground sources are likely to influence the observed EC fluxes. In this study, the CH_4 ground emissions were assumed to be negligible for F_{animal} estimation. The IPCC Tier 2 estimated CH_4 emissions from solid manure in feedlot pens is approximately 5.4 g animal^{-1} d^{-1} (FAO, 2009; Van Haarlem et al., 2008). However, previous studies showed that CH_4 ground emissions from feedlots can be quite variable, ranging from 3.8 to 38 g animal^{-1} d^{-1} (Borhan et al., 2011; Rahman et al., 2013). Aguilar et al. (2014) conducted an incubation study of soil samples from pens of the same feedlot from this study. They reported negligible CH_4 fluxes under dry conditions, but CH_4 fluxes from the soil samples reached 0.5 µmol m^{-2} s^{-1} under wet conditions. Assuming that the average stocking density during this study was similar to our study (~19 m^2 animal^{-1}), this value would be equivalent to ~13 g animal^{-1} d^{-1}. Under wet conditions and high temperature, manure can produce a significant quantity of CH_4 as it decomposes anaerobically (EPA, 2001; FAO, 2009). The high CH_4 emission values observed in August could be partially attributed to high ambient temperature and higher soil water content in the pen surface (Fig. 3.1), which resulted in higher anaerobic decomposition rates of the manure on the pen surfaces. Future studies in feedlots should monitor the soil temperature and water content in the pens to identify a possible correlation between those variables and the measured flux. Alternatively, manure could be removed from the area sampled by the tower to reduce CH_4 ground emissions from pen surfaces.

3.5. Conclusions

The source area predicted by KM01 was 5 to 6 times larger than FFP. The two pens immediately south from the flux tower, which correspond to less than 2% of the feedlot area, were responsible for 71% (FFP) and 48% (KM01) of the contributions to the measured fluxes. The results also showed that the presence of non-pen surfaces within the feedlot influenced the measured CH_4 flux. The magnitude of this effect varied substantially with the location and size of the flux footprint.

On average, F_{pens} was 8% (FFP) to 14% (KM01) higher than the raw EC flux. The monthly average F_{animal}, calculated using F_{pens} and the footprint weighed stocking density, ranged from 83 to 125 g animal^{-1} d^{-1} (KM01) and 75 to 114 g animal^{-1} d^{-1} (FFP). These emission values are consistent with the results from previous studies in feedlots. However, our results show that changes in stocking density due to animal movement in the source area are likely to affect F_{pens} and F_{animal} estimates. Additional studies are necessary to quantify the magnitude of CH_4 emission uncertainties introduced by discrepancies between footprint models and by changes in stocking density due to animal movement in the source area. Overall, our results are encouraging and provide further evidence that the EC technique could be used to measure greenhouse gas emissions from livestock systems.

Chapter 4 - Comparing methane emissions estimated using a backward-Lagrangian stochastic model and the eddy covariance technique in a beef cattle feedlot

4.1. Abstract

Accurate methodologies to measure emissions of greenhouse gases (GHG) from livestock systems are necessary to improve the emission coefficients used in national GHG inventories and to evaluate mitigation strategies. The objective of this study was to compare methane (CH_4) emissions estimated using the eddy covariance (EC) technique and a backward-Lagrangian stochastic (bLS) model. A closed-path EC system was used to measure CH_4 fluxes in a commercial beef cattle feedlot. The EC fluxes were scaled from the feedlot to the animal scale using a footprint analysis. The EC measurements of CH_4 concentration and wind data were used with the bLS model to infer CH_4 emissions. The average CH_4 emissions (± standard deviation) during the experiment were 87 (± 30) g animal^{-1} d^{-1} and 85 (± 27) g animal^{-1} d^{-1} for EC and bLS techniques, respectively. These values are consistent with the results from previous studies with similar animal and feed characteristics. Both techniques were able to capture a pronounced daytime and nighttime variation in CH_4 emissions, with higher CH_4 emissions during the day and lower emissions at night. Our results indicate that the eddy covariance technique combined with footprint models can be successfully used to accurately measure enteric CH_4 from cattle.

4.2. Introduction

Enteric fermentation, i.e., the breakdown of complex carbohydrates into simple molecules by microbes in the stomach of ruminants with production of CH_4 as a byproduct, accounts for up to one third of the global anthropogenic CH_4 emissions (IPCC, 2014). The

magnitude of CH_4 emissions from ruminants is quite variable and depends on several factors, including cattle breed, animal weight, feed intake and ration composition (Broucek, 2014). Accurate measurements of CH_4 emissions from livestock systems are necessary to evaluate mitigation strategies to reduce livestock greenhouse gas (GHG) emissions, to improve the accuracy of current GHG national inventories and whole farm models, and to understand the mechanisms controlling the CH_4 global cycle.

Chambers and the sulfur hexafluoride (SF_6) tracer technique are used to measure enteric greenhouse gas emissions from ruminants (Harper, 2005; Johnson et al., 1994; Lassey et al., 2011). These techniques are useful for comparing the effect of different diets, ration additives and genetic differences on CH_4 emissions from individual animals (Harper et al., 2011). Nevertheless, chamber and the SF_6 tracer techniques are labor intensive, often limited to a small number of animals and can interfere with animal behavior, introducing uncertainties in CH_4 emission measurements (Harper et al., 2011; Johnson et al., 1994). Micrometeorological techniques, such as backward Lagrangian stochastic dispersion analysis (bLS), mass balance and flux-gradient approaches, have been used to estimate ruminant CH_4 emissions at the farm level (Harper et al., 1999; Laubach et al., 2008; Leuning et al., 1999; McGinn et al., 2011). The major benefits of these techniques over non-micrometeorological methods are that they are non-intrusive, can be used to integrate fluxes from large herds reducing measurement uncertainties due to animal-to-animal variability, and provide high temporal resolution (< 1 h) flux measurements (McGinn, 2013).

The bLS technique is a micrometeorological method widely used to estimate CH_4 emissions from livestock systems. It requires gas concentration measurements taken downwind, within the source or upwind from the source area along with measurements of wind speed, wind

direction and turbulence statistics (Flesch et al., 2005a; Flesch et al., 2004; Flesch et al., 2005b; Flesch et al., 1995; Wilson et al., 2013). The bLS technique calculates the advection of a gas by predicting the trajectory of particles from a source to a sensor. This technique relies on the basic assumption that the flow is horizontally homogenous and is described by Monin-Obukhov similarity relationships. One of the limitations of bLS is the need to accurately measure background and downwind concentration, requiring cross-calibrations of different gas analyzers used to measure those concentrations (Laubach et al., 2013; McGinn, 2013). In addition, the accuracy of bLS estimates is compromised under low wind speeds and strong stable and unstable atmospheric stratification reducing the amount of usable data (McGinn, 2013).

The eddy covariance (EC) technique is considered the most direct meteorological method and has been widely used to measure carbon dioxide (CO_2) and energy exchange in ecosystems around the world (Baldocchi, 2003). Recently, with the development of new optical sensors, the EC technique has also been applied to quantify CH_4 emissions from livestock (Coates et al., 2018; Dengel et al., 2011; Felber et al., 2015; Prajapati and Santos, 2017; Taylor et al., 2017). Dengel et al. (2011) used the EC technique for the first time to measure CH_4 emissions from grazing sheep using an EC open-path CH_4 gas analyzer. They observed close agreement between annual CH_4 emissions per animal estimated using the EC technique and IPCC CH_4 emission estimates for sheep. However, they acknowledged that the EC CH_4 emission estimate may have been biased due to lack of information on the number of moving sheep within the flux footprint. Felber et al. (2015) used EC flux measurements, an analytical footprint model and GPS location of dairy cows to interpret CH_4 emissions estimates from a grazing system. Overall, they reported that CH_4 emissions estimated using the EC were similar to estimates reported by others (Hindrichsen et al., 2006; Münger and Kreuzer, 2006; van Dorland et al., 2007). However,

Felber et al. (2015) observed a systematic underestimation of CH_4 emission estimates from animals far from the flux tower, which they attributed to uncertainties in the analytical footprint model used to scale their fluxes. Coates et al. (2017) combined the EC technique with a Lagrangian stochastic model to estimate CH_4 emissions from eight-point sources within a limited area in a CH_4 controlled release study. They reported similar accuracy for the EC technique when compared with other micrometeorological techniques used to estimate livestock CH_4 emissions. Prajapati and Santos (2018b) compared two footprint models (Kljun et al., 2015; Kormann and Meixner, 2001) to estimate CH_4 emission from beef cattle in a feedlot. Their results showed large differences in the source areas estimated by the two footprint models. Nevertheless, their estimated CH_4 emissions per animal agreed with reported studies with similar animal characteristics and diets.

These studies show that quantifying CH_4 emissions from livestock using the EC technique are promising, but so far, the assessment of EC performance to estimate CH_4 emissions from cattle has been restricted to comparisons with CH_4 emissions from previous studies and estimates based on animal diet and intake. Evaluations of the EC technique and other herd-scale micrometeorological techniques are necessary to identify the potential sources of error and to evaluate the performance of the EC method under a wide range of atmospheric conditions. Large commercial feedlots where thousands of heads of cattle are confined to a well-defined area provide a unique experimental site for comparing the EC technique with the bLS model. The objective of this study was to compare CH_4 emissions obtained using the EC technique combined with a footprint analysis (EC_{FFP}) with CH_4 emission estimates provided by the well-stablished bLS model.

4.3. Material and Techniques

4.3.1. Experimental site description

Field measurements were conducted at a commercial beef cattle feedlot in Kansas from August 2013 to May 2014. The site is 622 m above sea level over a near flat terrain (slope < 5%). The monthly average air temperature during the measurement period ranged from 2 to 26 ^{o}C and accumulated monthly precipitation varied from 7 to 83 mm (National Climatic Data Center, 2017). The feedlot has a total surface area of approximately 59 ha with a holding capacity of approximately 30,000 animals. Roads and alleys used for cattle and feed transportation account for approximately 21% of the total feedlot surface area. The pens near the flux tower, which were expected to contribute to the majority of the measured fluxes, were occupied by steers and heifers weighing 350 kg on average at the beginning of the experiment. The cattle were fed a corn-product based died. Further information on the ration composition is provided by Prajapati and Santos (2018b). The total feedlot occupancy was 24,116 animals during the summer and early fall months (August 2013 to November 2013) with an average stocking density of 19 m^2 $animal^{-1}$ (~ 526 animals ha^{-1}). In the late fall and spring months (December 2013 to April 2014), the number of animals was reduced by about 15% resulting in an average stocking density of 22 m^2 $animal^{-1}$ (~455 animals ha^{-1}).

4.3.2. Flux measurements and calculations

A detailed description of the flux measurements and calculations at the experimental site is provided by Prajapati and Santos (2017). Here, we summarize the description of these measurements for completeness. Fluxes of CH_4 were measured using a closed-path EC system. The wind velocity components (*u, v, w*) and sonic temperature were measured with a sonic anemometer (CSAT3, Campbell Sci., Logan, UT). A wavelength-scanned closed-path analyzer

(G2311-f, Picarro Inc., Santa Clara, CA) was used to measure CH_4, CO_2 and H_2O mixing ratios. In this study, only CH_4 mixing ratios were used for flux calculations.

The closed-path analyzer air intake consisted of a rain diverter connected to an in-line filter (Polypropylene/polyethylene 10 µm membrane, Pall Corporation, AnnArbor, MI). The downstream part of the filter was attached to a 7-m long high-density polyethylene tube with an inner diameter of 5.3 mm. The other end of this tube was connected to a second filter (Acrodisc Gelman 1µm, PTFE membrane, Pall corporation) that was attached to the gas analyzer inlet. The sampling line was heated to prevent condensation of water on the tube walls. The flow rate within the sampling tube was maintained at 5 L min^{-1} using the closed-path analyzer internal mass flow controller and a vacuum pump (Vacuubrand GmbH, Wertheim, Germany). Field calibrations were performed at least every two weeks using certified calibration gas (CH_4 at 1.9 and 4.0 ppm, ±1%). The anemometer and the gas analyzer air intake were mounted on the tower at 5 m above the ground at the northern edge of the feedlot. All the data were recorded at 10 Hz using a datalogger (CR1000, Campbell Sci.).

The high frequency data from the sonic anemometer and gas analyzer were initially tested for time stamp consistency to identify possible gaps in the data series. Next, calibrations were applied to the concentration files using a custom Matlab code (version 8.3.0.532, The Mathworks Inc., Natick, MA). Half-hourly CH_4 fluxes were then calculated using an EC software application (EddyPro, v. 6.0, Licor). The CH_4 flux calculations followed the common procedures for EC flux calculations: spike removal, double coordinate rotation, time lag compensation (Fan et al., 1990) and spectral corrections (Horst, 1997). Typical spectral corrections ranged from 20% to 30% during the experiment. Prajapati and Santos (2017) observed the closed-path analyzer CH_4 and CO_2 frequency responses were similar and reported

good agreement (slope = 1.05) and correlation (R^2 = 0.98) between CO_2 fluxes measured using the same closed-path analyzer and an established EC open-path analyzer (LI-7500, LI-COR Biogeosciences, Lincoln, NE). These previous results show that the closed-path EC system is capable of providing reliable EC measurements.

The quality control system developed by Foken et al. (2004) was used to eliminate half-hourly periods in which the atmospheric conditions were unsuitable for EC measurements.

4.3.3. Scaling of raw EC flux to flux per animal using flux footprint model

Fluxes measured using the EC technique were scaled from the feedlot scale to the animal scale based on the relative contributions of pens and non-pen surfaces within the feedlot to the measured flux, following Neftel et al. (2008) and Baum et al. (2008). Further details on the flux scaling approach is provided by sections 3.3.5 and 3.3.6 of chapter 3.

4.3.3.1. Kljun et al. (2015) flux footprint parameterization

A parameterized version of a two-dimensional footprint model developed by Kljun et al. (2015), FFP was used to estimate the source area distribution contributing to the measured EC fluxes. The FFP model is based on the Lagrangian stochastic particle dispersion footprint model by Kljun et al. (2002) and is applicable to a broader range of boundary layer conditions compared to the footprint parameterization by Kljun et al. (2004). A detail description of the model and calculation of model input parameters are given in section (3.3.3) of this dissertation.

4.3.3.2. Estimating methane emission rate per animal

The relative contribution of pens was estimated using the FFP model and raw EC CH_4 fluxes were used to estimate CH_4 emission rate per animal as described in sections 3.3.5 and 3.3.6 of this dissertation.

4.3.4. Estimation of CH_4 emissions using the backwards-Lagrangian Stochastic technique

Methane emission rates were calculated in 30-min time increments using the bLS model (Flesch et al., 2004; Flesch et al., 1995). A brief overview of the underlying concepts of this inverse model is provided in this section. In the bLS model, the relationship between a tracer gas emission rate (Q; g m^{-2} day^{-1}) and the resulting increase in downwind concentration (C; g m^{-3}) from an source area is estimated by modelling trajectories of particles "released" from the concentration sensor and followed upwind to the source region (Flesch et al., 1995). The bLS model accounts for the location of the particles' impact with the ground and the subsequent reflection of the particles back into the atmosphere. This information is used to define the ratio of the modeled concentration to the emission rate $(C/Q)_{\mathrm{sim}}$ as follows:

$$(C/Q)_{\mathrm{sim}} = \frac{1}{N}\sum \frac{2}{|w_0|} \tag{4.1}$$

where N is the number of simulated particles released and w_0 is the vertical particle velocity at touchdown. Only the realized particles that touchdown within the source area, and therefore contribute to trace gas fluxes, are included in the inner summation in Eq. 4.1. For each 30-min simulation, N = 50,000 particles were released. The estimation of $(C/Q)_{\mathrm{sim}}$ requires the prior knowledge of turbulence statistics for the surface layer. The quotient $(C/Q)_{\mathrm{sim}}$ is then used to estimate the trace gas emission rate as follows:

$$Q = \frac{C - C_{\mathrm{b}}}{(C/Q)_{\mathrm{sim}}} \tag{4.2}$$

where C_b is background CH_4 concentration.

The CH_4 emission rate expressed in g animal^{-1} day^{-1} is calculated using the average stocking density in the source area, as follows:

$$F_{\text{animal}} = \frac{A_{\text{t}}}{N} Q \tag{4.3}$$

where, A_t is the total pen area and N is the number of cattle in the feedlot.

In our study, the bLS calculations were performed using the software WindTrax (v. 2.0.8.9, Thunder Beach Scientific, Nanaimo, Canada). The bLS simulations require the specification of turbulence statistics for the surface layer. The average wind velocity and air temperature (T_a); variances and covariances of temperature and wind velocity data were derived from the sonic anemometer measurements. The wind velocity data were processed using the software EddyPro, using the following steps: the sonic anemometer diagnostic flag was used to screen the high frequency data, spikes were removed, a double rotation method was applied to the wind velocity components and then wind statistics were calculated for 30-min intervals.

In addition, the spatial dimensions and location of the feedlots pens (source area) and the position of the wind velocity and concentration measurements were also specified in the WindTrax project map. Since CH_4 concentrations were measured by a single gas analyzer at the north edge of the feedlot, we had to rely on a conditional sampling approach i.e., concentration data associated with northerly wind directions were assumed to represent the background concentration and the upwind concentration was associated with southerly winds (see section 4.3.5).

The data were screened following Flesch et al. (2004) and flux values were removed when: 1) $u_* < 0.15$ m s^{-1}, 2) $|L| \leq 2$ m (strongly stable/unstable atmosphere) and 3) where $z_0 \geq 1$ m (error associated with wind profile calculations).

4.3.5. Background CH_4 concentration

The bLS technique implementation requires measurements of the background and either in-source or downwind concentrations of the gas of interest (Eq. 4.1). The CH_4 concentration was measured at a single point at the northern edge of the feedlot (Fig 4.1). The CH_4 background concentration was determined using a conditional sampling procedure based on wind direction (Wilson et al., 2013). Measured concentrations associated with periods of northerly winds flowing over agricultural fields were assumed to represent the background concentration (Fig 4.1).

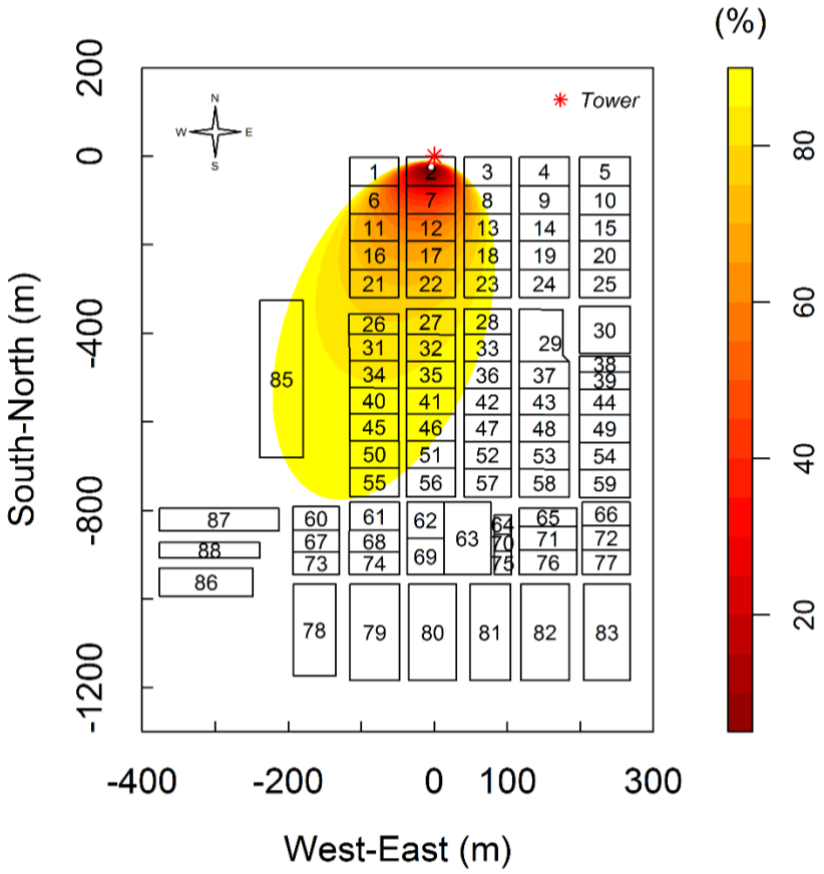

Figure 4.1. Schematic diagram showing a flux footprint overlaid over the feedlot. The footprint contour lines range from 10% to 90%. The location of the tower is represented by the asterisk in the map. The polygons in feedlot map show different feedlot surfaces. The polygons: 63, 85, 86 and 87 represent run-

off water storage lagoons and the polygon 30 represents a barn. The other remaining numbered polygons represent pens. Roads and transfer alleys are located among pens and around the edges of the feedlot.

The background gas concentration was derived using periods with northerly wind directions (300° - 60°). The bLS simulation was conducted on days with northerly wind directions that were followed by a day with southerly wind direction (120° - 240°). Only a small portion of data out of the total data period met this criterion (section 4.5.2). We relied on the assumptions that in the absence of strong sources or sinks of CH_4 in the fields surrounding the feedlot, the CH_4 background concentration did not change substantially within a 24-hour period. This is a reasonable assumption as fields located north of the feedlot had negligible CH_4 fluxes (~2% of feedlot flux magnitudes) in comparison to the feedlot fluxes (Prajapati and Santos, 2018b).

4.4. Statistical analysis

The Pearson and concordance coefficients were calculated for the relationship between bLS and EC CH_4 emissions following Lawrence and Lin (1989). The Pearson coefficient indicates the precision of CH_4 emission estimates by the EC technique, while the concordance coefficient was used to determine accuracy by quantifying the best-fit line deviation from the 1:1 line. Significant differences were declared at $P < 0.05$.

4.5. Results and Discussions

4.5.1. Methane concentration temporal and spatial dynamics

The average CH_4 mixing ratio (± standard deviation) for southerly (90°– 269°) and northerly (270° – 89°) wind sectors were approximately 2.7 ± 0.5 µmol mol^{-1} and 1.9 ± 0.1 µmol mol^{-1} respectively. The CH_4 mixing ratio for the northern sector typically ranged from 1.8 to 2.1

μmol mol^{-1}, with the exception of a few days in summer when cattle were present in the agricultural fields at the Northern edge of the feedlot. Only periods with CH_4 EC fluxes smaller than 0.5 μmol m^{-2} s^{-1} were included in the bLS calculation since higher flux values were likely caused by the presence of cattle outside the feedlot. High CH_4 mixing ratios (> 3 μmol mol^{-1}) were associated with light southerly winds occurring usually during the night (Fig. 4.2).

The average background CH_4 concentration was slightly lower (~1.92 μmol mol^{-1}) during the day in comparison to nighttime (~1.95 μmol mol^{-1}). These differences in CH_4 concentration between day and night periods can be explained by the atmospheric boundary layer dynamics. Stieger et al. (2015) measured the CH_4 concentrations from a grazing system in Switzerland using vertical CH_4 concentration profiles within the atmospheric boundary layer. They found that the CH_4 concentration remained relatively low (~ 1.9 ppm) during the daytime and was higher at night (~3.1 ppm). They attributed these diel differences in CH_4 concentration to convective mixing during the daytime and entrapment of CH_4 emissions within the stable nocturnal boundary layer at nighttime. In this study, the small variation in CH_4 concentration between daytime and nighttime confirms the absence of strong sources or sinks of CH_4 in the agricultural field located north of the feedlot.

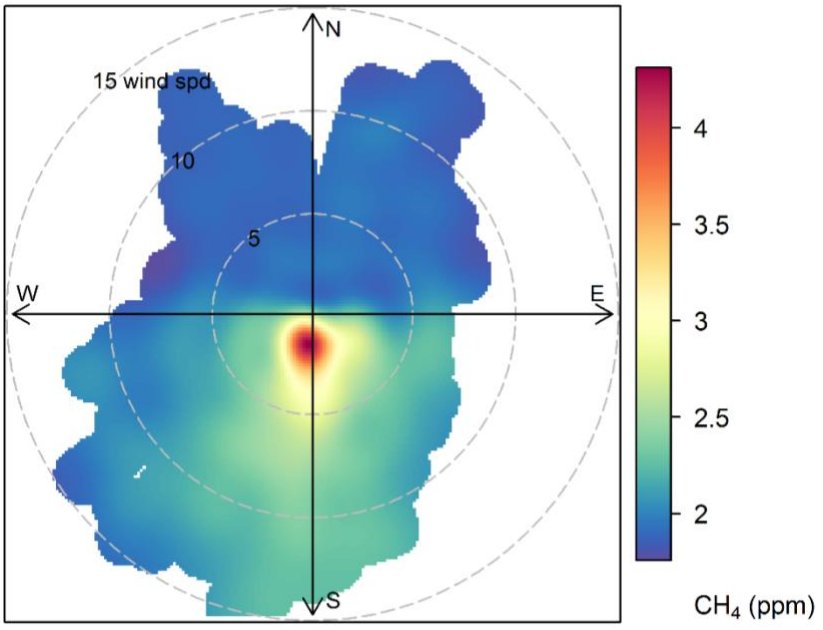

Figure 4.2. Relationship between CH_4 concentration (µmol mol^{-1}), wind speed and wind direction. The outline of the colored area indicates the maximum observed wind speed for each wind direction. The colored area indicates the average weighted CH_4 concentration associated with different wind speeds and directions.

4.5.2. Data screening

After applying the EC quality control screening criteria, 4377 half-hourly periods were associated with wind originating from the southern sector (90º – 269º, feedlot) and 2959 periods were with wind originating from the northern sector (270º – 89º, agricultural fields). Data were retained (1634 half-hour periods) based on wind direction (as in section 4.3.5) to obtain the CH_4 background concentration. About 8% of these data points were removed based on atmospheric turbulence and stability conditions as suggested by Flesch et al. (2004), described in section 4.5.2. Approximately 31% (Ω_{80}) and 49% (Ω_{90}) of the 30-min data were excluded due to fetch requirements using the FFP model (section 4.3.3.1). The exclusion of data points for fetch-limited periods were aimed to increase the representativeness of the EC measurements, i.e., the degree to which the flux measurements are influenced by surface area of the interest, as

discussed in chapter 3. The data screening described above was based on the source areas contributing to 80% (Ω_{80}) and 90% (Ω_{90}) of the measured EC flux, resulting in the retention of a total of 992 (Ω_{80}) and 695 (Ω_{90}) half-hourly periods.

4.5.3. Influence of diel variation in background concentration on bLS estimates

The bLS technique implementation requires measurements of horizontal gas concentration gradients which are usually obtained using arrays of line-averaging concentration sensors located downwind or within the source area, and upwind from the source area (Flesch et al., 2004; Flesch et al., 2007; Laubach et al., 2013; Loh et al., 2009). In our study, single point concentration measurements, obtained using a close-path analyzer, were used to determine downwind and background CH_4 concentrations by assuming that the background concentration variation over a 24-hour period was negligible (section 4.3.5). This assumption is likely to increase uncertainties in Q estimation (Eq. 4.2). To quantify Q uncertainties related to C_b temporal variability, the diel fractional uncertainty of Q values (D_Q) was estimated using the C_b ensemble half-hourly standard deviation (D_{C_b}), as follows:

$$D_Q = D_{C_b}/C - C_b \quad (4.4)$$

The estimated values of D_Q ranged from 5 to 15% in this study. Nonetheless, the uncertainties in D_Q estimated by Eq. 4.13 are also driven by $C - C_b$. Furthermore, D_Q decreases when $C - C_b$ or scalar fluxes are large. The term $C - C_b$ is largely affected at the feedlot by wind speed and direction and atmospheric stability conditions (Fig. 4.2). Smaller values of $C - C_b$ under certain wind directions are expected to increase the uncertainties in bLS estimates.

4.5.4. Comparisons between EC and bLS technique CH_4 emissions

The use of the scaling approach described in section 4.3.3 requires the definition of the source area bounded by the footprint model isopleth (Fig. 4.1) which is done by selecting a

fraction (*P*) of the source area contributing to the large majority of the observed fluxes. Kljun et al. (2015) recommended that for FFP, values of *P* should be smaller than 90% and that a *P* of 80% should be suitable to define the outer limit of the source area (Ω_P) for most applications. We investigated the effect of Ω_P to screen the flux data for fetch limitations. In addition, we examined the influence of the scaling approach (section 4.3.3) on the agreement between EC and bLS techniques. To do that, EC data were initially screened for fetch limitations using Ω_{80} or Ω_{90}. Then we compared unscaled and scaled EC F_{animal} estimates with F_{animal} estimated using the bLS technique. Unscaled flux computations did not account for the influence of non-emitting surfaces within the feedlot on measured EC fluxes. Furthermore, unscaled fluxes were estimated using the average stocking density in the feedlot instead of the footprint averaged stocking density. On the other hand, scaled fluxes were calculated following the procedures described in section 4.3.3.

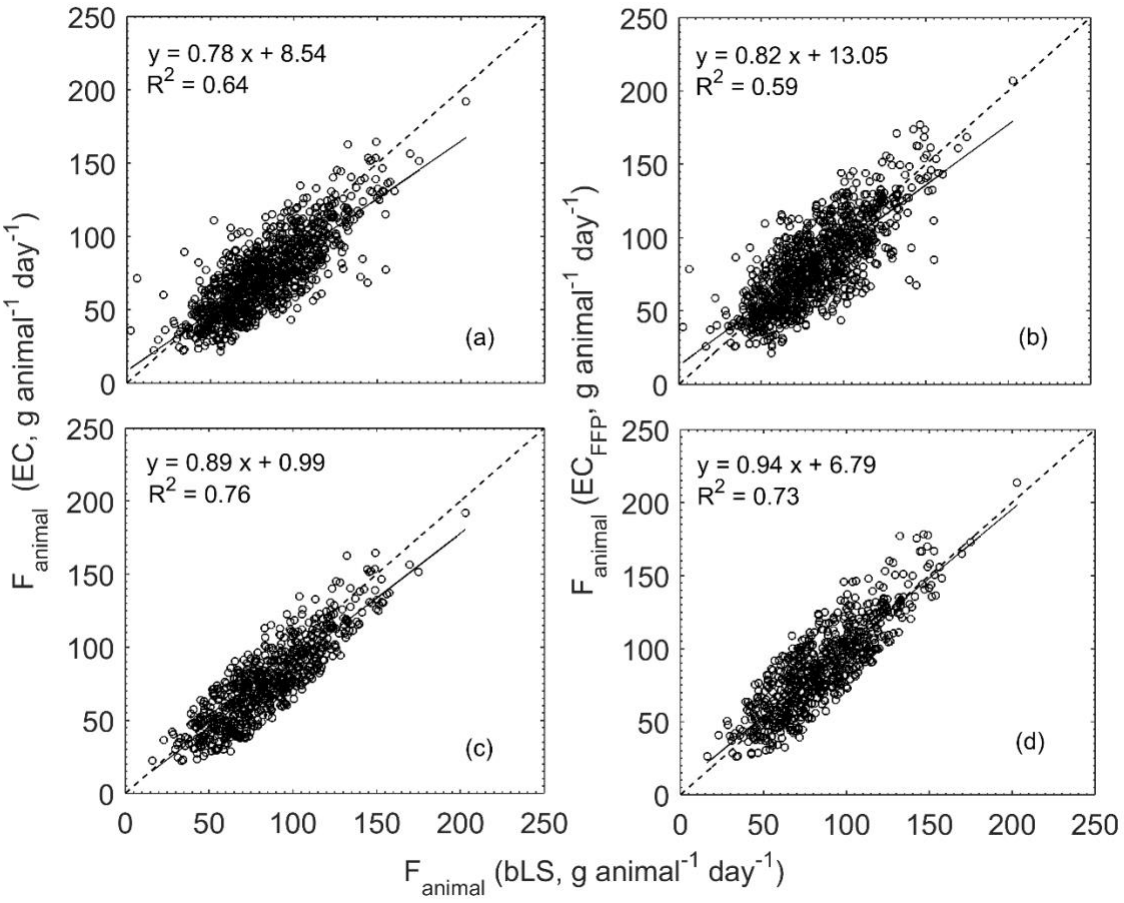

Figure 4.3. Relationships between CH_4 animal emissions (F_{animal}) estimated using the bLS technique and F_{animal} estimated using unscaled (EC, a and c) and scaled (EC_{FFP}, b and d) eddy covariance fluxes. The eddy covariance fluxes were scaled and/or screened for fetch limitations based on the estimated source area contributing to 80% (a and b) and 90% (c and d) of the measured flux, estimated using a flux footprint parameterization (Kljun et al., 2015).

The R^2 value, expressing the strength of the linear relationship between EC F_{animal} and bLS F_{animal} values, was greater when using Ω_{90} (Fig. 4.3c) than when Ω_{80} was used to screen the EC flux data (Fig. 4.3a). The footprint scaling approach improved the agreement between bLS and EC_{FFP} estimates while slightly reducing the correlation (R^2) between bLS and EC_{FFP} F_{animal} estimates (Fig. 4.3b and d). The Pearson coefficient (r), which expresses the precision of EC_{FFP} F_{animal} estimates in relation to bLS estimates, was 0.76 and 0.85 for EC fluxes screened and

scaled using FFP estimates of Ω_{80} and Ω_{90}, respectively (Table 4.1). The EC_{FFP} estimates also showed good accuracy, expressed by the bias correction factor (C_f), when compared to bLS emissions. The concordance coefficient was greater using Ω_{90} (0.84) than for Ω_{80} (0.72) when deriving EC F_{animal}.

Table 4.1. Pearson and concordance coefficient for the relationship between CH_4 animal emission rates estimated using a backward-Lagrangian model and the eddy covariance technique combined with a flux footprint model (EC_{FFP}). The EC_{FFP} fluxes were scaled based on the source area contributing to 80% (Ω_{80}) and 90% (Ω_{90}) of the observed fluxes.

Parameter	Ω_{80}	Ω_{90}
No of half hours	992	695
Pearson coefficient (r)	0.76	0.85
Bias correction factor (C_f)	0.95	0.99
Concordance coefficient (r. C_f)	0.72	0.84

Our results confirm that the effect of non-emitting surfaces within the feedlot should be taken into account when scaling fluxes from landscape to pen or animal scales. Baum et al. (2008) aggregated the results of a one-dimensional footprint model to scale CO_2 fluxes measured using the EC technique above a feedlot. They found that scaling EC fluxes using their flux footprint approach resulted in an increase of 11–31% of the measured EC fluxes. More recently, Prajapati and Santos (2018b) used a two-dimensional footprint analysis to scale CH_4 emissions estimates in the same feedlot as the one in this study. They found that the footprint scaling factor, which is determined by the relative contribution of non-emitting surfaces to the measured EC fluxes, ranged from 0 to 27%, depending on the wind direction and atmospheric conditions. The good agreement between bLS and EC_{FFP} (Table 4.1) is encouraging and shows that this scaling approach is a viable option to use the EC technique for locations in which the underlying

surfaces over which fluxes are measured violates the surface homogeneity assumptions for the EC method.

4.5.5. Influence of the source area on the relationship between EC and bLS CH_4 emissions

The footprint distances for Ω_{90} (x_{90}) and Ω_{80} (x_{80}) were 471 and 227 m, respectively (Fig 4.4). The greater values for EC_{FFP}/bLS (>1.6) were associated with easterly winds while lower EC_{FFP}/bLS values (< 0.8) were generally associated with higher x_{80} and x_{90} values. The adoption of Ω_{90} to screen and scale EC fluxes eliminated most of the highest values of EC_{FFP}/bLS resulting in good agreement (C_f = 0.99, Table 4.1) between EC_{FFP} and bLS F_{animal} estimates.

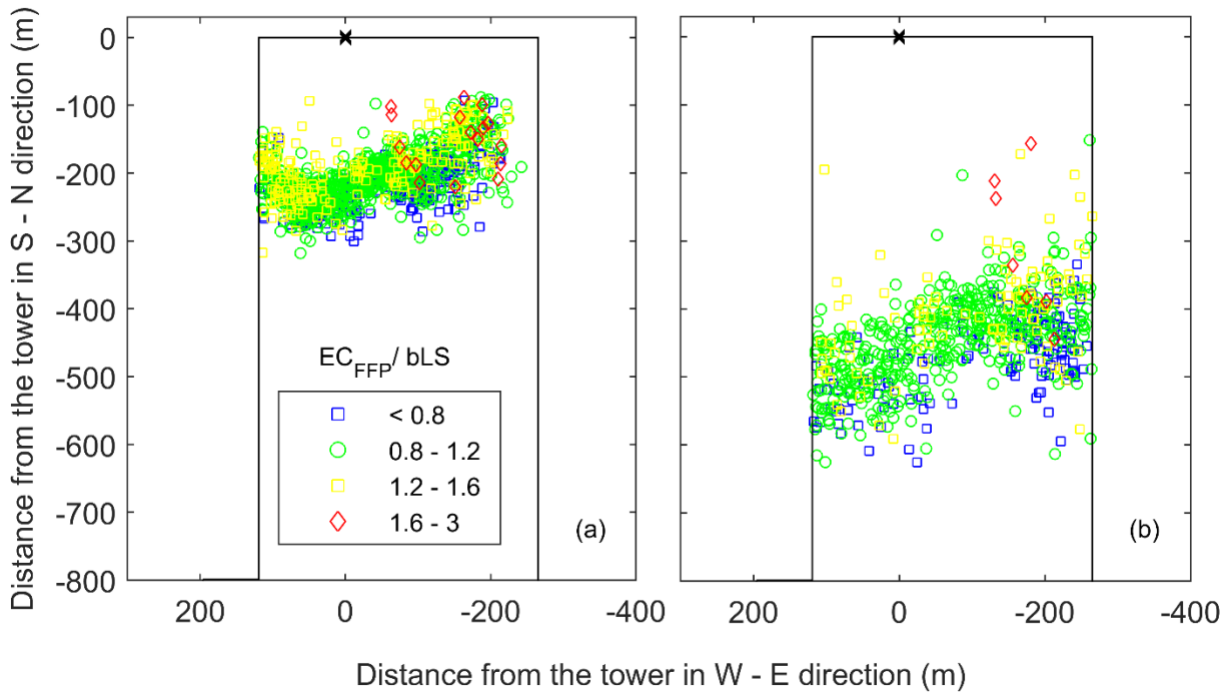

Figure 4.4. Relationship between EC_{FFP} and bLS CH_4 animal emission estimates and the maximum extent of 80% (a) and 90% (b) crosswind-integrated footprints estimated using the FFP model. The flux tower location is represented by the "x" in the graph and the feedlot border is shown by the larger rectangle within the figure.

We hypothesize that three main factors could explain the dependence between bLS and EC F_{animal} estimates agreement and the Ω_P value: 1) enhancement of the spatial representativeness of EC measurements by using a more rigorous fetch screening criterion, based on Ω_{90}; 2) reduction of bLS uncertainties by indirectly increasing the number of "touch-downs" within pen surfaces by using a stricter fetch criterion; and 3) improvement in the agreement between source areas influencing bLS and EC_{FFP} F_{animal} estimates, by screening out EC and bLS flux measurements from periods in which fluxes were from areas with higher source heterogeneity, i.e. with higher contribution from non-emitting surfaces in the feedlot.

The source area concept can be used to estimate the spatial representativeness of flux measurements by determining the most dominant surfaces contributing to scalar fluxes (Schmid, 1997). Prajapati and Santos (2018b) used FFP to estimate the source area in this feedlot and determined that beyond Ω_{80}, the contributions to the measured fluxes were negligible (< 1%) in relation to the source weighting value at the FFP source weighting function peak location. Consequently, a scalar point source located beyond Ω_{80} needs to be approximately 100 times stronger than a point source at isopleth Ω_{10}, where the peak value of the footprint function is found, to have the same effect on the measured fluxes. In this feedlot, CH_4 fluxes originating from agricultural field located north of the feedlot corresponded to approximately 2% of the magnitude of fluxes from the feedlot (Prajapati and Santos, 2018b). Considering the large discrepancies between CH_4 source strengths, contributions from agricultural fields around the feedlot may have introduced uncertainties in F_{animal} estimates. Therefore, a more rigorous fetch screening criterion, i.e. Ω_{90}, may be necessary to minimize the influence of non-emitting surfaces beyond the feedlot boundaries on the measured fluxes. However, the comparison of EC_{FFP} F_{animal} estimates scaled using Ω_{80} and Ω_{90} showed excellent agreement (slope = 0.99, R^2 = 0.99; data not

shown). This is due to the fact that the data used for the comparison does not include 30-min periods with presumably larger influence from non-emitting surfaces outside the feedlot. Those 30-min periods, associated primarily with southeast winds, were excluded using the fetch criterion based on Ω_{90}. Additional studies are needed to further investigate the influence of the source area extent on scaled EC fluxes.

Depending on the wind direction, the number of "touch-downs" within feedlot pens was reduced due to the presence of roads and areas extending beyond the feedlot boundaries. Flesch et al. (2007) used the bLS technique to estimate NH_3 emissions from a feedlot in Texas. They observed that for some wind directions, the NH_3 simulated plume only glanced the path of their open-path lasers. Under those conditions, the bLS technique accuracy according to Flesch et al. (2007) is compromised due to three factors: 1) the plume edge trajectories are less predictable resulting in greater emission uncertainties, 2) the spatial representativeness of bLS estimates is also compromised since the plume scalar concentration is influenced by a smaller pen surface area and 3) small errors in wind direction observations can lead to large errors in emission estimates. To minimize these issues, Flesch et al. (2007) removed periods in which number of touch-downs were less than 10% of the pen area. In this study, the number of touch-downs within the feedlot was indirectly increased by adopting a stricter fetch screening criterion based on Ω_{90} (Fig. 4.4).

Furthermore, discrepancies between the EC and bLS technique source areas are likely to affect the agreement between F_{animal} estimates provided by the two techniques. The bLS model uses the scalar concentration measurements within an emission plume to infer the emission rate of a source area based on the concentration footprint (Flesch et al., 2004). On the other hand, the EC instrumentation provides a more direct measurement of scalar fluxes, which can be scaled

from landscape to source scale emissions using a flux footprint model (section 4.3.3). Schmid (1994) demonstrated through model simulations that source areas for fluxes (e.g. EC technique) tend to be smaller by one order of magnitude than concentration source areas (bLS approach). Therefore, discrepancies between flux and concentration source areas were likely to affect the agreement between EC and bLS estimates in this study because the two methods are essentially estimating fluxes from different areas in the feedlot.

The near-rectangular shape of the feedlot in this study as well as the presence of main roads and transfer alleys running in the north-south directions (Fig. 4.1) leads to considerable variability of the source area with the wind direction. The effect of this variability on CH_4 emission estimates can be quantified by estimating the magnitude of the EC_{FFP} scaling factor (*SF*), given by Eq. 3.11 in chapter 3.

Fig. 4.5 shows that *SF* increased as the wind direction departed from the south owing to growing contributions from non-emitting surfaces within this feedlot to the measured fluxes. Based on these results, we would expect greater differences between flux and concentration source areas to occur as the source area became more heterogeneous, i.e. as the wind direction departed from the south. The use of Ω_{80} to screen fluxes included more half-hour periods with greater influence from roads and alleys and areas outside the feedlot and, consequently, greater *SF* (up to 30%) than for fluxes screened using Ω_{90}. This likely resulted in greater differences between bLS and EC_{FFP} source areas, consequently affecting the agreement between the two techniques (Fig. 4.3b). Conversely, a better agreement between the two methods is expected when bLS and EC_{FFP} sampled more homogenous areas in the feedlot (Fig. 4.3d) with lower *SF*. The results shown in Fig. 4.5 also indicate considerable run-to-run variation for F_{animal} ratio.

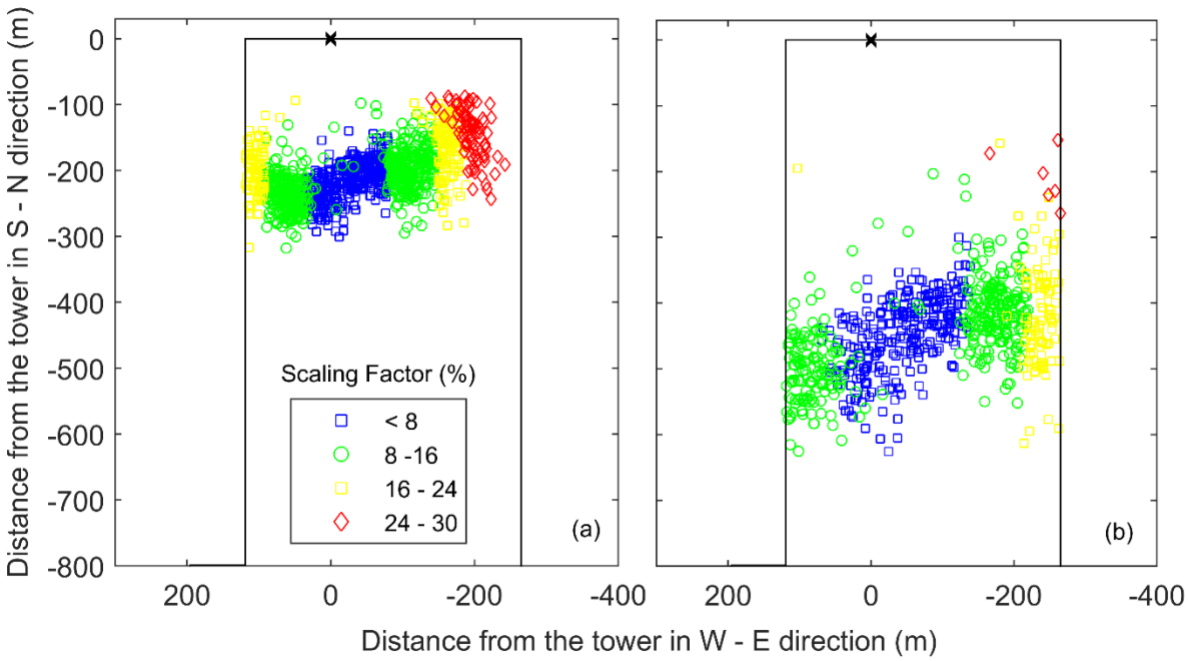

Figure 4.5. Relationship between the eddy covariance flux scaling factor and the extent of 80% (a) and 90% (b) crosswind-integrated footprints estimated using the FFP model. The flux tower location is represented by the "x" in the graph and the feedlot border is shown by the larger rectangle within the figure.

This high variability in CH_4 emissions over short time scales (30-min) is in agreement with the results by Laubach et al. (2013) who compared-herd scale techniques to estimate CH_4 emissions from cattle, including the bLS technique. They also found high run-to-run variability among different techniques, which they attributed to several possible reasons: real changes in animal emissions related to digestion processes, instrument random error, influence of wind speed and direction on the ability of the instruments to resolve gradients of concentration, differences in source area among different methods, and variability in the source location due to animal movement. Prajapati and Santos (2018b) evaluated how the half hour emission estimates from EC_{FFP} technique depend upon half-hourly footprint area. Their emission estimates showed higher fluctuation for a smaller footprint area compared to a larger footprint area. Most of these fluctuations were associated with feeding times when the animals were usually concentrated near

feed bunks. This indicates that animal movement introduces uncertainties in the EC measurements by altering the stocking density in the flux footprint.

4.5.6. Diel CH_4 emission patterns

The CH_4 emissions showed a similar diel trend for both techniques (Fig. 4.6). Daily mean emission values ± standard deviation ranged from 44 ± 10.1 to 115.8 ± 34.7 g animal^{-1} d^{-1} and 50.5 ± 16.4 to 114.6 ± 40.9 g animal^{-1} d^{-1}, for EC_{FFP} and bLS, respectively. Night time F_{animal} values were significantly lower (EC_{FFP}: 80.9; bLS: 81.5 g animal^{-1} d^{-1}) than the daytime (0800 – 2000 h) CH_4 F_{animal} (EC_{FFP}: 100.4; bLS: 94.2 g animal^{-1} d^{-1}) when tested with a two-sample t-test at a 5% significance level. Both techniques were able to detect a distinct CH_4 emission peak close to the feeding times. During the study period, cattle were fed at three different periods throughout the day: 0600 to 0830, 1100 to 1330, and 1500 to 1730. The average F_{animal} (± standard deviation) estimated using the EC_{FFP} technique was 86.8 ± 30.3 g animal^{-1} d^{-1} and 84.8 ± 27.4 g animal^{-1} d^{-1} for the bLS technique. Differences between the ensemble F_{animal} value estimates by the two methods (2.3%) were not statistically significant when tested with a two-sample t-test at a significance level of 0.05.

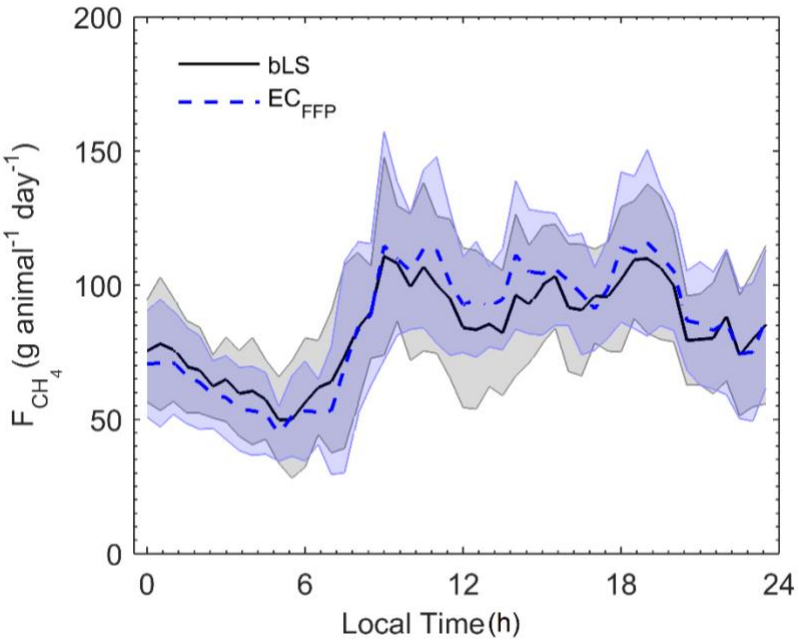

Figure 4.6. Composite diel CH_4 animal emissions (F_{animal}) in the feedlot estimated using a backward-Lagrangian model (bLS) and the eddy covariance technique combined with a flux footprint parameterization (EC_{FFP}). The EC_{FFP} estimates were scaled based on the source area contributing to 90% of the total flux. The shaded areas show ±1 SE (standard error) for EC_{FFP} (blue area) and bLS (grey area) CH_4 animal emission rates.

The diel CH_4 emission patterns in the feedlot are in agreement with results reported in the literature and are related to animal metabolism and feeding times (Dengel et al., 2011). Similar relationship between CH_4 emissions and feeding time has been reported in previous CH_4 emission studies for: confined dairy cattle (Gao et al., 2011; Jungbluth et al., 2001; Kinsman et al., 1995), grazing cattle (Felber et al., 2015; Harper et al., 1999), grazing sheep (Lockyer and Champion, 2001) and beef cattle feedlots (Van Haarlem et al., 2008). Furthermore, our results show that both EC and bLS technique were able to capture the expected CH_4 temporal patterns over a wide range of atmospheric conditions occurring during the daytime and at nighttime at the experimental site.

4.5.7. Comparative advantages and limitations of EC and bLS techniques

The bLS source area is expected to be larger than the source area influencing EC fluxes (section 4.5.5). The smaller EC source area can have implications on the sensitivity of the EC technique to animal movement at the feedlot. For small footprints, the source weight of each animal in the source area is relatively large. Therefore, under those conditions animal movement can result in large uncertainty in EC F_{animal} estimates. Considering that the bLS technique source area is much larger than the area contributing to EC fluxes, we would expect the bLS estimates to be less sensitive to animal movement in comparison to the EC measurements. Fortunately, the EC source area can easily be increased by raising the height of the EC instrumentation. A possible disadvantage of this approach is the reduction of data retention due to fetch limitations. In this feedlot, the deployment of the flux tower in the middle of the feedlot could result in larger data retention by minimizing the influence of areas outside the feedlot to our flux measurements.

Recent studies showed the dependence of the eddy covariance F_{animal} estimates on the accuracy of the footprint model estimates (Felber et al., 2015; Prajapati and Santos, 2018b). Felber et al. (2015) used the EC technique and an analytical footprint model to estimate CH_4 emissions from dairy cows. They observed that the CH_4 emissions from cows far from the tower were underestimated as a result of the overestimation of footprint weights downwind from the footprint function peak. Prajapati and Santos (2018b) compared F_{animal} estimates obtained from scaled EC fluxes using two footprint models. They reported differences in the extent of the source area predicted by the footprint model as well as in their F_{animal} estimates. These results indicate the need for studies on the experimental validation of footprint models and the quantification of uncertainties of those models; however, such studies are still rare (Arriga et al., 2017; Foken and Leclerc, 2004; Vesala et al., 2008). The bLS technique also relies on a

Lagrangian stochastic scalar concentration footprint model to infer scalar fluxes. Lagrangian stochastic models provide a more sophisticated description of the turbulent transport in the atmosphere than analytical models (Kljun et al., 2015; Wilson, 2015). The disadvantage of Lagrangian Stochastic models is their higher computational demand. An alternative could be the use of parameterizations of Lagrangian Stochastic models, such as FFP, that retain some of the skills of the more sophisticated Lagrangian models but allow for footprint computations (Schmid, 2002).

In terms of instrumentation, the EC technique only requires measurement of concentration and wind turbulence at a single point at time scales relevant for the turbulent transport (> 5 Hz). On the other hand, the bLS technique requires at least two concentration measurements (C and C_b), which are often measured using two line-averaging analyzers located upwind, in-source area in addition to downwind of the source (Flesch et al., 2007; Laubach et al., 2013; Todd et al., 2014). This setup requires regular cross-checks between gas analyzers to ensure good accuracy of bLS estimates by minimizing biases among gas analyzers (Laubach et al., 2013). In addition, line averaging sensors require careful alignment of laser emitter and retroreflector and their measurements may be affected by dust and precipitation, which may impose some challenges for the use of the bLS for continuous gas emission monitoring over long periods of time. Conversely, the calibration of an EC closed-path gas analyzer, such as the one of this study, can be automated using a multi-port manifold. In addition, closed-path gas analyzers are less prone to data losses during rainy periods and dust accumulations in sensor optical components. Nevertheless, the dusty conditions of the feedlot of this study required constant replacement (at least once every other week) of the air intake filter to ensure a constant flow rate in the sampling line and to maintain pressure in the analyzer cavity within the operating range.

4.6. Conclusions

Methane emissions from beef cattle in a feedlot were estimated using the bLS and EC techniques. The EC fluxes were scaled from landscape scale to animal scale using a parameterization of a Lagrangian stochastic footprint model. The results from EC and bLS comparisons show the need to consider the influence of non-emitting surfaces within the feedlot when scaling fluxes from feedlot to animal scales. In addition, better agreement between bLS and EC_{FFP} F_{animal} estimates was achieved by using a more restrictive fetch screening criterion, based on Ω_{90}. Daily mean emission values ± standard deviation ranged from 44 ± 10.1 to 115.8 ± 34.7 g animal^{-1} d^{-1} and 50.5 ± 16.4 to 114.6 ± 40.9 g animal^{-1} d^{-1}, for EC_{FFP} and bLS, respectively. Average emission values based on EC_{FFP} were not significantly different from bLS estimates despite fetch limited conditions in the feedlot and the difference in footprint functions used by bLS and EC_{FFP} techniques. Nonetheless, additional studies are still needed to quantify the uncertainties of flux footprint models at the field scale and to investigate the uncertainties caused by animal movement on the CH_4 emission measurements.

The results from this study indicate that the eddy covariance technique is a viable option to quantify gas emissions from a feedlot. The combination of EC flux measurements and footprint analysis can be applied to scale emissions of other trace gases, e.g. ammonia, N_2O, CO_2, etc., per source area allowing comparisons among different livestock systems. Algorithms for modelling 2-D flux footprint models could be included in EC computation software packages allowing easier scaling of EC fluxes. Moreover, the use of the EC approach can be particularly useful in grazing systems where small gradients of concentration make the implementation of other micrometeorological techniques difficult, such as the bLS approach. In those systems, however, tracking animal positions may be necessary for accurate CH_4 emission estimates.

Chapter 5 - Overall conclusions and recommendations

5.1. Summary of conclusions

Estimating CH_4 emissions from livestock production is challenging but crucial to improve the efficiency and sustainability of beef and dairy production systems. The eddy covariance technique is a well-established micrometeorological method used to measure fluxes of CO_2 and energy and hundreds of sites around the world, but only a few studies have applied this technique to measure gas exchange in livestock systems. In this thesis, the EC technique performance to estimate CH_4 emissions from cattle in a commercial feedlot was investigated. This evaluation included different aspects influencing EC measurements, such as instrumentation, fetch limitations and the effect of heterogeneities of the source area on flux estimates. The overall goal of this study was to evaluate if the EC technique can be used to measure CH_4 emissions from cattle in a feedlot and scale CH_4 emission from feedlot to animal level using existing flux footprint models. The following conclusions were drawn from this research.

1. The performance assessment of the closed-path EC system based on comparisons of flux and cospectra with open-path system showed that this system is suitable for EC measurements.
2. Footprint analysis indicate large spatial variability of EC fluxes throughout the feedlot suggesting possible inhomogeneity in source strength due to atmospheric conditions and fetch limitations. This suggests the need for considering the position and size of the source area contributing to the measured flux to interpret the EC measurements.
3. Two-dimensional footprint functions were used to interpret and estimate the contribution of different areas in the feedlot to measured flux. The results showed that the two pens

immediately south from the flux tower contributed to more than 50% of the measured fluxes, although these pens correspond to less than 2% of the feedlot area. The results also showed that non-pen surfaces within the feedlot influenced the measured CH_4 flux. The magnitude of this effect depended on the size and the extent of the source area defined by flux footprint models.

4. Scaling of fluxes from feedlot to pen scale (F_{pens}) increased F_{pens} by 8% (FFP) to 14% (KM01) compared to the measured EC flux. The monthly average CH_4 emission per animal (F_{animal}), ranged from 83 to 125 g animal^{-1} d^{-1} (KM01) and 75 to 114 g animal^{-1} d^{-1} (FFP). These emission values agree with the results from other studies in feedlots that used different micrometeorological techniques. Additional studies are necessary to quantify the magnitude of CH_4 emission uncertainties introduced by discrepancies between footprint models and by changes in stocking density due to animal movement in the source area.
5. The CH_4 emission estimates provided by EC and bLS techniques showed good agreement (concordance coefficient = 0.84). Average emission values based on EC_{FFP} were not significantly different from bLS estimates despite the different footprint model used by bLS and EC_{FFP} techniques and the presence of fetch limited conditions in the feedlot. This comparison study further indicate that the eddy covariance technique is a viable option to quantify gas emissions from a feedlot.

So far, very few studies have combined footprint models and the EC technique to estimate CH_4 fluxes from livestock. The results from this study provide important guidelines for estimating trace gas emissions from feedlots. Apart from CH_4, feedlots are also important sources of ammonia (NH_3) and nitrous oxide (N_2O). The flux footprint scaling approach used in

this study could also be used to estimate NH_3 and N_2O emissions per pen surface. This would allow long-term monitoring of livestock systems and bring new insights into the mechanism governing the exchange of trace gases in livestock system. However, additional studies are still needed to quantify the uncertainties of flux footprint models under field conditions and further address uncertainties associated with animal movement on the CH_4 emission measurements.

5.2. Recommendations for future studies

Based on the findings of this study, we have the following recommendations for improving future measurements of GHG emissions from livestock using the EC method:

1. The spectral response of closed-path EC systems could be improved in future studies by shortening the length of the air intake tubing to minimize the accumulation of dust and water vapor adsorption. Moreover, hydrophobic tubing materials made up of Teflon and Synflex tubing, and other types of air filters (e.g. Vortex air cleaner, Campbell Sci.) could be an option to improve frequency responses for active gases such as NH_3 and H_2O measured in closed-path EC systems.
2. The results from this study suggest that an increase in the source area sampled by the tower could reduce the influence of source area variability on EC flux measurements. However, in this feedlot, higher sensor heights would reduce data retention due to fetch limitations. In future studies, the retention of data could be increased by placing the tower closer to the center of the feedlot.
3. This study also showed that the animal movement within the pens especially during the feeding times poses additional challenges for CH_4 emission estimates. Monitoring the animal positions using digital photograph and computer algorithms would allow the

calculation of the true cattle stocking density and in scaling CH_4 emissions measured at landscape to animal level.

4. We observed high CH_4 emission values in August probably due to the higher ambient temperature and soil water content in the pen surfaces in comparison to the winter months. This likely resulted in high anaerobic decomposition rates of the manure on the pen surfaces. Future studies in feedlots should monitor the soil temperature and water content in the pens to identify possible dependence between CH_4 emissions and these variables. Alternatively, the removal of manure from pens closed by the tower that contribute majority of the measured flux would reduce CH_4 ground emissions from pen surfaces.
5. One of the most obvious shortcomings of the conditional sampling approach used in this study to determine background CH_4 concentration for estimating CH_4 emission was the reduction in the available flux data. In addition, some uncertainties in the bLS emission estimates could probably be reduced by using additional line-average concentration measurements along with the EC measurements.

References

Abraha, M., Chen, J., Chu, H., Zenone, T., John, R., Su, Y.J., Hamilton, S.K. and Robertson, G.P., 2015. Evapotranspiration of annual and perennial biofuel crops in a variable climate. GCB Bioenergy, 7(6): 1344-1356.

Aguilar, O.A., Maghirang, R., Trabue, S.L. and Erickson, L.E., 2014. Experimental research on the effects of water application on greenhouse gas emissions from beef cattle feedlots. International Journal of Energy and Environmental Engineering, 5(2-3): 103.

Amiro, B., 1998. Footprint climatologies for evapotranspiration in a boreal catchment. Agricultural and Forest Meteorology, 90(3): 195-201.

Arriga, N., Rannik, Ü., Aubinet, M., Carrara, A., Vesala, T. and Papale, D., 2017. Experimental validation of footprint models for eddy covariance CO_2 flux measurements above grassland by means of natural and artificial tracers. Agricultural and Forest Meteorology, 242: 75-84.

Aubinet, M., Vesala, T. and Papale, D., 2012. Eddy covariance: a practical guide to measurement and data analysis. Springer Science & Business Media.

Bai, M., Flesch, T.K., McGinn, S.M. and Chen, D., 2015. A Snapshot of Greenhouse Gas Emissions from a Cattle Feedlot. Journal of Environmental Quality, 44(6): 1974-1978.

Baker, J. and Griffis, T., 2005. Examining strategies to improve the carbon balance of corn/soybean agriculture using eddy covariance and mass balance techniques. Agricultural and Forest Meteorology, 128(3): 163-177.

Baldocchi, D., 2008. Breathing of the terrestrial biosphere: lessons learned from a global network of carbon dioxide flux measurement systems. Aust. J. Bot., 56(1): 1-26.

Baldocchi, D., Detto, M., Sonnentag, O., Verfaillie, J., Teh, Y.A., Silver, W. and Kelly, N.M., 2012. The challenges of measuring methane fluxes and concentrations over a peatland pasture. Agricultural and Forest Meteorology, 153: 177-187.

Baldocchi, D.D., 2003. Assessing the eddy covariance technique for evaluating carbon dioxide exchange rates of ecosystems: past, present and future. Global Change Biology, 9(4): 479-492.

Batchvarova, E. and Gryning, S.-E., 1991. Applied model for the growth of the daytime mixed layer. Boundary-Layer Meteorology, 56(3): 261-274.

Baum, K.A., Ham, J.M., Brunsell, N.A. and Coyne, P.I., 2008. Surface boundary layer of cattle feedlots: Implications for air emissions measurement. Agricultural and Forest Meteorology, 148(11): 1882-1893.

Beauchemin, K., McGinn, S., Benchaar, C. and Holtshausen, L., 2009. Crushed sunflower, flax, or canola seeds in lactating dairy cow diets: Effects on methane production, rumen fermentation, and milk production. Journal of Dairy Science, 92(5): 2118-2127.

Benvenutti, M.A., Coates, T.W., Imaz, A., Flesch, T.K., Hill, J., Charmley, E., Hepworth, G. and Chen, D., 2015. The use of image analysis to determine the number and position of cattle at a water point. Computers and Electronics in Agriculture, 118: 24-27.

Borhan, M.S., Capareda, S.C., Mukhtar, S., Faulkner, W.B., McGee, R. and Parnell, C.B., 2011. Greenhouse gas emissions from ground level area sources in dairy and cattle feedyard operations. Atmosphere, 2(3): 303-329.

Broucek, J., 2014. Production of methane emissions from ruminant husbandry: a review. Journal of Environmental Protection, 5(15): 1482.

Buendia, L., Miwa, K., Ngara, T. and Tanabe, K., 2006. IPCC Guidelines for National Greenhouse Gas Inventories. Prepared by the National Greenhouse Gas Inventories Programme. IGES, Hayama, Japan.

Burba, G., Schmidt, A., Scott, R.L., Nakai, T., Kathilankal, J., Fratini, G., Hanson, C., Law, B., McDermitt, D.K. and Eckles, R., 2012. Calculating CO_2 and H_2O eddy covariance fluxes from an enclosed gas analyzer using an instantaneous mixing ratio. Global change biology, 18(1): 385-399.

Burkholder, J., Libra, B., Weyer, P., Heathcote, S., Kolpin, D., Thorne, P.S. and Wichman, M., 2007. Impacts of waste from concentrated animal feeding operations on water quality. Environmental health perspectives, 115(2): 308.

Businger, J.A., Wyngaard, J.C., Izumi, Y. and Bradley, E.F., 1971. Flux-profile relationships in the atmospheric surface layer. Journal of the atmospheric Sciences, 28(2): 181-189.

Chadwick, D., Sommer, S., Thorman, R., Fangueiro, D., Cardenas, L., Amon, B. and Misselbrook, T., 2011. Manure management: implications for greenhouse gas emissions. Animal Feed Science and Technology, 166: 514-531.

Chen, H., Winderlich, J., Gerbig, C., Hoefer, A., Rella, C., Crosson, E., Van Pelt, A., Steinbach, J., Kolle, O. and Beck, V., 2010. High-accuracy continuous airborne measurements of greenhouse gases (CO_2 and CH_4) using the cavity ring-down spectroscopy (CRDS) technique. Atmospheric Measurement Techniques, 3(2): 375-386.

Coates, T.W., Benvenutti, M.A., Flesch, T.K., Charmley, E., McGinn, S.M. and Chen, D., 2018. Applicability of Eddy Covariance to Estimate Methane Emissions from Grazing Cattle. Journal of Environmental Quality, 47(1): 54-61.

Coates, T.W., Flesch, T.K., McGinn, S.M., Charmley, E. and Chen, D., 2017. Evaluating an eddy covariance technique to estimate point-source emissions and its potential application to grazing cattle. Agricultural and Forest Meteorology, 234: 164-171.

Crosson, P., Shalloo, L., O'Brien, D., Lanigan, G.J., Foley, P.A., Boland, T.M. and Kenny, D.A., 2011. A review of whole farm systems models of greenhouse gas emissions from beef and dairy cattle production systems. Animal Feed Science and Technology, 166-67: 29-45.

Dabberdt, W.F., Lenschow, D.H., Horst, T.W., Zimmerman, P.R., Oncley, S.P. and Delany, A.C., 1993. Atmosphere-surface exchange measurements. Science, 260(5113): 1472-1481.

Danielsson, R., Ramin, M., Bertilsson, J., Lund, P. and Huhtanen, P., 2017. Evaluation of a gas in vitro system for predicting methane production in vivo. Journal of dairy science, 100(11): 8881-8894.

Dengel, S., Levy, P.E., Grace, J., Jones, S.K. and Skiba, U.M., 2011. Methane emissions from sheep pasture, measured with an open-path eddy covariance system. Global Change Biology, 17(12): 3524-3533.

Denmead, O., 2008. Approaches to measuring fluxes of methane and nitrous oxide between landscapes and the atmosphere. Plant and Soil, 309(1-2): 5-24.

Detto, M., Verfaillie, J., Anderson, F., Xu, L. and Baldocchi, D., 2011. Comparing laser-based open-and closed-path gas analyzers to measure methane fluxes using the eddy covariance method. Agricultural and forest meteorology, 151(10): 1312-1324.

Dyer, A., 1974. A review of flux-profile relationships. Boundary-Layer Meteorology, 7(3): 363-372.

Eckard, R.J., Grainger, C. and de Klein, C.A.M., 2010. Options for the abatement of methane and nitrous oxide from ruminant production: A review. Livestock Science, 130(1-3): 47-56.
EPA, 2001. Emissions from animal feeding operations. https://www3.epa.gov/ttn/chief/ap42/ch09/draft/draftanimalfeed.pdf (accessed 2 Jul. 2017).
EPA, 2016. Inventory of U.S. Greenhouse Gas Emissions and Sinks: 1990 - 2014. U.S. Environmental Protection Agency, Washington, D.C.
EPA, 2017. Inventory of U.S. Greenhouse Gas Emissions and Sinks: 1990 - 2015. U.S. Environmental Protection Agency, Washington, D.C.
Eugster, W. and Merbold, L., 2015. Eddy covariance for quantifying trace gas fluxes from soils. SOIL, 1(1): 187-205.
Famulari, D., Nemitz, E., Di Marco, C., Phillips, G.J., Thomas, R., House, E. and Fowler, D., 2010. Eddy-covariance measurements of nitrous oxide fluxes above a city. Agricultural and Forest Meteorology, 150(6): 786-793.
Fan, S.M., Wofsy, S.C., Bakwin, P.S., Jacob, D.J. and Fitzjarrald, D.R., 1990. Atmosphere-biosphere exchange of CO_2 and O_3 in the central Amazon forest. Journal of Geophysical Research-Atmospheres, 95(D10): 16851-16864.
FAO, 2009. Global agriculture towards 2050. High Level Expert Forum Issues Paper. FAO, Rome. FAO (Food and Agriculture Organization of the United Nations). The state of food and agriculture: Livestock in the balance. Food and Agriculture Organization of the United Nations. Available at http://www.fao.org/docrep/012/i0680e/i0680e.pdf (accessed 12.20.14).
Feigenwinter, C., Vogt, R. and Christen, A., 2012. Eddy covariance measurements over urban areas, Eddy Covariance. Springer, pp. 377-397.
Felber, R., Muenger, A., Neftel, A. and Ammann, C., 2015. Eddy covariance methane flux measurements over a grazed pasture: effect of cows as moving point sources. Biogeosciences, 12(12): 3925-3940.
Finkelstein, P.L. and Sims, P.F., 2001. Sampling error in eddy correlation flux measurements. Journal of Geophysical Research-Atmospheres, 106(D4): 3503-3509.
Flesch, T., Harper, L., Powell, J. and Wilson, J., 2009. Inverse-dispersion calculation of ammonia emissions from Wisconsin dairy farms. Transactions of the ASABE, 52(1): 253-265.
Flesch, T., Wilson, J. and Harper, L., 2005a. Deducing ground-to-air emissions from observed trace gas concentrations: a field trial with wind disturbance. Journal of Applied Meteorology, 44(4): 475-484.
Flesch, T., Wilson, J., Harper, L., Crenna, B. and Sharpe, R., 2004. Deducing ground-to-air emissions from observed trace gas concentrations: a field trial. Journal of Applied Meteorology, 43(3): 487-502.
Flesch, T., Wilson, J., Harper, L., Todd, R. and Cole, N., 2007. Determining ammonia emissions from a cattle feedlot with an inverse dispersion technique. Agricultural and forest meteorology, 144(1): 139-155.
Flesch, T.K., Wilson, J.D., Harper, L.A. and Crenna, B.P., 2005b. Estimating gas emissions from a farm with an inverse-dispersion technique. Atmospheric Environment, 39(27): 4863-4874.

Flesch, T.K., Wilson, J.D. and Yee, E., 1995. Backward-time Lagrangian stochastic disersion models and their application to estimate gaseous emissions. Journal of Applied Meteorology, 34(6): 1320-1332.

Foken, T., Göckede, M., Mauder, M., Mahrt, L., Amiro, B.D. and Munger, J.W., 2004. Post-field data quality control. In: X. Lee, W. Massman and B. Law (Editors), Handbook of Micrometeorology: a guide for surface flux measurement and analysis. Kluwer, Dordrecht, pp. 181-208.

Foken, T. and Leclerc, M., 2004. Methods and limitations in validation of footprint models. Agricultural and Forest Meteorology, 127(3): 223-234.

Gao, Z., Desjardins, R.L. and Flesch, T.K., 2010. Assessment of the uncertainty of using an inverse-dispersion technique to measure methane emissions from animals in a barn and in a small pen. Atmospheric Environment, 44(26): 3128-3134.

Gao, Z., Mauder, M., Desjardins, R.L., Flesch, T.K. and van Haarlem, R.P., 2009. Assessment of the backward Lagrangian Stochastic dispersion technique for continuous measurements of CH4 emissions. Agricultural and Forest Meteorology, 149(9): 1516-1523.

Gao, Z., Yuan, H., Ma, W., Liu, X. and Desjardins, R., 2011. Methane emissions from a dairy feedlot during the fall and winter seasons in Northern China. Environmental Pollution, 159(5): 1183-1189.

Gash, J., 1986. A note on estimating the effect of a limited fetch on micrometeorological evaporation measurements. Boundary-Layer Meteorology, 35(4): 409-413.

Gerber, P.J., Steinfeld, H., Henderson, B., Mottet, A., Opio, C., Dijkman, J., Falcucci, A. and Tempio, G., 2013. Tackling climate change through livestock: a global assessment of emissions and mitigation opportunities. Food and Agriculture Organization of the United Nations (FAO).

Gibbs, M. and Leng, R., 1993. Methane emissions from livestock. Methane and Nitrous Oxide, RIVM report(481507003): 73-79.

Grainger, C. and Beauchemin, K., 2011. Can enteric methane emissions from ruminants be lowered without lowering their production? Animal feed science and technology, 166: 308-320.

Grainger, C., Clarke, T., McGinn, S.M., Auldist, M.J., Beauchemin, K.A., Hannah, M.C., Waghorn, G.C., Clark, H. and Eckard, R.J., 2007. Methane emissions from dairy cows measured using the sulfur hexafluoride (SF_6) tracer and chamber techniques. Journal of Dairy Science, 90(6): 2755-2766.

Griffith, D.W., Bryant, G.R., Hsu, D. and Reisinger, A.R., 2008. Methane emissions from free-ranging cattle: Comparison of tracer and integrated horizontal flux techniques. Journal of environmental quality, 37(2): 582-591.

Hammond, K.J., Crompton, L.A., Bannink, A., Dijkstra, J., Yáñez-Ruiz, D., O'Kiely, P., Kebreab, E., Eugène, M., Yu, Z. and Shingfield, K., 2016. Review of current in vivo measurement techniques for quantifying enteric methane emission from ruminants. Animal Feed Science and Technology, 219: 13-30.

Harper, L., Denmead, O., Freney, J. and Byers, F., 1999. Direct measurements of methane emissions from grazing and feedlot cattle. Journal of Animal Science, 77(6): 1392-1401.

Harper, L., Flesch, T., Powell, J., Coblentz, W., Jokela, W. and Martin, N., 2009. Ammonia emissions from dairy production in Wisconsin. Journal of dairy Science, 92(5): 2326-2337.

Harper, L.A., 2005. Ammonia: Measurement Issues. Agronomy Monograph No. 47 J.L. Hatfield, J.M. Baker (Eds.), Micrometeorology in Agricultural Systems, ASA-CSSA-SSSA, Madison, WI (2005): 345-380.

Harper, L.A., Denmead, O.T. and Flesch, T.K., 2011. Micrometeorological techniques for measurement of enteric greenhouse gas emissions. Animal Feed Science and Technology, 166-67: 227-239.

Haslwanter, A., Hammerle, A. and Wohlfahrt, G., 2009. Open-path vs. closed-path eddy covariance measurements of the net ecosystem carbon dioxide and water vapour exchange: A long-term perspective. Agricultural and Forest Meteorology, 149(2): 291-302.

Havlík, P., Valin, H., Herrero, M., Obersteiner, M., Schmid, E., Rufino, M.C., Mosnier, A., Thornton, P.K., Böttcher, H. and Conant, R.T., 2014. Climate change mitigation through livestock system transitions. Proceedings of the National Academy of Sciences, 111(10): 3709-3714.

Hill, J., McSweeney, C., Wright, A.-D.G., Bishop-Hurley, G. and Kalantar-zadeh, K., 2016. Measuring methane production from ruminants. Trends in biotechnology, 34(1): 26-35.

Hindrichsen, I., Wettstein, H.-R., Machmüller, A. and Kreuzer, M., 2006. Methane emission, nutrient degradation and nitrogen turnover in dairy cows and their slurry at different milk production scenarios with and without concentrate supplementation. Agriculture, ecosystems & environment, 113(1-4): 150-161.

Horst, T., 1997. A simple formula for attenuation of eddy fluxes measured with first-order-response scalar sensors. Boundary-Layer Meteorology, 82(2): 219-233.

Hsieh, C.I., Katul, G. and Chi, T., 2000. An approximate analytical model for footprint estimation of scaler fluxes in thermally stratified atmospheric flows. Advances in Water Resources, 23(7): 765-772.

Hudson, R.J., 2009. Management of agricultural, forestry and fisheries enterprises. Eloss Publisheres Company Limited.

Ibrom, A., Dellwik, E., Flyvbjerg, H., Jensen, N.O. and Pilegaard, K., 2007. Strong low-pass filtering effects on water vapour flux measurements with closed-path eddy correlation systems. Agricultural and Forest Meteorology, 147(3-4): 140-156.

IPCC, 2006. Guidelines for National Greenhouse Gas Inventory. http://www.ipcc-nggip.iges.or.jp/public/ (accessed 2 Aug. 2017).

IPCC, 2014. Climate Change 2014: Synthesis Report. Contribution of Working Groups I, II and III to the Fifth Assessment Report of the Intergovernmental Panel on Climate Change Core Writing Team, R.K. Pachauri, L.A. Meyer (Eds.)IPCC, Geneva, Switzerland (2014).

Johnson, K., Huyler, M., Westberg, H., Lamb, B. and Zimmerman, P., 1994. Measurement of methane emissions from ruminant livestock using a sulfur hexafluoride tracer technique. Environmental science & technology, 28(2): 359-362.

Johnson, K.A. and Johnson, D.E., 1995. Methane emissions from cattle. Journal of Animal Science, 73(8): 2483-2492.

Judd, M.J., Kellier, F.M., Ulyatt, M.J., Lassey, K.R., Tate, K.R., Shelton, D., Harvey, M.J. and Walker, C.F., 1999. Net methane emissions from grazing sheep. Global Change Biology, 5(6): 647-657.

Jungbluth, T., Hartung, E. and Brose, G., 2001. Greenhouse gas emissions from animal houses and manure stores. Nutrient cycling in Agroecosystems, 60(1-3): 133-145.

Kaimal, J., Wyngaard, J., Izumi, Y. and Coté, O., 1972. Spectral characteristics of surface-layer turbulence. Quarterly Journal of the Royal Meteorological Society, 98(417): 563-589.
Kinsman, R., Sauer, F., Jackson, H. and Wolynetz, M., 1995. Methane and carbon dioxide emissions from dairy cows in full lactation monitored over a six-month period. Journal of Dairy Science, 78(12): 2760-2766.
Klevenhusen, F., Kreuzer, M. and Soliva, C., 2011. Enteric and manure-derived methane and nitrogen emissions as well as metabolic energy losses in cows fed balanced diets based on maize, barley or grass hay. Animal, 5(03): 450-461.
Kljun, N., Calanca, P., Rotach, M. and Schmid, H., 2004. A simple parameterisation for flux footprint predictions. Boundary-Layer Meteorology, 112(3): 503-523.
Kljun, N., Calanca, P., Rotach, M. and Schmid, H., 2015. A simple two-dimensional parameterisation for Flux Footprint Prediction (FFP). Geoscientific Model Development, 8(11): 3695-3713.
Kljun, N., Kormann, R., Rotach, M. and Meixer, F., 2003. Comparison of the Langrangian Footprint. Boundary-layer meteorology, 106(2): 349-355.
Kljun, N., Rotach, M. and Schmid, H., 2002. A three-dimensional backward Lagrangian footprint model for a wide range of boundary-layer stratifications. Boundary-Layer Meteorology, 103(2): 205-226.
Knapp, J., Firkins, J., Aldrich, J., Cady, R., Hristov, A., Weiss, W., Wright, A. and Welch, M., 2011. Cow of the Future research priorities for mitigating enteric methane emissions from dairy. Innovation Center for US Dairy.
Knapp, J., Laur, G., Vadas, P., Weiss, W. and Tricarico, J., 2014. Invited review: Enteric methane in dairy cattle production: Quantifying the opportunities and impact of reducing emissions. Journal of Dairy Science, 97(6): 3231-3261.
Kormann, R. and Meixner, F.X., 2001. An analytical footprint model for non-neutral stratification. Boundary-Layer Meteorology, 99(2): 207-224.
Lassey, K., Pinares-Patiño, C., Martin, R., Molano, G. and McMillan, A., 2011. Enteric methane emission rates determined by the SF_6 tracer technique: Temporal patterns and averaging periods. Animal feed science and technology, 166: 183-191.
Laubach, J., 2010. Testing of a Lagrangian model of dispersion in the surface layer with cattle methane emissions. Agricultural and Forest Meteorology, 150(11): 1428-1442.
Laubach, J., Bai, M., Pinares-Patino, C.S., Phillips, F.A., Naylor, T.A., Molano, G., Cardenas Rocha, E.A. and Griffith, D.W.T., 2013. Accuracy of micrometeorological techniques for detecting a change in methane emissions from a herd of cattle. Agricultural and Forest Meteorology, 176: 50-63.
Laubach, J. and Kelliher, F.M., 2004. Measuring methane emission rates of a dairy cow herd by two micrometeorological techniques. Agricultural and Forest Meteorology, 125(3-4): 279-303.
Laubach, J. and Kelliher, F.M., 2005. Measuring methane emission rates of a dairy cow herd (II): results from a backward-Lagrangian stochastic model. Agricultural and Forest Meteorology, 129(3): 137-150.
Laubach, J., Kelliher, F.M., Knight, T.W., Clark, H., Molano, G. and Cavanagh, A., 2008. Methane emissions from beef cattle - a comparison of paddock-and animal-scale measurements. Australian Journal of Experimental Agriculture, 48(1-2): 132-137.
Lawrence, I. and Lin, K., 1989. A concordance correlation coefficient to evaluate reproducibility. Biometrics: 255-268.

Leclerc, M. and Thurtell, G., 1990. Footprint prediction of scalar fluxes using a Markovian analysis. Boundary-Layer Meteorology, 52(3): 247-258.
Leclerc, M.Y. and Foken, T., 2014. Footprints in micrometeorology and ecology. Springer, 239 pp.
Leuning, R., Baker, S.K., Jamie, I.M., Hsu, C.H., Klein, L., Denmead, O.T. and Griffith, D.W.T., 1999. Methane emission from free-ranging sheep: a comparison of two measurement methods. Atmospheric Environment, 33(9): 1357-1365.
Lockyer, D. and Champion, R., 2001. Methane production by sheep in relation to temporal changes in grazing behaviour. Agriculture, ecosystems & environment, 86(3): 237-246.
Lockyer, D. and Jarvis, S., 1995. The measurement of methane losses from grazing animals. Environmental Pollution, 90(3): 383-390.
Loh, Z., Chen, D., Bai, M., Naylor, T., Griffith, D., Hill, J., Denmead, T., McGinn, S. and Edis, R., 2008. Measurement of greenhouse gas emissions from Australian feedlot beef production using open-path spectroscopy and atmospheric dispersion modelling. Australian Journal of Experimental Agriculture, 48(1-2): 244-247.
Loh, Z., Leuning, R., Zegelin, S., Etheridge, D., Bai, M., Naylor, T. and Griffith, D., 2009. Testing Lagrangian atmospheric dispersion modelling to monitor CO_2 and CH_4 leakage from geosequestration. Atmospheric Environment, 43(16): 2602-2611.
Madsen, J., Bjerg, B.S., Hvelplund, T., Weisbjerg, M.R. and Lund, P., 2010. Methane and carbon dioxide ratio in excreted air for quantification of the methane production from ruminants. Livestock Science, 129(1): 223-227.
Makkar, H. and Vercoe, P., 2007. Measuring methane poduction from ruminants. Springer, Dordrecht, The Netherlands.
Martin, C., Morgavi, D. and Doreau, M., 2010. Methane mitigation in ruminants: from microbe to the farm scale. Animal, 4(3): 351-365.
McBain, M. and Desjardins, R., 2005. The evaluation of a backward Lagrangian stochastic (bLS) model to estimate greenhouse gas emissions from agricultural sources using a synthetic tracer source. Agricultural and forest meteorology, 135(1): 61-72.
McDermitt, D., Burba, G., Xu, L., Anderson, T., Komissarov, A., Riensche, B., Schedlbauer, J., Starr, G., Zona, D., Oechel, W., Oberbauer, S. and Hastings, S., 2011. A new low-power, open-path instrument for measuring methane flux by eddy covariance. Applied Physics B-Lasers and Optics, 102(2): 391-405.
McDermitt, D., Xu, L., Lin, X., Amen, J. and Welding, K., 2013. Impact of changes in barometric pressure on landfill methane emission, EGU General Assembly Conference Abstracts, pp. 5435.
McGinn, S., Beauchemin, K., Coates, T. and Colombatto, D., 2004. Methane emissions from beef cattle: Effects of monensin, sunflower oil, enzymes, yeast, and fumaric acid. Journal of animal science, 82(11): 3346-3356.
McGinn, S. and Flesch, T., 2018. Ammonia and greenhouse gas emissions at beef cattle feedlots in Alberta Canada. Agricultural and Forest Meteorology.
McGinn, S., Flesch, T., Harper, L. and Beauchemin, K., 2006. An approach for measuring methane emissions from whole farms. Journal of environmental quality, 35(1): 14-20.
McGinn, S.M., 2006. Measuring greenhouse gas emissions from point sources in agriculture. Canadian Journal of Soil Science, 86(3): 355-371.
McGinn, S.M., 2013. Developments in micrometeorological methods for methane measurements. Animal, 7: 386-393.

McGinn, S.M., Turner, D., Tomkins, N., Charmley, E., Bishop-Hurley, G. and Chen, D., 2011. Methane Emissions from Grazing Cattle Using Point-Source Dispersion. Journal of Environmental Quality, 40(1): 22-27.

Moncrieff, J., Clement, R., Finnigan, J. and Meyers, T., 2004. Averaging, detrending, and filtering of eddy covariance time series, Handbook of micrometeorology. Springer, pp. 7-31.

Moncrieff, J.B., Massheder, J.M., Bruin, H.d., Elbers, J., Friborg, T., Heusinkveld, B., Kabat, P., Scott, S., Soegaard, H. and Verhoef, A., 1997. A system to measure surface fluxes of momentum, sensible heat, water vapour and carbon dioxide. Journal of Hydrology (Amsterdam), 188-189(1/4): 589-611.

Moravek, A., Trebs, I. and Foken, T., 2013. Effect of imprecise lag time and high-frequency attenuation on surface-atmosphere exchange fluxes determined with the relaxed eddy accumulation method. Journal of Geophysical Research: Atmospheres, 118(17).

Münger, A. and Kreuzer, M., 2006. Methane emission as determined in contrasting dairy cattle breeds over the reproduction cycle, International Congress Series. Elsevier, pp. 119-122.

National Climatic Data Center, 2017. Available at http://www.rcc-acis.org/docs_datasets.html (accessed on 3/17/2017).

Neftel, A., Spirig, C. and Ammann, C., 2008. Application and test of a simple tool for operational footprint evaluations. Environmental Pollution, 152(3): 644-652.

Nordbo, A., Launiainen, S., Mammarella, I., Leppäranta, M., Huotari, J., Ojala, A. and Vesala, T., 2011. Long-term energy flux measurements and energy balance over a small boreal lake using eddy covariance technique. Journal of Geophysical Research: Atmospheres (1984–2012), 116(D2).

Norris, S.J., Brooks, I.M., Hill, M.K., Brooks, B.J., Smith, M.H. and Sproson, D.A., 2012. Eddy covariance measurements of the sea spray aerosol flux over the open ocean. Journal of Geophysical Research: Atmospheres (1984–2012), 117(D7).

O'Mara, F.P., 2011. The significance of livestock as a contributor to global greenhouse gas emissions today and in the near future. Animal Feed Science and Technology, 166: 7-15.

Opio, C., Gerber, P., Mottet, A., Falcucci, A., Tempio, G., MacLeod, M., Vellinga, T., Henderson, B. and Steinfeld, H., 2013. Greenhouse gas emissions from ruminant supply chains–A global life cycle assessment. Food and agriculture organization of the United Nations (FAO), Rome: 1-214.

Peltola, O., Mammarella, I., Haapanala, S., Burba, G. and Vesala, T., 2013. Field intercomparison of four methane gas analyzers suitable for eddy covariance flux measurements. Biogeosciences, 10(6): 3749-3765.

Phillips, F., Leuning, R., Baigent, R., Kelly, K. and Denmead, O., 2007. Nitrous oxide flux measurements from an intensively managed irrigated pasture using micrometeorological techniques. Agricultural and Forest Meteorology, 143(1-2): 92-105.

Pinares-Patiño, C., Lassey, K., Martin, R., Molano, G., Fernandez, M., MacLean, S., Sandoval, E., Luo, D. and Clark, H., 2011. Assessment of the sulphur hexafluoride (SF_6) tracer technique using respiration chambers for estimation of methane emissions from sheep. Animal feed science and technology, 166: 201-209.

Pinares-Patiño, C., Waghorn, G., Machmüller, A., Vlaming, B., Molano, G., Cavanagh, A. and Clark, H., 2007. Methane emissions and digestive physiology of non-lactating dairy cows fed pasture forage. Canadian Journal of Animal Science, 87(4): 601-613.

Place, S.E., Pan, Y., Zhao, Y. and Mitloehner, F.M., 2011. Construction and operation of a ventilated hood system for measuring greenhouse gas and volatile organic compound emissions from cattle. Animals, 1(4): 433-446.

Prajapati, P. and Santos, E.A., 2017. Measurements of methane emissions from a beef cattle feedlot using the eddy covariance technique. Agricultural and Forest Meteorology, 232: 349-358.

Prajapati, P. and Santos, E.A., 2018a. Comparing methane emissions estimated using a backward-Lagrangian stochastic model and the eddy covariance technique in a beef cattle feedlot. Agricultural and Forest Meteorology, 256: 482-491.

Prajapati, P. and Santos, E.A., 2018b. Estimating methane emissions from beef cattle in a feedlot using the eddy covariance technique and footprint analysis. Agricultural and Forest Meteorology, 258: 18-28.

Rahman, S., Borhan, M.S. and Swanson, K., 2013. Greenhouse gas emissions from beef cattle pen surfaces in North Dakota. Environmental technology, 34(10): 1239-1246.

Ramin, M. and Huhtanen, P., 2013. Development of equations for predicting methane emissions from ruminants. Journal of Dairy Science, 96(4): 2476-2493.

Raupach, M., 2001. Inferring biogeochemical sources and sinks from atmospheric concentrations: general considerations and applications in vegetation canopies, Global biogeochemical cycles in the climate system. Elsevier, pp. 41-59.

Raupach, M.R., 1994. Simplified expressions for vegetation roughness length and zero-plane displacement as functions of canopy height and area index. Boundary-Layer Meteorology, 71(1-2): 211-216.

Ro, K.S., Johnson, M.H., Stone, K.C., Hunt, P.G., Flesch, T. and Todd, R.W., 2013. Measuring gas emissions from animal waste lagoons with an inverse-dispersion technique. Atmospheric environment, 66: 101-106.

Sanz, A., Misselbrook, T., Sanz, M.J. and Vallejo, A., 2010. Use of an inverse dispersion technique for estimating ammonia emission from surface-applied slurry. Atmospheric Environment, 44(7): 999-1002.

Sawford, B., 2001. Project Prairie Grass—a classic atmospheric dispersion experiment revisited, 14th Australian fluid mechanics conference, Adelaide.

Schmid, H., 1994. Source areas for scalars and scalar fluxes. Boundary-Layer Meteorology, 67(3): 293-318.

Schmid, H., 1997. Experimental design for flux measurements: matching scales of observations and fluxes. Agricultural and Forest Meteorology, 87(2): 179-200.

Schmid, H. and Lloyd, C., 1997. Source area/footprint modeling over sparse savannah: how the sensors perceive the Tigerbush, Preprints 12th AMS Symp. on Boundary-Layers and Turb, pp. 555-556.

Schmid, H. and Oke, T., 1990. A model to estimate the source area contributing to turbulent exchange in the surface layer over patchy terrain. Quarterly Journal of the Royal Meteorological Society, 116(494): 965-988.

Schmid, H.P., 2002. Footprint modeling for vegetation atmosphere exchange studies: a review and perspective. Agricultural and Forest Meteorology, 113(1): 159-183.

Schuepp, P., Leclerc, M., MacPherson, J. and Desjardins, R., 1990. Footprint prediction of scalar fluxes from analytical solutions of the diffusion equation. Boundary-Layer Meteorology, 50(1-4): 355-373.

Sejian, V., Shekhawat, I., Ujor, V., Ezeji, T., Lakritz, J. and Lal, R., 2012. Global climate change: enteric methane reduction strategies in livestock, Environmental Stress and Amelioration in Livestock Production. Springer, pp. 469-499.
Shibata, M. and Terada, F., 2010. Factors affecting methane production and mitigation in ruminants. Animal Science Journal, 81(1): 2-10.
Steinfeld, H., Gerber, P., Wassenaar, T., Castel, V., Rosales, M. and Haan, C.d., 2006. Livestock's long shadow: environmental issues and options. Food and Agriculture Organization of the United Nations (FAO).
Stieger, J., Bamberger, I., Buchmann, N. and Eugster, W., 2015. Validation of farm-scale methane emissions using nocturnal boundary layer budgets. Atmospheric Chemistry and Physics, 15(24): 14055-14069.
Storm, I.M.L.D., Hellwing, A.L.F., Nielsen, N.I. and Madsen, J., 2012. Methods for measuring and estimating methane emission from ruminants. Animals, 2(2): 160-183.
Stull, R., 1988. Boundary conditions and surface forcing. An Introduction to Boundary Layer Meteorology: 251-289.
Subharat, S., Shu, D., Zheng, T., Buddle, B.M., Janssen, P.H., Luo, D. and Wedlock, D.N., 2015. Vaccination of cattle with a methanogen protein produces specific antibodies in the saliva which are stable in the rumen. Veterinary immunology and immunopathology, 164(3-4): 201-207.
Sun, K., Tao, L., Miller, D.J., Zondlo, M.A., Shonkwiler, K.B., Nash, C. and Ham, J.M., 2015. Open-path eddy covariance measurements of ammonia fluxes from a beef cattle feedlot. Agricultural and Forest Meteorology, 213: 193-202.
Taylor, A.M., Amiro, B.D., Tenuta, M. and Gervais, M., 2017. Direct whole-farm greenhouse gas flux measurements for a beef cattle operation. Agriculture, Ecosystems & Environment, 239: 65-79.
Todd, R., Cole, N., Casey, K., Hagevoort, R. and Auvermann, B., 2011. Methane emissions from southern High Plains dairy wastewater lagoons in the summer. Animal feed science and technology, 166: 575-580.
Todd, R.W., Altman, M.B., Cole, N.A. and Waldrip, H.M., 2014. Methane Emissions from a Beef Cattle Feedyard during Winter and Summer on the Southern High Plains of Texas. Journal of Environmental Quality, 43(4): 1125-1130.
Todd, R.W., Cole, N.A., Clark, R.N., Flesch, T.K., Harper, L.A. and Baek, B.H., 2008. Ammonia emissions from a beef cattle feedyard on the southern High Plains. Atmospheric Environment, 42(28): 6797-6805.
USDA, 2016. Overview of the United States Cattle Industry. Available at http://usda.mannlib.cornell.edu/usda/current/USCatSup/USCatSup-06-24-2016.pdf (accessed on 03.29.2017).
USEPA, 2015. U.S. greenhouse gas inverntory report: 1990–2013. USEPA, Washington, DC.
van Dorland, H.A., Wettstein, H.-R., Leuenberger, H. and Kreuzer, M., 2007. Effect of supplementation of fresh and ensiled clovers to ryegrass on nitrogen loss and methane emission of dairy cows. Livestock Science, 111(1-2): 57-69.
Van Haarlem, R., Desjardins, R., Gao, Z., Flesch, T. and Li, X., 2008. Methane and ammonia emissions from a beef feedlot in western Canada for a twelve-day period in the fall. Canadian Journal of Animal Science, 88(4): 641-649.

Velasco, E., Pressley, S., Allwine, E., Westberg, H. and Lamb, B., 2005. Measurements of CO_2 fluxes from the Mexico City urban landscape. Atmospheric Environment, 39(38): 7433-7446.

Vesala, T., Kljun, N., Rannik, Ü., Rinne, J., Sogachev, A., Markkanen, T., Sabelfeld, K., Foken, T. and Leclerc, M., 2008. Flux and concentration footprint modelling: State of the art. Environmental Pollution, 152(3): 653-666.

Vickers, D. and Mahrt, L., 1997. Quality control and flux sampling problems for tower and aircraft data. Journal of Atmospheric and Oceanic Technology, 14(3): 512-526.

Vranken, L., Avermaete, T., Petalios, D. and Mathijs, E., 2014. Curbing global meat consumption: emerging evidence of a second nutrition transition. Environmental Science & Policy, 39: 95-106.

Webb, E., Pearman, G. and Leuning, R., 1980. Correction of flux measurements for density effects due to heat and water vapour transfer. Quarterly Journal of the Royal Meteorological Society, 106(447): 85-100.

Wilczak, J.M., Oncley, S.P. and Stage, S.A., 2001. Sonic Anemometer Tilt Correction Algorithms. Boundary-Layer Meteorology, 99(1): 127-150.

Wilson, J., 2015. Computing the flux footprint. Boundary-Layer Meteorology, 156(1): 1-14.

Wilson, J., Flesch, T. and Crenna, B., 2013. Estimating Surface-Air Gas Fluxes by Inverse Dispersion Using a Backward Lagrangian Stochastic Trajectory Model. Lagrangian Modeling of the Atmosphere: 149-162.

Wilson, J.D. and Yee, E., 2007. A critical examination of the random displacement model of turbulent dispersion. Boundary-Layer Meteorology, 125(3): 399-416.

Wright, A., Kennedy, P., O'Neill, C., Toovey, A., Popovski, S., Rea, S., Pimm, C. and Klein, L., 2004. Reducing methane emissions in sheep by immunization against rumen methanogens. Vaccine, 22(29-30): 3976-3985.